NASA Technical Paper 1484

Two-Phase Choked Flow of Cryogenic Fluids in Converging-Diverging Nozzles

Robert J. Simoneau and Robert C. Hendricks

JULY 1979

NASA

NASA Technical Paper 1484

Two-Phase Choked Flow of Cryogenic Fluids in Converging-Diverging Nozzles

Robert J. Simoneau and Robert C. Hendricks
Lewis Research Center
Cleveland, Ohio

NASA
National Aeronautics
and Space Administration

Scientific and Technical
Information Branch

1979

SUMMARY

Data are presented for the two-phase choked flow of three cryogenic fluids - nitrogen, methane, and hydrogen - in four converging-diverging nozzles. Oxygen data were reported earlier. The data cover a range of inlet stagnation conditions, all single phase, from well below to well above the thermodynamic critical conditions. In almost all cases the nozzle throat conditions were two phase.

The results indicate that the choked flow rates were not very sensitive to nozzle geometry. However, the axial pressure profiles, especially the throat pressure and the point of vaporization, were very sensitive to both nozzle geometry and operating conditions.

A modified Henry-Fauske model correlated all the choked-flow-rate data to within ±10 percent. Neither the equilibrium model nor the Henry-Fauske model predicted throat pressures well over the whole range of data. Above the thermodynamic critical temperature the homogeneous equilibrium model was preferred for both flow rate and pressure ratio.

Like the oxygen data, the data of the three fluids could be normalized by the principle of corresponding states.

INTRODUCTION

The space program involves the storage, handling, and transfer of large quantities of pressurized liquid cryogens. Many of these fluids can be dangerous, and good management of them requires a knowledge of their flow characteristics. Anytime a pressurized liquid cryogen is caused to flow - whether by design or by accident - the potential for vaporization and two-phase choked flow exists. The flow discharge passage can be a variety of geometries: an orifice, a nozzle, a long or short tube, a crack, or a slit. The potential range of fluid conditions is also quite extensive. At the Lewis Research Center an experimental program has been conducted to measure the two-phase choked flow of various cryogenic fluids in a number of geometries over a wide range of initial conditions. The present report documents the work done with converging-diverging nozzles.

The general field of two-phase choked flow has been well surveyed in references 1 to 3. Reference 4 also contains some good articles on the subject. No attempt will be made herein to review the field. The literature for subcooled inlet conditions is sparse.

Our experiments with cryogens (refs. 5 to 12) include four fluids: nitrogen, oxygen, methane, and hydrogen in nozzles, orifices, tubes, and slits. The experiments cover a wide range of single-phase inlet stagnation conditions. Some of the nitrogen data to be reported are discussed in the literature in references 5 to 7. The only other data on choked flow of subcooled liquids through nozzles are the water data of Sozzi and Sutherland (ref. 13) and Schrock, et al. (ref. 14). There have been a few experiments on subcooled liquids in orifices and tubes. These are cited in references 10 to 12.

Attempts at analyses generally fall into two categories: first, an isentropic homogeneous equilibrium analysis; and second, some attempt to account for thermodynamic nonequilibrium. The isentropic homogeneous equilibrium model is considered standard thermodynamics and is rarely given authorship. An early work would be that of Tangren, et al. (ref. 15). The equilibrium analysis used in this report is summarized in the appendix. A recent paper by Collins (ref. 16) also presents the equilibrium analysis. It is widely accepted that two-phase choked flow experiences some degree of thermodynamic nonequilibrium, mainly in the form of some delay in vaporization as the fluid passes through the saturation pressure. An attempt at describing this phenomenon proposed by Henry and Fauske (ref. 17) is frequently used in nuclear thermal-hydraulic safety analyses. With a small modification the Henry-Fauske model is used herein. This model is also summarized in the appendix. We have had considerable success applying the principle of corresponding states, in addition to these flow models, to two-phase choked flows (refs. 18 and 19). This can be a considerable aid in extending the applicability of the data.

In many of these calculations it is important to have a good description of the thermophysical properties. We used a property program called GASP developed by Hendricks, Baron, and Peller (ref. 20).

The present report emphasizes the experiment and the data. The experimental facilities are described in some detail, especially the test sections. All the converging-diverging nozzle data are tabulated. Fairly extensive data plots are presented to aid in interpretation. Comparisons are made between the data and conventional equilibrium and nonequilibrium analyses. The data presented cover a wide range: four converging-diverging nozzles; three fluids - nitrogen, methane, and hydrogen; and inlet stagnation temperatures of $0.65 < T_0/T_c < 1.40$, where T_0 is the temperature at stagnation conditions and T_c is the temperature at thermodynamic critical conditions. These data are companion data to the oxygen and nitrogen data reported earlier (ref. 8). The data are primarily two-phase choked flow rates and the associated axial pressure profiles for these extensive inlet conditions. Some gaseous nitrogen data are also included both for calibration and as a reference base for data comparisons.

SYMBOLS

A	cross-sectional area, cm^2
D	hydraulic diameter, cm
G	mass flux, $g/cm^2 \cdot sec$
L	length, cm
N	constant, eq. (A19)
P	pressure, N/cm^2
r	radius, cm
S	entropy, $J/g \cdot K$
T	temperature, K
u	velocity, cm/sec
v	specific volume, cm^3/g
W	mass flow rate, g/sec
X	axial distance, cm
x	quality
Z	compressibility factor
ρ	density, g/cm^3

Subscripts:

b	back conditions
c	thermodynamic critical conditions
calc	calculated
e	thermodynamic equilibrium conditions
g	saturated vapor conditions
l	saturated liquid conditions
max	maximum, choked-flow, conditions
meas	measured
o	stagnation conditions
sat	saturation conditions
t	throat conditions

1, 2, . . ., n axial stations

Superscript:

* flow-normalizing parameter

DESCRIPTION OF EXPERIMENTS

General Flow Facilities

The experiments were carried out in two separate "once through" cryogenic flow facilities. The facilities are illustrated schematically in figures 1 and 2. They have the same basic characteristics. The essential elements include a low-pressure liquid supply, a high-pressure vessel, a gas-pressurizing system, a primary flowmeter, the test-section assembly, a backpressure valve, a heat exchanger, and a secondary orifice flowmeter near the exit. In addition the high-pressure gas system was arranged so that the gas could be used to warm the liquid. The pressure vessel, primary flowmeter, and test section were enclosed in a vacuum envelope to minimize heat leaks. Fluid pressures and temperatures were measured at appropriate points in the flow system, as indicated. The facility of reference 8 was also of this type. Individual components are discussed in detail later.

The general operation of the flow facility was as follows: After the pressure vessel was filled with liquid from the low-pressure supply, the liquid was warmed to the desired stagnation temperature by bubbling a warm gas of the same type through the liquid. Subsequently, the supply pressure was set by applying the pressurizing gas to the top of the liquid. The stagnation conditions were the pressure and temperature that existed in the inlet mixing chambers, as shown in figures 1 and 2. Flow was begun by fully opening the backpressure control valve. Once a steady flow was established, choking was demonstrated by varying the backpressure and observing that it did not change the flow rate or throat pressure. From here on the operation of the two test facilities differed, and this difference had a bearing on the results.

In the smaller, 110-liter, rig shown in figure 1 the procedure was to take discrete data points, normally only one for each fill of the pressure vessel with liquid nitrogen. The object was to maintain all the data points as close as possible to a predetermined stagnation isotherm T_o. In reality, since the system would normally drift steadily in temperature, several records of data would be taken for each fill and subsequent flow and then the record closest to the desired isotherm would be selected for data. Also the backpressure was regularly varied throughout the flow so that choking was established for every data point. This procedure produced close control; however, it was very time consuming and used large quantities of fluid.

The larger, 375-liter, system shown in figure 2 was operated differently. Once the steady flow and the choking phenomenon were established, a series of data points were recorded, each at a different stagnation pressure P_0. The stagnation pressure was normally varied from some high subcooled value down to near saturation for a single tankful. This was done by adjusting the control valve between the high-pressure tank and the test section. This procedure was much faster and more efficient in the use of fluid, but it did result in a wider tolerance on the nominal stagnation "isotherm" than the other procedure. This technique was absolutely essential for the hydrogen and methane data, where fluid cost was high and setup time was long. It also allowed data to be taken for many isotherms near the thermodynamic critical point with nitrogen in order to obtain detailed information on that region.

Test-Section Assemblies

In these experiments the four converging-diverging nozzle configurations were obtained by using three separate test sections. They are illustrated in figures 3 to 5. The essential dimensions of these test sections are listed in tables I to III. The fourth nozzle was obtained by flowing the conical nozzle (fig. 3) in both directions.

The test section illustrated in figure 3, as originally designed, had a truncated cone of nominally 7° half-angle convergence and a cone of nominally 3.5° half-angle divergence. It was designated the 7° conical nozzle. The throat region had a constant-area section 3.2 diameters in length. The transition from the converging cone to the constant-area throat section was smoothed with a radius of curvature of approximately 10 times the throat radius. The transition from the constant-area throat section to the diverging cone was a sharp corner. (With a 3.5° half-angle cone the term "sharp" can be questioned. It merely means that the cone was machined with a straight wall with no attempt to radius the transition to the constant-area section.) This sharp corner was designated the throat. The test section was instrumented with 15 pressure taps concentrated near the throat. Later in the testing this nozzle was turned around in the rig in order to assess the effect of the convergence angle and approach curvature on the pressure profile. In this orientation the nozzle was designated the 3.5° conical nozzle.

The test section illustrated in figure 4 was rectangular in cross section. The side walls were parallel. The convergence was effected by linearly tapering one wall at nominally 7°. The divergence was achieved by tapering the same wall at nominally 3°. The opposite wall was straight. The throat region had a constant-area section that was 8.3 times the throat height in length ($L/D = 4.15$). This constant-area throat section had a width-height ratio of 9.3. The transitions between sections were the same as for the conical nozzle. The straight wall, which could be considered as the imaginary centerline of a symmetrical nozzle, was instrumented with 12 pressure taps concentrated near the throat. At three key locations a pressure tap was located on the contoured wall opposite a straight-wall counterpart.

The test section illustrated in figure 5 was a conventional venturi flowmeter and was designed according to the ASME long-radius flow nozzle guidelines (ref. 21). Pressure taps were installed as illustrated. The converging section had a 2:1 elliptical curvature that transitioned smoothly into a constant-area section 2.1 diameters in length. The transition from the constant-area throat section to the 4° half-angle divergence cone was a sharp corner. This sharp corner was designated the throat. Table III gives two values for overall length. The smaller value, 6.80 centimeters, was the distance from the beginning of the elliptical converging section to the end of the 4° diverging section. The larger number was the distance from the inlet plenum to the beginning of the downstream straight section. The smaller dimension was probably more relevant, since this was really the nozzle shape under consideration. This nozzle was not as heavily instrumented in the throat region as the other two.

The dimensions listed in tables I to III were determined in two ways: They were measured mechanically in an inspection laboratory and were scaled from X-ray photographs of the test-section cross section. The tolerances represented discrepancies between these measurements. One additional measurement of importance was the alinement of the curved and straight walls in the constant-area section of the two-dimensional nozzle. From the various measurements we estimated that the misalinement in this area did not exceed 0.002 to 0.003 centimeter of the 0.109-centimeter height over the 0.905-centimeter length, a variation of 2 to 3 percent. Because of the very small divergence angle in all the test sections, the location of the exact point of divergence was very difficult to pinpoint, and the axial tap location tolerance was primarily an estimate of this difficulty.

All the nozzles were made of stainless steel with their internal surfaces finished to at least 16 rms. Care was taken to deburr all pressure taps.

In addition to the obvious geometric differences, the four nozzles can be compared in terms of convergence rates. Using the elliptical nozzle and taking the beginning of the ellipse as a reference, the ratio of entrance area to throat area was 14.3 and the nozzle converged to the beginning of the constant-area throat region in 0.751 centimeter. For the 7° conical nozzle, the convergence from the position where the area ratio was 14.3 to the beginning of the throat region required a distance of 4.14 centimeters. For the 3.5° conical nozzle, this distance was 7.48 centimeters. For the two-dimensional nozzle, this distance was 12.1 centimeters.

The inlet and outlet plenum mixing chambers for these test sections were an important part of the assembly. For the conical and two-dimensional nozzles they were identical and are shown in figure 6. The labyrinth path was designed to avoid any jetting into the nozzle entrance and to break up any stratification in the flow. The cross-sectional area of the innermost passage was 19 cm^2, as compared with approximately 6 cm^2 at the inlet of the conical and two-dimensional nozzles. The pressure and temperature measured in the inlet plenum were taken as stagnation conditions. The backpressure and temperature were measured in the outlet plenum. The elliptical nozzle had only an inlet plenum, and it was welded directly to the nozzle as shown in figure 7. The cross-sectional area of the stagnation chamber was 6 cm^2, as compared with 0.5 cm^2 at the nozzle inlet. There was a mixing chamber in the flow system downstream of the elliptical nozzle (cf. fig. 2) where the backpressure was measured. However, there was a length of straight pipe between the nozzle exit and this chamber.

Instrumentation

Pressure and temperature sensors. - The only physical measurements made in this experiment were pressure and temperature. Pressures were all measured with strain-gage transducers. In the 110-liter rig shown in figure 1 all the static pressures (except the static pressure at the downstream orifice) were measured on a matched set of 689-N/cm^2 (1000-psig) transducers rated at ±0.2 percent of full scale. The differential transducers and the transducer used to measure the downstream orifice static pressure were rated at ±0.3 percent of full scale. The transducers were calibrated in a standards laboratory and normally exceeded rated accuracy.

The fluid temperatures were measured throughout the flow system, as shown in figure 1, by use of platinum resistance thermometers. The thermometers and accompanying bridge circuits were calibrated in a standards laboratory and were considered accurate to ±0.1 percent of full scale (±0.1 kelvin). Two thermometers were located in each of the inlet and outlet mixing chambers.

In the 375-liter rig (fig. 2) a wider range of transducers was used to accommodate the wider range of the experiments undertaken therein. The same accuracy statements made for the 110-liter rig apply here also. In addition to platinum thermometers in key locations, as shown in figure 2, this rig also had Chromel-constantan thermocouples at various points. They are less accurate than the platinum thermometers and were used as backup measurements.

Flowmeters. - In the smaller rig the flow was measured in two locations, as shown in figure 1, by sharp-edged-orifice flowmeters. The primary flowmeter was located immediately upstream of the test section and metered liquid flow. Because of limited space a special orifice was built, as shown in figure 8. Because of the unusually short entrance region (L/D = 6) a special fitting that had the same configuration as the actual installation was made for use in calibration. The flowmeter was calibrated in a standards laboratory. According to the resulting calibration curve, flowmetering was considered accurate to within ±0.4-percent error. Most of the flow rates in the experiment were high enough to be in the extrapolated asymptotic region of the curve. A secondary or backup orifice flowmeter was located downstream of the test section and the heat exchanger, as shown in figure 1, and metered gas flow.

In the larger rig the flow was metered with a venturi located at the bottom of the dip tube in the high-pressure Dewar, as shown in figure 2. The venturi was approximately 4 meters ahead of the test section. It was a fairly conventional instrument and was calibrated in the same standards laboratory as the flowmeter for the smaller rig. It can be considered accurate to within ±0.3 percent error. This facility also employed an orifice flowmeter at the exit as a backup or secondary instrument.

Recording and monitoring. - All the data were recorded on a central data acquisition system known as CADDE II, which is described in reference 22. The system uses a solid-state scanner and a four-place integrating digital voltmeter coupled with a binary-coded decimal (BCD) encoding unit. It can sample up to 200 inputs at 1 to 40 signals per second, with 20 signals per second being the normal rate. These raw signals were available for immediate playback on a typewriter at the test facility. In addition, the signals were transmitted directly to a time-sharing computer for further processing at the test cell by means of a computer terminal link. Thus, such computed parameters as mass flow rate were rapidly available. The inputs are recorded as percentage of full scale over seven ranges from 10 millivolts to 10 volts. Each signal in succession can be recorded in one of these seven ranges. The overall recording system was rated accurate to within ±0.04-percent error or ±10 microvolts, whichever was more accurate. The signals necessary for control and monitoring of the test facility were isolated and amplified through high-impedance differential amplifiers and displayed on panel-mounted digital voltmeters.

Data Accuracy

Accuracy is as much a function of how an instrument is used as it is of its manufactured tolerance. For example, if a 690-N/cm^2 transducer is used to measure a 69-N/cm^2 pressure, the absolute error remains unchanged but the relative error increases by a factor of 10. Although this is obvious, it is often overlooked or reported inaccurately. Also some data, such as flow rate, involve the accuracy of both measured data and computed parameters such as fluid density. With these thoughts in mind, two accuracy estimates for each measurement taken in the two facilities (figs. 1 and 2) are listed in table IV. One is the absolute value based on the full range of the instruments used. The other, which is really more useful, is the percentage of error based on the average value over the actual range of the measurement.

The flow-rate measurement depends on the accuracy of computing properties - most importantly, density. The thermophysical properties were computed by using a computer subroutine called GASP, which is described by Hendricks, Baron, and Peller in reference 20. The main component of the program is an equation of state by Bender (ref. 23). Transport properties were refit by the authors of GASP. Bender (ref. 23) gives error estimates of ±0.26 percent for gas, ±0.18 percent for liquid, and ±1.47 percent in the critical region. (The critical region is defined by Bender as 0.66 ρ_c to 1.5 ρ_c, from the saturation locus to 1.25 T_c.) These error estimates in computing the density of the fluid were included in the error estimates for flow rate presented in table IV.

Because all the pressure readings on the smaller rig were taken on a matched set of 690-N/cm^2 transducers, it was possible to condition the data to improve internal consistency. At the beginning of each day's run the system was closed and pressurized to about midrange and a zero-flow pressure record was established. The relation of any individual transducer to the median was remarkably consistent over the many months of the experiment (e.g., transducer 5 was always 0.05 to 0.19 percent above the median). Because of this consistency the computer was programmed to adjust all static pressures by the percentage observed in the daily zero-flow readings. Although this did nothing to improve absolute accuracy, it did help to establish an internal consistency between the axial pressure profile measurements.

Finally, redundant instrumentation was used throughout both facilities. No critical measurements, such as stagnation pressure and temperature or mass flow rate, were made without a backup. Such system checks as flowing with gas and the no-flow check already mentioned were routinely performed.

RESULTS

Range of Experiments

These experiments investigated the two-phase choked flow of cryogenic fluids in four converging-diverging nozzles. Three separate fluids - nitrogen, methane, and hydrogen - were investigated. The hydrogen and methane data were obtained in the elliptical nozzle. Only nitrogen was investigated in all four nozzles. (The liquid-oxygen and -nitrogen data of ref. 8 were taken in the elliptical and the conical nozzles.) In all cases the initial conditions were single phase. A very extensive range of initial conditions was investigated. The entire investigation is summarized in table V. Throughout the experiments an attempt was made to acquire the data along lines of constant stagnation temperature T_O; thus, the data are organized along isotherms for presentation.

An interesting way to look at the experimental range is on a temperature-entropy diagram, as shown in figure 9. Since the process is frequently assumed to be isentropic, this sketch gives a good overview of the location of the stagnation conditions in relation to the two-phase locus. Figure 9 shows that the range of initial conditions extends from a "hard" liquid to a highly compressible fluid. However, the data are not uniformly distributed throughout the crosshatched region. For example, most of the data have an initial entropy that is less than the critical entropy. Only about 30 of the 545 data runs were at $S_o/S_c > 1.0$. Also only the nitrogen data extended to high temperature. The methane data were below $T_o/T_c = 1.05$ and the hydrogen data were below $T_o/T_c = 1.0$. Most of the data were choked in the two-phase region; however, some of the high-temperature nitrogen data were sufficiently compressible to choke in the single-phase region above the saturation locus. This is not to say, however, that none of the $S_o/S_c > 1.0$ data were two phase. In fact, 21 of these 30 data runs had throat pressures below the isentropic intercept with the saturation locus. In any case, the overwhelming majority of the data had stagnation conditions that fell into two categories: (1) those of a highly subcooled liquid and (2) those of a very dense but compressible fluid.

Data Tables

The data from these experiments are presented in tables VI to XIII, with a summary in table V. The data in these tables are described briefly here. The results are discussed in detail later. In all cases in these tables, the "throat" pressure used in the P_t/P_o column is the pressure read at the tap immediately upstream of the point of divergence.

The data of tables VI to VIII were all taken in the smaller rig (fig. 1) with nitrogen as the fluid. The emphasis was on acquiring data along specific isotherms within close tolerance. The five isotherms - 95, 110, 119, 124, and 130 K - were chosen to span the region from incompressible liquid to the highly compressible dense fluid near the thermodynamic critical region (126.3 K). The pressures ranged from just above saturation to twice the thermodynamic critical pressure. The two conical nozzles and the two-dimensional nozzle were employed. For the two-dimensional nozzle, pressures 1 to 12 were taken on the straight wall and 13 to 15 were taken on the contoured wall. Measurements 6 and 13, 8 and 14, and 9 and 15 were made directly opposite each other. Emphasis was placed on obtaining a comprehensive set of pressure profiles. For each data set, two readings were taken at two different backpressure levels to demonstrate choking. The reading included in the data tables was that closest to the isotherm. This explains the irregular pattern in the backpressure data. At the end of each of tables VI to VIII an ambient-temperature gas run is included for reference. For the data of table VII the 3.5^o conical nozzle was used (i.e., the 7^o conical nozzle installed backwards). This reversal of flow through the conical nozzle was performed to investigate the influence of the throat turning-radius on the pressure profiles.

Nitrogen data taken in the larger rig (fig. 2) with the elliptical nozzle are presented in table IX. The summary table (table V) shows that the special emphasis was on isotherms near the thermodynamic critical temperature (126.3 K). Also the pressure range was substantial, reaching to almost three times the thermodynamic critical pressure. In most instances the number of data runs per isotherm was not large; however, the isotherms were closely spaced.

Data for methane and hydrogen, also taken using the larger rig with the elliptical nozzle, are presented in tables X and XI, respectively. Because of the handling difficulties and the expense associated with these fuels, the data are somewhat more limited; nevertheless, a substantial range has been covered, especially for methane. The primary purpose of these data is to allow normalized comparisons on corresponding-states principles. The data for the three fluids presented herein, along with the oxygen data already reported (ref. 8), provide a good basis for such comparisons.

The data presented in tables XII and XIII were acquired in a different facility and are summarized in reference 5. Since they were never documented, they are included herein for convenience and completeness. They have two important features: Some of the points are very close to the thermodynamic critical point, probably closer than any other data in these experiments. Other points are very close to the saturation locus, again probably closer than any other data in these experiments. The experiment, however, was somewhat less precise than the others reported herein. For a description of the experiment, see reference 5.

Although it was standard practice with the conical and two-dimensional nozzles to establish choking for every run, it was not normal to obtain profiles over a wide range of choked and unchoked backpressures. Two such sets obtained with nitrogen and the 3.5° conical nozzle are presented in table XIV. A gas data set is included for reference. The data also offer some insight into system drift. There is a tendency for stagnation temperature to drift upward and, sometimes, for stagnation pressure to drift downward. The 1331-1334 set (table XIV) spanned 3.4 minutes.

Axial Pressure Profiles

In addition to the data tabulations, the data can be presented in certain graphical forms that are useful for analysis. Primary among them are the axial pressure profiles and plots of the flow rate and the ratio of throat to stagnation pressure as functions of stagnation conditions.

Axial pressure profiles for various conditions are plotted in figures 10 to 16. The first of these contains nitrogen gas data. Because the nozzles were of varying lengths and all had constant-area sections separating convergence from divergence, a special abscissa had to be invented to normalize the plots. The pressures in the converging and diverging sections are plotted as a function of area ratio A/A_t. The pressures in the constant-area section are plotted as a function of the fraction of that section where the pressure was measured X/L. (Note that the point of divergence, the nominal throat, is located at X/L = 1.) All the two-phase pressure profiles have one common characteristic, which is a function of the tendency of the system to drift upward in temperature during operation. From figure 9 it is clear that such a drift in stagnation temperature at constant stagnation pressure will increase the isentropic intersection with the saturation locus. Also, the increased average temperature will decrease average density. It is known that the saturation (vaporization) pressure is closely related to the throat pressure in two-phase choked flow. Thus, the combination of decreased pressure difference between stagnation and saturation, as well as decreased density, will cause a drift downward in flow rate as the stagnation temperature increases.

Flow Data Plots

The choked flow rates and the ratios of throat to stagnation pressure are plotted for each of the four nozzles in figures 17 to 24. Figures 17 and 18 present all the data from table VI for the 7° conical nozzle. Most of the data fall on the listed isotherm to within ±0.3 kelvin. The symbols for the data that fall outside this tolerance are tailed in the figures. If the tail is on the bottom of the symbol, the temperature is low, and conversely. Figures 19 and 20 present the data from table VIII for the two-dimensional nozzle. All the remarks made for figures 19 and 20 apply to these data as well. The isotherms for the two nozzles are quite close in value and thus should be good for comparisons. Figures 21 and 22 present the data from table VII for the 3.5° conical nozzle. Only two isotherms were run for this nozzle. Again, the same remarks concerning tolerances and plotting apply. In general, the conical-nozzle data have the closest temperature tolerance.

The data in figures 23 and 24 are for the elliptical nozzle and are drawn from two sources. They include the data of table IX, open symbols, and also the data of table XIII, solid symbols. There is some mismatch in the isotherms and the tolerances are greater; thus the stagnation temperatures shown on the figures should be treated as nominal and the tables should be consulted for specific detail. The one set was generally at low pressure, and the other was at high pressure. Both sets are needed to get a full picture of the performance of the nozzle.

DISCUSSION OF RESULTS

Choked Flow Rates and Pressure Ratios

The data for nitrogen taken in the four separate nozzle configurations and presented in figures 17 to 24 are summarized in figures 25 and 26. The isotherms selected for summary were ones where there was reasonable correspondence from nozzle to nozzle. (Only the 110 and 119 K isotherms include data from all four nozzles.) The lines faired through the data in figures 17 to 24 are reproduced in figures 25 and 26. The values of the isotherms are much more nominal in these figures, and they are used primarily for qualitative remarks. See figures 17 to 24 and the data tables for quantitative details.

Beginning with the flow-rate data (fig. 25), the first observation is that there is strong agreement between the data from the various nozzles in most regions of the experimental parameters. In general the flow-rate data from the two-dimensional nozzle fall a few percent below those from the 7^{o} conical nozzle, which in turn fall below those from the elliptical nozzle, over the whole range of the experiment. An exception occurs along the 124 and 130 K isotherms at the low-pressure end where the curves fold over. This small change in trend in these regions may reflect a greater sensitivity to geometry near the thermodynamic critical point, where density gradients are very steep. The biggest difference from nozzle to nozzle occurs at the low-pressure end of the 110 and 119 K isotherms. Here, in the most significant case, the difference in flow rate was as much as 34 percent between nozzles. This is also the region of greatest differences in the ratios of throat to stagnation pressure. This is discussed in conjunction with the axial pressure profiles in the next section.

The summary plots of the ratio of throat to stagnation pressure as a function of stagnation conditions (fig. 26) exhibit much less agreement from nozzle to nozzle. The question is whether this is a nozzle geometry effect, or whether it merely reflects the difference in the location of the nozzle "throat" pressure tap. The data appear to suggest both. For example, from the gas pressure profiles (fig. 10), the two-dimensional nozzle would be expected to read a higher "throat" pressure than the conical nozzle, but only by about 8 percent. At T_o = 130 K and P_o = 600 N/cm^2 this is true, with the difference being about 6 percent; however, at T_o = 95 K and P_o = 600 N/cm^2, the two-dimensional nozzle's throat pressure was almost 100 percent above that of the conical nozzle. It would appear that in this region the pressures are very sensitive to geometry.

Axial Pressure Profiles

Gas profiles. - Pressure profiles from the gas runs were normalized and are plotted in figure 10. In most of the cases shown, profiles for two separate backpressures are plotted. It is clear from the data of figure 10 that all four nozzles performed similarly in gas flows. The converging-region profiles are almost identical, even in the very sensitive throat region. They could all be readily choked. The measured flows all range from 96 to 98 percent of the computed isentropic expansion.

On the other hand, there are small differences and deviations that should be noted to aid interpretation of the data. For example, although there was good overall profile agreement, there were differences in the "throat" pressures from nozzle to nozzle. The throat pressure measured in the 7° conical nozzle was in perfect agreement with the calculated throat pressure. However, this pressure tap was 0.185 centimeter ahead of the point of divergence, which was designated as the throat. Thus, it could be reading a little low, or the throat location could be slightly in error. Actually, extrapolations of the "throat" pressure readings of the 3.5° conical nozzle and the two-dimensional nozzle to the point of divergence are closer to the computed value. Although these differences are small, they should be considered when evaluating the choked-flow pressure ratio data.

The gas profiles serve as a convenient reference for discussing the two-phase-choked-flow data. If the flow were ideal, there would be no pressure drop in the constant-area flow region. However, despite only a 3 to 4 percent deviation from ideal flow, all the nozzles show strong linear pressure drops in this region, roughly 10 percent of the total. The pressure profiles in the constant-area region for the 7°, rounded-entrance and the 3.5°, sharp-corner-entrance conical nozzle geometries are nearly parallel. This suggests that the strong pressure drop was not the result of some small geometric differences from nozzle to nozzle but was, in fact, phenomenological. Computing the friction in the entrance of a tube for the conditions of figure 10 indicates a friction pressure drop of about 8 N/cm^2, or about 2 percent of the total nozzle pressure drop. If it were assumed that the 3- to 4-percent flow deviation from ideal was due to the area change from this same boundary-layer growth, the required 3- to 4-percent area change would produce a 6- to 8-percent pressure drop. Thus, a friction boundary layer in the throat that was only 1.5 to 2.0 percent of the throat radius could produce pressure drops of the order shown in figure 10.

In summary, the gas profiles show that a small constant-area section of 2- to 4-L/D length in the throat region of a converging-diverging nozzle produces a strong pressure gradient. However, the two-phase situation is much more complex.

Two-phase profiles. - With the gas behavior as background, the pressure profiles associated with the two-phase choked flow of subcooled nitrogen can be examined. The first subject of interest from the two-phase profiles is the nature of the choking phenomenon. This can be described by reference to a series of axial pressure profiles in which the flow was both choked and unchoked. Such a series was obtained for the 3.5° conical nozzle (fig. 11). The distinguishing feature of the data in figure 11(a) is that the stagnation pressure is substantially above the saturation pressure. The average values of both the isothermal and isentropic saturation pressures are indicated in figure 11(a). A band is shown because these values drift with stagnation temperature. See the appendix for further discussion of the saturation pressures.

The profiles in figure 11(a) are all remarkably similar up to the diverging end of the constant-area throat section. Since P_o was the same for all readings, the mass flux data G (see fig. 11(a) key) indicate that the first two profiles (readings 1331 and 1332) are unchoked. Also, they are probably for an all-liquid phase since the lowest pressure is 40 N/cm^2 above saturation. The profiles for readings 1333 and 1334 appear to be choked. (The small difference in G is the drift previously discussed.) The pressure drops in the constant-area region were very similar in all four cases. This led to the conclusion that the flow was dominated by liquid to the exit end of the constant-area region.

The profiles in figure 11(b) present a different picture. They are characterized by the stagnation pressure being close to saturation. The profile for the first reading (1350) is very similar to the profiles in figure 11(a). Depending on which thermodynamic path was selected, the constant-area throat pressures were either slightly above or slightly below the saturation pressure. The flow was not choked. The remaining four profiles are clearly different, and in every case the pressures in the constant-area region were clearly below saturation regardless of the thermodynamic path. A profile for nitrogen gas (reading 1344) is also shown in figure 11(b). In the constant-area region the gas pressure distribution was very similar to that for the four two-phase profiles (1351 to 1354). This profile similarity certainly seems to imply that vapor dominated the constant-area region for all these nozzle profiles except the first reading (1350).

The combination of the data shown in figures 11(a) and (b) strongly implies (1) that for P_o near $P_{sat}(S_o)$ the profiles show a fairly steep pressure drop in the constant-area region and reflect a vapor-dominated flow; and (2) that for P_o well above $P_{sat}(S_o)$ the profiles have a very strong initial gradient dP/dx and then almost level off in the constant-area region and appear to reflect a liquid-dominated flow to the point of divergence.

The three profiles in figure 12 give us a little closer look at the effect of subcooling. They are axial pressure profiles for a range of stagnation pressures from slightly above saturation to three times the saturation pressure. In the first case (triangles), the flow expanded below the saturation pressure well upstream of the throat; in the second case (squares), the saturation pressure appeared to occur right at the entrance to the throat region. In both cases the pressure drop in the constant-area (throat) region is similar to the gas profiles. This would suggest that vaporization occurred at, or upstream of, the throat and that vapor was present and dominant in the constant-area region. In the final case (circles), the isentropic saturation pressure coincided with the pressure at the last two taps in the throat. The shape of the profile and the fact that all pressures were above saturation strongly suggest that the flow was liquid dominated to the exit of the throat region and that any vapor was present in very small quantities.

Another way of looking at the pressure is in terms of what the pressure would ideally be if there were no vapor present (i. e., all-liquid flow). For the measured G, a pressure was computed that would produce that mass flux if the flow were all liquid. The points are shown in figure 12. In each case this computed pressure was very close to the pressure measured at the entrance to the constant-area region and substantially above the value nominally designated as the throat pressure. In the two cases where vapor was clearly present (readings 1546 and 1531), this is not too surprising; but in the case where liquid appeared to dominate the flow (reading 1584) something, either a vena contracta or a small amount of vapor, must be constricting the flow.

Another point of interest is the shape of the profiles in the diffuser, particularly in the first two cases (readings 1546 and 1531). Further downstream the profiles are virtually identical; however, just downstream of the throat there are substantial differences. This could represent separation or it could be the result of some nonequilibrium behavior.

As has been pointed out, so that we could explore questions of nozzle geometry, the 7° conical nozzle was turned around and installed in reverse to its normal flow direction, forming the 3.5° conical nozzle (cf. fig. 3). The difference between the two nozzle configurations was small. One nozzle had a 7° convergence with a rounded throat entrance and a sharp divergence at 3.5°. The other nozzle was the reverse of this. At these small angles, the difference between "sharp" and "rounded" is more a matter of specification on a drawing than it is a fact. Thus, we are talking about the effect of small differences. Selected isotherms were repeated. Profiles from two of these cases are shown in figures 13 and 14. In both cases the data are characterized by very close control on the stagnation parameters.

In the first case (fig. 13) the profiles and flow rates for the two flow directions are very similar. The small differences may be significant in terms of mechanism, but they make little difference in the results. On the other hand, at stagnation conditions closer to saturation the two nozzle configurations produced a substantial shift in the pressure profiles and a 10-percent difference in flow rate. Thus, it would appear that, if the potential for vaporization is present (such as in fig. 14 with a relatively high saturation pressure), the small differences in nozzle configuration can be significant. In the more highly subcooled case (fig. 13), the differences are less significant, at least in their effect on the flow rate.

The same phenomena appear when all the nozzle profiles are compared in a single plot, such as shown in figures 15(a) and (b). In figure 15(a), for example, with highly subcooled conditions the pressure profile in the constant-area (throat) region varies in shape from nozzle to nozzle; however, the resulting "throat" pressure and flow rate are not significantly affected. On the other hand, when the saturation pressure is higher, as in figure 15(b), the pressure profiles are even more varied and the influence on "throat" pressure and flow rate is strong. These variations in sensitivity have already been pointed out in the overall summary in figures 25(a) and 26(a).

Before we leave this subject, one final point - drawn from figures 11 to 15 - is in order. The term "throat" has become very imprecise for these flows. Recall from the test-section descriptions that the constant-area regions were introduced to ensure a pressure tap at the throat. It was initially expected that very little vapor would exist upstream of the point of nozzle divergence; consequently, negligible pressure drop was expected in the constant-area region. The data show this to be true only in the highly subcooled case; but, as P_o approached $P_{sat}(S_o)$, the small 2- to 4-L/D constant-area section played a role in the pressure drop. The point of vaporization, the amount of vapor, and the location of the "throat" all seem to depend on relative subcooling. This makes consistent reporting difficult and offers a complex challenge to analytical modeling.

The effect of varying stagnation temperature on the pressure profiles in the two-dimensional nozzle is shown in figure 16. For this plot the pressure difference $P_o - P_{sat}(S_o)$ was held roughly constant; thus, the flow was initiated at roughly the same distance from the saturation locus for each case. The first and most obvious observation is that the shift in the profiles follows the trend in the saturation pressures. This would suggest that perhaps the flow could be predicted if the isentropic saturation pressure were known. Although in a gross sense this is probably true, a close examination reveals that it is not quite so simple. If the pressure data in the constant-area throat are linearly extrapolated to the point of divergence ($X/L = 1$), the trend is not consistent with respect to $P_{sat}(S_o)$. For the three highest temperature isotherms this extrapolated pressure is below $P_{sat}(S_o)$. For the 109.8 K isotherm it almost coincides with $P_{sat}(S_o)$. And for the lowest temperature isotherm, 95.8 K, the extrapolated pressure is above $P_{sat}(S_o)$. Thus, in terms of modeling, the isentropic pressure is not a simple barometer of the flow characteristics.

Another interesting observation from figure 16 is that the profile for the 129.9 K isotherm, which is greater than $T_c = 126.3$ K, has the same shape in the converging region and the throat area as the other four isotherms. This suggests that the expansion was isentropic or nearly isentropic (definitely not isothermal). The initial entropy for this case was $S_o/S_c = 0.833$; and thus, like the other isotherms in figure 16, the expansion was through the liquid locus into the two-phase region.

The pressure profiles from the two-dimensional nozzle also offer some insight into the validity of a one-dimensional flow model. Figure 4 and table II show that the two-dimensional nozzle was really a half nozzle with one wall straight and one wall contoured. Most of the pressure taps were on the straight wall but at three locations: one just upstream of, one in, and one just downstream of the constant-area throat region. Pressure taps were placed in the contoured wall, nominally opposite its straight-wall counterpart (cf. table II). At the upstream location the contoured-wall pressure was consistently 2 to 6 N/cm^2 higher than the straight-wall pressure; however, it was measured slightly farther upstream. In the constant-area region the nominal "throat" tap frequently read the same as its contoured-wall counterpart. Occasionally, the contoured-wall pressure was 1 to 3 N/cm^2 higher. In this case, however, the contoured-wall tap was slightly farther downstream. Just downstream, the pressures were virtually identical again, with the contoured-wall pressure occasionally slightly higher, at 1 to 2 N/cm^2. In this case, the contoured-wall tap was slightly upstream, and again position alone could account for these small differences. Also remember that the error band on the pressure transducers was ±1.4 N/cm^2. The evidence in these pressure profiles testifies strongly to the validity of one-dimensional modeling.

On the other hand, in the two-dimensional nozzle there were no precipitous pressure drops coming into the constant-area region, such as observed in the conical nozzle at high subcooling. Thus, it is possible that separation at the inlet (i.e., two-dimensional effects) could be occurring in one nozzle and not the other. This would indicate an extreme sensitivity to small machining differences since both nozzles converged and diverged at the same angles.

Throat Pressure Anomaly

Returning to the summaries of the ratios of throat to stagnation pressure (fig. 26), we observe an anomalous flat region, particularly along the 110 and 119 K isotherms. As is shown in the next section, the commonly used theories do not describe this flat region. This presents problem to the analyst. Although the effect was most prominent in the conical nozzle, it appears in the data of all the nozzles.

Presenting the "throat" pressure data in the manner of figure 26, although it is based on a long-standing tradition, tends to mask the trend since P_o appears in both the ordinate and the abscissa. Figure 27 is a plot of "throat" pressure as a function of stagnation pressure for the conical nozzle in the reversed-flow orientation along the 119.3 K isotherm. This nozzle and isotherm were chosen because the data exhibit the trend well and the isotherm was in extraordinarily close tolerance, with all points being within 0.2 kelvin of 119.3 K. The variation of the isentropic saturation pressure with stagnation pressure was plotted for reference. The isothermal saturation pressure was also marked. Beginning at the low-pressure end (the first stagnation data point is only 6 N/cm^2 above saturation), the "throat" pressure decreased to a minimum at around $P_o = 305\ N/cm^2$ and then increased steadily until at high stagnation pressure it began to merge along the isentropic saturation pressure locus.

In figure 28, data for the 7^o conical nozzle are added to those for the 3.5^o conical nozzle. The isothermal tolerance had to be increased to ±0.3 kelvin in order to get enough data points. The general trend for the 3.5° nozzle was strongly reinforced, although the minimum point shifted slightly to $P_0 = 330\ N/cm^2$. This could be related to a small difference in the physical location of the "throat" pressure tap (-0.185 cm in the 7° nozzle and -0.083 cm in the 3.5° nozzle).

A careful study of the axial pressure profiles (tables VI(c) and VII(b)) in the manner of figure 12 revealed that the pressure profiles underwent changes in shape, especially in the constant-area region. These shape changes corresponded to the slope changes in "throat" pressure in figure 28.

Data points from the two-dimensional and elliptical nozzles that fall within the isothermal tolerance of ±0.3 kelvin are added in figure 29. Although these points tend to support the overall trend, the variance from the conical-nozzle data would weaken any phenomenological conclusions we might draw, especially with regard to the location of the minimum and the correspondence to the isentropic saturation pressure. Nevertheless, the general trend does appear to be phenomenological and presents real problems for any predictive models.

Comparison of Theory with Data

The theoretical models for two-phase choked flow in most common use today are the homogeneous equilibrium model and a nonequilibrium model developed by Henry and Fauske (ref. 17). The isentropic, homogeneous equilibrium expansion is really rather basic fluid mechanics and thermodynamics and is rarely given authorship today. The equations as they apply to the two-phase choked flow of cryogenic fluids were presented some time ago by the authors in reference 6. They are summarized in the appendix. The model of Henry and Fauske (ref. 17) is particularly popular because, since it was developed as a departure from equilibrium, equilibrium calculations can be used as a base. For comparison with the data herein the Henry-Fauske calculation was modified to have an isentropic path in the single-phase part of the expansion from stagnation to saturation. Thus, the saturation pressure corresponds to the stagnation entropy S_0. This is also discussed in the appendix.

The flow-rate summaries of figure 25 are compared with the two theories in figure 30. The mean lines of the data from the four nozzle configurations fall in the cross-hatched bands shown in figure 30. Part of the spread is due to variations in geometry and part is due to slight differences in stagnation temperature from nozzle to nozzle. The calculations were carried out along stagnation isotherms, as indicated in figure 30. Detailed comparisons are not warranted herein but can be made by going to figures 17, 19, 21, and 23.

The first, and most important, observation from the data is that the modified Henry-Fauske model correlates all the flow-rate data herein to within ±10 percent.

However, keeping in mind that in general the flow-rate data are well correlated, there are two very obvious deviations. First, the theory appears to consistently overpredict at high stagnation pressures (i.e., high subcooling). Second, the data and theory slopes are slightly different. The flow discrepancy can be at least partially accounted for in the nonideal nature of the nozzles. Recall that the ratios of the measured to ideal gas flow for the conical and two-dimensional nozzles were 0.96 to 0.97 (cf. fig. 10). At $P_0 = 650\ N/cm^2$, for example, the theory overpredicts the average of the data by a consistent 7 percent. Thus, if the nonideal correction were applied to the theory, the correlation would be quite accurate. This type of calibration, of course, does not identify the source of the departure from ideal one-dimensional flow; it merely quantifies it. For the nozzles in question the most likely candidate is a small boundary-layer buildup in the constant-area region. Another possibility would be a poor radius entering the constant-area region. It has also been pointed out that it is not clear where vaporization begins. Thus, taking the flow into account, both theories predict the high-stagnation-pressure (i.e., high subcooling) data quite well.

The slope difference is a little more complex. Let us examine first the 95 K isotherm. The modified Henry-Fauske nonequilibrium model consistently overpredicts the data by about 7 percent over the whole isotherm; thus, it predicts very well over the whole isotherm when the flow coefficient is considered. The equilibrium model does not do this. It substantially underpredicts as P_0 approaches $P_{sat}(S_0)$. This is discussed more later. When the throat-pressure anomaly appears, such as along the 119.5 K isotherm, the slope change is no longer explainable in terms of flow coefficient, and both models begins to underpredict. As discussed earlier this seems to be a physical phenomenon in the flow, and it is clear from the data trends that neither model comprehends it.

We see from figure 30 that the two models run parallel and only a couple percent apart at high P_0. Then, as the stagnation pressure decreases, they begin to diverge until, as P_0 approaches $P_{sat}(S_0)$, the equilibrium prediction may be 50 percent below the nonequilibrium. This deviation tends to be greater along the lower temperature isotherms, where the single-phase fluid is nearly incompressible. As T_0 increases toward the thermodynamic critical temperature the two models tend to come closer until, along the 130 K isotherm, they have almost completely converged. In fact, at this point the equilibrium model is more accurate, as shown in the following discussion on pressure. The nonequilibrium model of Henry and Fauske really only makes sense for $S_0 < S_c$, and thus is restricted accordingly.

The ability of the theoretical models to predict ratios of throat to stagnation pressure (fig. 31) is much less impressive. First, of course, the data themselves show a much wider variation from nozzle to nozzle. Part of this is the result of the "throat" pressure-tap location being slightly different for each nozzle, as discussed earlier. More likely though, it reflects a sensitivity to geometry. The one-dimensional analyses, however, make no recognition of geometry and thus cannot account for these variations. This is especially true in the anomalous flat regions most prominent along the 110.0 and 119.5 K isotherms. Although the analytical models cannot be expected to reflect geometry variations, they should show proper trends. Both models substantially overpredict pressure ratios near saturation. At low stagnation pressures the fluid passes through the saturation pressure substantially farther upstream than the models predict.

An exception to all this is the prediction by the homogeneous equilibrium model along the 130.0 K isotherm. The prediction of flow rate and pressure ratio is excellent. The peak in the pressure ratio corresponds to the point where the throat pressure begins to be less than the saturation pressure. Where P_t/P_o peaks, the computed throat pressure is the saturation pressure. In the stagnation pressure region above the point where P_t/P_o peaks, the volumetric expansion due to vaporization is so great that it chokes immediately. Colins (ref. 16) refers to this as "discontinuous choking." In the stagnation pressure region below the point where P_t/P_o peaks, the pressure at the throat is predicted to be below saturation. The data agree well with this prediction. If the calculation is continued, the sharp change occurs as S_o passes through S_c and the expansion begins to pass through the vapor locus rather than the liquid locus. Finally, the calculation converges to a single-phase choking and the expected $P_t/P_o = 0.53$ for gaseous nitrogen (i.e., a diatomic ideal gas).

In general, there are few data to verify these trends; however, a couple of data points from the two-dimensional nozzle tend to support them. The first four runs in table VII(e) have entropies in excess of the critical entropy, and the pressure ratio is dropping in the manner predicted by the homogeneous theory. The other isotherms computed by the equilibrium model also show the peak, but none of the data along those isotherms support it.

In general, on the liquid side ($S_o < S_c$) the nonequilibrium model of Henry and Fauske (ref. 17), as modified herein, is more reliable than the equilibrium model for stagnation temperatures below the thermodynamic critical temperature, especially near the saturation locus. For temperatures at or above T_c the homogeneous equilibrium model is preferred. For $S_o > S_c$, only the homogeneous equilibrium model is applicable.

Data Normalization by Corresponding-States Principle

In addition to the extensive investigation of nitrogen, methane and hydrogen were also explored by using the elliptical nozzle in the larger rig (fig. 2). One reason for doing this was to see if the principle of corresponding states could be applied to choking flow. Basically, the principle of corresponding states says that a given thermophysical property of various fluids can be generalized onto a single curve through normalization by the appropriate critical constants of the fluid. Although this is a well-established principle for static equilibrium properties, it has not been used for the correlation of dynamic flow parameters. The choice of fluids was based on an interest in handling hydrogen and methane (or liquified natural gas) as liquids and on a unique capability for handling such fuels that existed in the larger rig.

It was fairly straightforward to derive a flow normalization parameter (ref. 18)

$$G^* = \sqrt{\frac{\rho_c P_c}{Z_c}}$$

However, it was quite difficult to obtain data over a wide range in all three fluids along lines of constant reduced temperature T_o/T_c. A feel for the problem can be obtained by examining the range of critical parameters in table XV. It simply was not possible to obtain fine control over this whole range in a single facility.

The data that best met constant reduced isotherms were selected from tables IX to XI and are plotted for reduced choked flow rate in figure 32 and for ratios of throat to stagnation pressure in figure 33. Three symbols were used to identify T_o/T_c levels, and three shadings to represent the various fluids. Although the data are limited, the results in figures 32 and 33 appear to justify the application of the corresponding-states principle to two-phase choked flow. Data over a very wide area are brought tightly together on a single plot. To appreciate the extent to which the flow-rate curves have been collapsed, we must examine the critical constants in table XV. For the three fluids, G^* varies by a factor of 5. Most of the deviations can be explained in terms of stagnation temperature deviations from the nominal isotherm. The G^* normalization appears to be correct.

In separate papers (refs. 18 and 19) all the data of tables IX to XI were smoothed, crossplotted, and compared with the homogeneous equilibrium analysis for a more complete study. This study supported these results more completely. Subsequent work in another facility with oxygen and nitrogen (ref. 8) mapped a wide range with very close control and established the principle convincingly. In the case of hydrogen, because of its quantum nature, the normalization parameters for corresponding states are different, and G^* must be modified to include a function that covers the full temperature range (ref. 19). The essential message herein is that corresponding-states normalization works for two-phase choked flow.

SUMMARY OF RESULTS

Experiments were conducted to investigate two-phase choked flow of subcooled cryogens in four converging-diverging nozzles using three separate fluids. There were three axisymmetric nozzles: one with a 7° half-angle conical convergence, one with a 3.5° half-angle conical convergence, and one with a 2:1 elliptical convergence. The fourth nozzle was two dimensional with a 7° convergence. The primary fluid investigated was nitrogen. The other two fluids were methane and hydrogen.

Data were acquired over a range of stagnation conditions:

(1) $0.65 < T_o/T_c < 1.40$

(2) $0.20 < P_o/P_c < 2.80$ (4.50 for hydrogen)

(3) $0.30 < S_o/S_c < 1.45$

where T_o, P_o, and S_o are the temperature, pressure, and entropy at stagnation conditions and T_c, P_c, and S_c are these measurements at thermodynamic critical conditions. The data were not uniformly distributed over these ranges. In general, the stagnation conditions can be classified into one of two categories: (1) a highly subcooled liquid or (2) a very dense but compressible fluid. In almost every case the throat conditions were two phase. For the most part, data were acquired parametrically along lines of constant stagnation temperature.

The report includes tabulations and selected plots of data from 545 separate runs over these ranges. The primary data acquired were the choked-flow rates and the accompanying nozzle pressure profiles.

The major results of the data are as follows:

1. Along a given stagnation isotherm the choked flow rates were not strongly variant from nozzle to nozzle. On the other hand, the ratio of throat to stagnation pressure was very sensitive to nozzle geometry.

2. The axial pressure profiles of the various nozzles indicate that the pressure at which vaporization occurred was very sensitive to geometry and initial conditions.

3. The variation in throat pressure as a function of stagnation pressure along a given isotherm was not monotonic. At low, near saturation, stagnation pressures the throat pressure decreased as stagnation pressure increased. At intermediate stagnation pressures the throat pressure increased with stagnation pressure, yielding an almost constant ratio of throat to stagnation pressure. Finally, at high stagnation pressures the throat pressure was relatively constant near the isentropic saturation value.

4. A modified Henry-Fauske nonequilibrium model correlated all the choked-flow-rate data to within ±10 percent and is recommended for $T_o < T_c$. Homogeneous equilibrium calculations were more accurate above the thermodynamic critical temperature and are recommended for that region. No model did a particularly good job of predicting throat pressure over the whole range of the experiment; however, the equilibrium model was very good above the thermodynamic critical temperature.

5. The flow-rate and pressure-ratio data for the three fluids investigated - nitrogen, methane, and hydrogen - could be normalized to universal curves by the thermodynamic critical constants in accordance with the principle of corresponding states.

Lewis Research Center,
National Aeronautics and Space Administration,
Cleveland, Ohio, January 4, 1979,
506-21.

APPENDIX - HOMOGENEOUS TWO-PHASE-CHOKED-FLOW EQUATIONS

The basic equations for two-phase choked flow in a nozzle are quite straightforward. They are summarized here for the convenience of the reader. The equations presented are for homogeneous one-dimensional flow. Simply, this means that the flow is uniform across the nozzle cross-section and that both phases are traveling at the same velocity. The equations are more frequently derived without the latter assumption, allowing each phase to have a different velocity; however, this makes the presentation more complex and, in practice, the velocities are assumed to be equal anyhow. Since this was the case in the present work, the two velocities are assumed to be equal at the outset and are denoted by u. Friction is neglected because of the high acceleration that occurs in a nozzle.

Under these assumptions the one-dimensional momentum equation in the absence of friction is

$$-A\ dP = d\left[u(W_g + W_l)\right] \tag{A1}$$

With the definition for mass flux

$$G = \frac{W}{A} \tag{A2}$$

and with the one-dimensional continuity equation

$$W = W_g + W_l = \text{Constant} \tag{A3}$$

equation (A1) becomes

$$-\frac{1}{G} = \frac{du}{dP} \tag{A4}$$

To express u in terms of measurable quantities, we introduce the concept of quality (fluid vapor fraction).

$$x = \frac{W_g}{W} \tag{A5}$$

where

$$W_g = \frac{uA_g}{v_g} \tag{A6}$$

and manipulate

$$xGv_g = u\left(\frac{A_g}{A}\right)$$

$$= u\left(1 - \frac{A_l}{A}\right)$$

$$= u\left(1 - \frac{W_l v_l}{uA}\right)$$

$$= u\left\{1 - \left[\frac{(1 - x)Wv_l}{uA}\right]\right\}$$

$$= u - (1 - x)v_l G$$

Thus

$$u = G\left[xv_g + (1 - x)v_l\right] \tag{A7}$$

The term in brackets on the right side of the equation is recognized as the definition of the two-phase specific volume

$$v = xv_g + (1 - x)v_l \tag{A8}$$

After this definition of the two-phase specific volume is substituted into equation (A7), the momentum equation (A4) becomes

$$-1 = G\frac{d(vG)}{dP} \tag{A9}$$

Multiplying by v gives

$$-v = vG \frac{d(vG)}{dP}$$

or

$$-v = \frac{1}{2} \frac{d(vG)^2}{dP} \tag{A10}$$

Equation (A10) can then be integrated, subject to the condition that $G = 0$ when $P = P_o$, as

$$G^2 = -\frac{2}{v^2} \int_{P_o}^{P} v \, dP \tag{A11}$$

Carrying out the differentiation in equation (A9) yields

$$-1 = G \left[v \frac{dG}{dP} + G \frac{dv}{dP} \right] \tag{A12}$$

The choked-flow criterion is

$$\left. \frac{dG}{dP} \right]_t = 0 \tag{A13}$$

Thus, equation (A12) at the point of choking becomes

$$G_{max}^2 = - \left. \frac{dv}{dP} \right]_t^{-1} \tag{A14}$$

By using the definition (A8), equation (A14) can be written as

$$G_{max}^2 = - \left[x \frac{dv_g}{dP} + (1 - x) \frac{dv_l}{dP} + (v_g - v_l) \frac{dx}{dP} \right]_t^{-1} \tag{A15}$$

Either equation (A14) or equation (A15) can be solved, together with equation (A11), to determine the choked flow rate and the choking pressure.

The specific volume is, of course, a function of two variables, so a path must be determined. For a nozzle an isentropic path is an appropriate choice. As with specific volume, the entropy for a two-phase medium is defined as a percentage contribution from the liquid component and the vapor component:

$$S = xS_g + (1 - x)S_l = \text{Constant} = S_o \tag{A16}$$

Since the entropy is constant, equation (A16) defines the quality as long as the system is in thermodynamic equilibrium.

The model of Henry and Fauske (ref. 17) proposes a departure from thermodynamic equilibrium that they feel is consistent with the observations made in various two-phase-choked-flow experiments. The basic equations, (A11) and (A14), remain valid. The modifications are in the definitions of the specific volume, equation (A8), and the volume derivative, equation (A15). The basic statement is that there is insufficient time for any significant change in quality during the acceleration to the throat; however, the rate of quality change would still be significant. Thus, the quality is assumed to be constant at the stagnation value, and equation (A8) becomes

$$v = x_o v_g + (1 - x_o)v_l \tag{A17}$$

and for the present case of subcooled, liquid inlet-stagnation conditions this reduces to

$$v = v_l \tag{A18}$$

Henry and Fauske also assumed $dv_l/dP \approx 0$ and proposed that the nonequilibrium derivative of the quality could be related to equilibrium by

$$\left.\frac{dx}{dP}\right]_t = N \left.\frac{dx}{dP}\right]_t \tag{A19}$$

where

$$N = \begin{cases} \dfrac{x_e}{0.14} & \text{for } x_e < 0.14 \\ 1.0 & \text{for } x_e \geq 0.14 \end{cases}$$

Thus, equation (A15) becomes

$$G_{max}^2 = -\left[x_o \frac{dv_g}{dP} + (v_g - v_l)N \frac{dx_e}{dP}\right]_t^{-1} \tag{A20}$$

which for subcooled inlets reduces to

$$G_{max}^2 = -\left[(v_g - v_l)N \frac{dx_e}{dP}\right]_t^{-1} \tag{A21}$$

As a computational convenience, Henry and Fauske (ref. 17) differentiated equation (A16) and used the subcooled-inlet condition to express equation (A21) in the following entropy terms:

$$G_{max}^2 = -\left[\frac{N(v_g - v_l)}{(S_g - S_l)} \frac{dS_l}{dP}\right]_t^{-1} \tag{A22}$$

where S_g and S_l were assumed to be at the saturation conditions corresponding to T_o. For the present work the stagnation conditions were frequently too far from the saturation locus to allow that assumption, so the Henry-Fauske program was modified to compute v_l, S_g, and S_l at the saturation pressure corresponding to an isentropic expansion from the stagnation conditions to the saturation locus. This is designated $P_{sat}(S_o)$. For the convenience of the reader and to point out the differences, both $P_{sat}(S_o)$ and $P_{sat}(T_o)$ are included in the data tables. Because of this modification, we refer to the model as the modified Henry-Fauske model.

REFERENCES

1. Hsu, Y. Y.: Review of Critical Flow Rate, Propagation of Pressure Pulse, and Sonic Velocity in Two-Phase Media. NASA TN D-6814, 1972.
2. Henry, R. E.; Grolmes, M. A.; and Fauske, H. K.: Pressure Drop and Compressible Flow of Cryogenic Liquid-Vapor Mixtures. Heat Transfer at Low Temperatures, W. Frost, ed., Plenum Press, 1975, pp. 229-259.
3. Smith, R. V.; Randall, K. R.; and Epp, R.: Critical Two-Phase Flow for Cryogenic Fluids. (NBS TN-633, National Bureau Standards; NASA Order W-13300.) NASA CR-130793, 1973.
4. Lahey, R. T., Jr.; and Wallis, G. B., eds.: Nonequilibrium Two-Phase Flows, American Society of Mechanical Engineers, 1975.
5. Simoneau, R. J.; et al.: Two-Phase Critical Discharge of Liquid Nitrogen. Progress in Refrigeration Science and Technology, Proceedings of the 13th International Congress of Refrigeration. Vol. 1, International Institute of Refrigeration by Avi. Publ. Co., Inc., 1973, pp. 293-297.
6. Hendricks, R. C.; Simoneau, R. J.; and Ehlers, R. C.: Choked Flow of Fluid Nitrogen with Emphasis on the Thermodynamic Critical Region. Advances in Cryogenic Engineering, Vol. 18, K. D. Timmerhaus, ed., Plenum Press, 1973, pp. 150-161.
7. Simoneau, R. J.: Pressure Distribution in a Converging-Diverging Nozzle During Two-Phase Choked Flow of Subcooled Nitrogen. Nonequilibrium Two-Phase Flows, R. T. Lahey, Jr., and G. B. Wallis, eds., American Society of Mechanical Engineers, 1975, pp. 37-45.
8. Hendricks, R. C.; Simoneau, R. J.; and Barrows, R. F.: Two-Phase Choked Flow of Subcooled Oxygen and Nitrogen. NASA TN D-8149, 1976.
9. Hendricks, R. C.; Simoneau, R. J.; and Hsu, Y. Y.: A Visual Study of Radial Inward Choked Flow of Liquid Nitrogen. Advances in Cryogenic Engineering, Vol. 20. K. D. Timmerhaus, ed., Plenum Press, 1975, pp. 370-382.
10. Simoneau, R. J.: Two-Phase Choked Flow of Subcooled Nitrogen Through a Slit. Proceedings of the Tenth Southeastern Seminar on Thermal Sciences, R. G. Watts and H. H. Sogin, eds., Tulane Univ., 1974, pp. 225-238.
11. Simoneau, R. J.: Maximum Two-Phase Flow Rates of Subcooled Nitrogen Through a Sharp-Edged Orifice. Advances in Cryogenic Engineering, Vol. 21. K. D. Timmerhaus and D. H. Weitzel, eds., Plenum Press, 1975, pp. 299-306.

12. Hendricks, R. C.; and Simoneau, R. J.: Two-Phase Choked Flow in Tubes with Very Large L/D. Advances in Cryogenic Engineering, Vol. 23. K. D. Timmerhaus, ed., Plenum Press, 1978, pp. 265-275.

13. Sozzi, G. L.; and Sutherland, W. A.: Critical Flow of Saturated and Subcooled Water at High Pressure. Nonequilibrium Two-Phase Flows, R. T. Lahey, Jr., and G. B. Wallis, eds., American Society of Mechanical Engineers, 1975, pp. 19-25.

14. Schrock, V. E.; Starkman, E. S.; and Brown, R. A.: Flashing Flow of Initially Subcooled Water in Convergent-Divergent Nozzles. J. Heat Transfer, vol. 99, no. 2, May 1977, pp. 263-268.

15. Tangren, R. F.; Dodge, C. H.; and Seifert, H. S.: Compressibility Effects in Two-Phase Flow. J. Appl. Phys., vol. 20, no. 7, July 1949, pp. 637-645.

16. Collins, R. L.: Choked Expansion of Subcooled Water and the I.H.E. Flow Model. J. Heat Transfer, vol. 100, no. 2, May 1978, pp. 275-280.

17. Henry, R. E.; and Fauske, H. K.: The Two-Phase Critical Flow of One-Component Mixtures in Nozzles, Orifices, and Short Tubes. J. Heat Transfer, vol. 93, no. 2, May 1971, pp. 179-187.

18. Hendricks, R. C.; and Simoneau, R. J.: Application of the Principle of Corresponding States to Two-Phase Choked Flow. NASA TM X-68193, 1973.

19. Hendricks, R. C.; Normalizing Parameters for the Critical Flow Rate of Simple Fluids Through Nozzles. Proceedings of the Fifth International Cryogenic Engineering Conference, K. Mendelssohn, ed., IPC Science and Technology Press, (England), 1974, pp. 278-281. (Also NASA TM X-71545, 1974.)

20. Hendricks, R. C.; Baron, A. K.; and Peller, I. C.: GASP: A Computer Code for Calculating the Thermodynamic and Transport Properties for Ten Fluids: Parahydrogen, Helium, Neon, Methane, Nitrogen, Carbon Monoxide, Oxygen, Fluorine, Argon, and Carbon Dioxide. NASA TN D-7808, 1975.

21. Bean, Howard S., ed.: Fluid Meters, Their Theory and Application. Sixth ed. American Society of Mechanical Engineers, 1971, p. 216.

22. Mealey, C.; and Kee, L.: Computer-Controlled Central Digital Data Acquisition System. NASA TN D-3904, 1967.

23. Bender, E.: Equations of State Exactly Representing the Phase Behavior of Pure Substances. Proceedings of the Fifth Symposium on Thermophysical Properties. American Society of Mechanical Engineers, 1970, pp. 227-235.

TABLE I. - CONICAL CONVERGING-

DIVERGING NOZZLE

(a) Dimensions

Overall length, cm	31.1
Throat diameter, cm	0.3555±0.0007
Throat area, cm^2	0.09926
Length of constant-area section, cm	1.135±0.020
Length-diameter ratio	3.20
Radius of curvature, cm	1.77
Pressure-tap diameter, cm	0.051
Convergence half-angle, deg	6.79±0.05
Divergence half-angle, deg	3.78±0.23

(b) Tap locations (referenced to throat)

Station (tap)	Axial distance, X, cm ±0.014 cm	Radius, r, cm	Ratio of area to throat area, A/A_t
0	-9.1	-----	[a]∞
1	-5.062	0.645	13.18
2	-3.066	.408	5.26
3	-2.263	.312	3.08
4	-1.984	.279	2.46
5	-1.692	.244	1.88
6	-1.052	.178	1.00
7	-.536	.178	1.00
8	-.185	.178	1.00
9	.112	.185	1.08
10	.455	.208	1.37
11	.940	.240	1.82
12	1.933	.306	2.95
13	7.943	.703	15.61
14	12.939	1.033	33.73
15	17.943	1.363	58.79
B	22.0	-----	[b]∞

[a]Inlet mixing chamber.
[b]Outlet mixing chamber.

TABLE II. - TWO-DIMENSIONAL CONVERGING-DIVERGING NOZZLE

(a) Dimensions

Overall length, cm	31.1
Channel width, cm	1.011±0.001
Throat height, cm	0.109±0.001
Throat area, cm^2	0.1104
Length of constant-area section, cm	0.905±0.020
Length-diameter ratio	4.15
Radius of curvature, cm	2.54
Pressure-tap diameter, cm:	
Stations 6 to 9	0.074
Stations 1 to 5, 10 to 12	0.151
Convergence half-angle, deg	[a]6.84
Divergence half-angle, deg	[a]2.98

(b) Tap locations (referenced to throat)

Station (tap)	Axial distance, X, cm ±0.015 cm		Channel height, cm	Ratio of area to throat area, A/A_t
	Straight wall	Contoured wall		
0	-21.0	------	-----	[b]∞
1	-15.824	------	1.899	17.34
2	-11.824	------	1.419	13.02
3	-7.826	------	.939	8.61
4	-4.072	------	.489	4.49
5	-2.065	------	.248	2.28
6	-1.349	-1.355	.162	1.49
7	-.876	------	.109	1.00
8	-.231	-.224	.109	1.00
9	.508	.491	.135	1.24
10	1.392	------	.181	1.66
11	3.828	------	.308	2.83
12	6.370	------	.441	4.05
B	10.1	------	-----	[c]∞

[a]Not possible to make tolerance estimate.
[b]Inlet mixing chamber.
[c]Outlet mixing chamber.

TABLE III. - ELLIPTICAL CONVERGING-

DIVERGING NOZZLE

(a) Dimensions

Overall length, cm	6.80 (11.30)
Throat diameter, cm	0.2934±0.0007
Throat area, cm^2	0.06760
Length of constant-area section, cm	0.617±0.010
Length-diameter ratio	2.10
Curvature (2:1 ellipse):	
r_1	0.78
r_2	0.39
Pressure-tap diameter, cm	0.080
Converging taper (half-angle), deg	10.1
Divergence half-angle, deg	4.00
Diverging taper (half-angle), deg	10.0
Diameter of straight (constant area) section, cm	0.808

(b) Tap locations (referenced to throat)

Station (tap)	Axial distance, X, cm	Radius, r, cm	Ratio of area to throat area, A/A_t
0	-4.605	-----	[a]∞
1	-2.390	0.747	25.82
2	-1.115	.274	3.47
3	-.747	.164	1.25
4	-.297	.147	1.00
5	-.150	.147	1.00
6	.373	.216	2.16
7	1.430	.290	3.89
8	3.942	.467	10.09
9	6.452	.721	24.06

[a]Inlet mixing chamber.

TABLE IV. - ERROR ESTIMATES

(a) For parameters measured in 110-liter rig

Parameter	Range	Percent of average value	Absolute
Pressure, N/cm^2:			
Stagnation, P_o	60 - 680	±0.4	±1.4
Throat, P_t	33 - 275	±.9	-------
Back, P_b	20 - 100	±2.3	-------
Axial, P	30 - 550	±.5	-------
Temperature, K:			
Stagnation, T_o	90 - 130	±.1	±.1
Back, T_b	84 - 104	±.1	±.1
Mass flux, G, $g/cm^2 \cdot sec$:			
95 - 125 K isotherms	1600 - 9000	±1.4	±75
130 K isotherm	1700 - 6000	±2.1	±80

(b) For parameters measured in 375-liter rig

Parameter	Range	Percent of average value	Absolute
Pressure, N/cm^2:			
Nitrogen	150 - 950	±0.4	±2.5
Methane	150 - 925	±.4	±2.5
Hydrogen	130 - 425	±.5	±2.0
Temperature, K:			
Nitrogen	87 - 235	±.15	±.25
Methane	121 - 200	±.10	±.20
Hydrogen	27.2 - 32.3	±.25	±.10
Mass flux, $g/cm^2 \cdot sec$:			
Nitrogen	200 - 10600	±2.0	±5 - 140
Methane	1700 - 7100	±2.5	±100
Hydrogen	900 - 2500	±3.0	±30

TABLE V. - SUMMARY OF DATA TABLES

Table	Nozzle	Fluid	Stagnation temperature, T_o, K	Number of runs
VI(a)	Conical	Nitrogen	95.0	17
(b)			110.0	28
(c)			119.3	20
(d)			124.3	22
(e)			130.3	30
VII(a)	Conical reversed		110.1	21
(b)			119.3	23
VIII(a)	Two dimensional		95.3	19
(b)			109.9	17
(c)			118.9	17
(d)			124.3	18
(e)			129.5	18
IX(a)	Elliptical		89	7
(b)			97	14
(c)			104	8
(d)			111	7
(e)			117	5
(f)			120	10
(g)			122	6
(h)			124	6
(i)			125	7
(j)			126	12
(k)			127	10
(l)			130	10
(m)			131	7
(n)			132	7
(o)			133	5
(p)			134	7
(q)			135	8
(r)			138	4
(s)			140	8
(t)			156	6
(u)			177	5
(v)			234	3
X(a)		Methane	123	9
(b)			126	8
(c)			133	5
(d)			154	11
(e)			167	3
(f)			184	6
(g)			195	3
(h)			200	3
XI(a)		Hydrogen	28	6
(b)			30	9
(c)			32	7
XII		Near-critical nitrogen	118 - 131	30
XIII		Nitrogen	90 - 125	[a]33
			Total	545

[a]Flow-rate and pressure-ratio data only - no profiles.

TABLE VI. - DATA FOR NITROGEN - 7° CONICAL NOZZLE

(a) Stagnation temperature, T_o, 95.0 K

Reading	Stagnation temperature, T_o, K	Stagnation pressure, P_o, N/cm²	Pressures at stations 1 to 15, N/cm² P_1	P_2	P_3	P_4	P_5	P_6	P_7	P_8	P_9	P_{10}	P_{11}	P_{12}	P_{13}	P_{14}	P_{15}	Back-pressure P_b, N/cm²	Temperature at back condition, T_b, K	Ratio of throat pressure to stagnation pressure, P_t/P_o	Maximum mass flux, G_{max}, g/cm² · sec	Stagnation entropy, S_o, J/g · K	Saturation pressure at stagnation entropy, $P_{sat}(S_o)$, N/cm²	Saturation pressure at stagnation temperature, $P_{sat}(T_o)$, N/cm²
101-562	95.0	60	59	59	57	56	53	40	35	33	26	23	22	24	24	24	25	25	86.2	0.543	1580	0.840	54	54
551	94.7	78	76	76	73	72	67	47	43	39	30	24	19	18	20	20	20	21	84.1	.504	2000	.830	52	53
504	95.0	90	89	88	85	82	76	49	47	44	34	29	31	32	34	36	37	37	90.6	.491	2290	.836	53	54
559	94.9	111	110	109	103	100	90	51	48	48	37	30	23	21	25	25	26	26	86.9	.434	2840	.830	52	53
547	94.8	130	129	127	120	115	102	51	47	49	39	32	25	24	30	31	32	33	88.0	.376	3240	.827	52	↓
491	95.3	142	141	139	131	125	110	53	48	49	40	33	30	38	50	54	55	55	95.2	.346	3450	.837	54	↓
544	94.8	195	193	189	178	168	145	54	46	50	41	35	28	20	33	36	39	40	90.7	.257	4350	.821	51	↓
541	95.1	246	244	238	223	209	179	56	46	51	42	36	29	35	83	84	85	85	95.5	.207	5050	.822	51	54
500	95.0	284	282	275	257	240	204	58	45	50	42	36	29	20	43	55	58	58	95.5	.177	5540	.815	49	54
539	95.3	338	336	327	304	285	241	61	46	51	43	37	30	21	52	70	71	72	95.9	.151	6130	.817	50	55
498	95.5	407	405	393	366	341	287	60	46	51	43	38	31	21	41	57	63	64	96.4	.125	6770	.814	49	56
529	95.2	411	408	397	368	344	288	63	44	50	42	37	↓	22	34	43	51	53	94.8	.121	6850	.808	48	55
532	94.9	473	471	456	423	394	330	64	43	49	41	36	↓	21	59	71	87	87	95.8	.103	7440	.796	46	54
524	95.3	535	532	515	478	445	371	68	44	49	42	37	↓	22	46	71	77	77	96.3	.092	7950	.799	47	55
556	95.7	594	590	572	530	493	412	73	46	51	43	38	32	23	54	88	91	91	96.8	.085	8400	.801	47	57
488	94.9	646	642	622	576	535	444	73	42	46	40	35	30	22	22	26	30	32	89.1	.071	8840	.781	44	54
506	94.5	659	655	634	587	545	454	74	42	47	40	35	30	20	33	42	55	61	95.9	.071	8960	.771	42	52

TABLE VI. - Continued.

(b) Stagnation temperature, T_o, 110.0 K

Reading	Stagnation temperature, T_o, K	Stagnation pressure, P_o, N/cm^2	Pressures at stations 1 to 15, N/cm^2															Backpressure, P_b, N/cm^2	Temperature at back condition, T_b, K	Ratio of throat pressure to stagnation pressure, P_t/P_o	Maximum mass flux, G_{max}, g/cm^2 · sec	Stagnation entropy, S_o, J/g · K	Saturation pressure at stagnation entropy, $P_{sat}(S_o)$, N/cm^2	Saturation pressure at stagnation temperature, $P_{sat}(T_o)$, N/cm^2
			P_1	P_2	P_3	P_4	P_5	P_6	P_7	P_8	P_9	P_{10}	P_{11}	P_{12}	P_{13}	P_{14}	P_{15}							
101-906	109.9	162	161	160	154	149	138	85	78	71	52	42	33	26	24	27	28	29	87.5	0.441	2840	1.164	145	146
920	110.3	169	167	166	159	155	143	88	80	73	53	42	34	26	23	27	28	28	87.1	.436	2860	1.173	148	149
480	109.6	178	177	176	168	162	148	88	80	73	55	42	34	29	42	45	46	46	93.1	.411	3120	1.154	141	143
857	109.9	200	199	196	188	182	166	99	91	84	61	46	35	30	48	49	51	52	94.8	.423	3340	1.155	141	145
478	109.7	216	215	213	204	196	179	106	97	87	62	45	35	40	55	58	61	61	96.7	.404	3510	1.149	139	144
863	110.3	241	239	236	226	218	200	124	112	101	71	50	36	28	51	54	56	57	96.5	.418	3660	1.158	143	149
874	109.8	251	250	247	236	228	208	128	117	108	77	54	39	26	28	34	36	36	89.9	.428	3780	1.145	138	145
457	110.4	265	264	260	250	240	220	130	123	113	80	56	40	27	44	48	51	51	94.4	.426	3880	1.156	142	151
865	110.5	268	267	263	252	243	221	135	124	115	82	58	41	27	40	45	47	48	93.8	.429	3940	1.156	142	151
868	109.9	283	281	277	264	254	230	133	123	119	86	62	43	28	28	35	37	38	90.8	.421	4170	1.140	136	146
879	109.9	295	294	288	275	264	238	133	123	121	87	63	45	29	56	61	64	65	97.7	.409	4360	1.137	135	146
889	109.8	307	306	300	286	274	246	133	122	122	89	65	46	30	53	60	63	64	97.3	.398	4530	1.135	134	145
476	110.0	319	318	312	297	284	254	135	124	123	91	67	48	32	65	73	76	76	99.7	.388	4630	1.136	134	146
902	110.4	336	335	328	312	298	267	138	127	127	94	69	49	35	82	91	93	93	103.0	.379	4800	1.141	136	150
461	110.1	348	347	340	323	308	274	135	123	126	93	68	48	30	55	62	66	67	98.0	.362	4980	1.134	134	148
881	110.3	367	366	358	340	323	288	139	125	128	96	71	51	32	71	81	84	84	101.5	.347	5180	1.135	134	150
891	109.9	376	374	366	346	330	292	135	120	124	95	71	51	32	44	52	57	58	96.1	.331	5310	1.124	130	146
907	110.5	390	389	380	360	342	303	140	125	129	98	73	52	33	50	59	64	65	97.5	.331	5400	1.134	134	151
482	110.0	391	390	382	361	342	302	137	120	124	96	71	52	34	61	72	76	76	100.0	.317	5480	1.124	130	147
910	110.1	426	424	414	391	371	326	138	120	125	97	73	53	34	35	43	48	50	94.0	.294	5820	1.120	129	↓
894	110.0	454	452	441	416	393	344	137	117	124	97	74	54	34	36	44	50	52	94.4	.273	6110	1.115	127	↓
921	110.0	472	470	459	432	409	357	139	118	125	98	75	55	35	66	80	85	86	101.5	.265	6250	1.112	126	↓
895	109.9	520	518	505	475	448	388	139	115	123	98	75	55	35	78	98	101	101	104.2	.236	6710	1.103	123	146
914	110.1	543	541	527	495	467	404	140	115	124	99	76	56	35	37	47	54	56	95.5	.228	6910	1.103	123	147
456	109.8	566	564	549	515	485	419	138	111	121	96	75	55	34	18	34	34	37	90.7	.214	7130	1.093	120	145
474	110.3	617	614	598	561	527	454	145	114	123	99	76	57	37	48	64	73	74	99.5	.199	7510	1.097	121	150
918	109.9	645	642	625	585	550	472	145	112	122	98	77	58	37	38	49	58	61	96.8	.189	7710	1.086	117	146
460	109.9	664	660	642	601	564	484	142	109	120	97	75	56	35	19	30	36	40	91.7	.181	7890	1.083	116	146

TABLE VI. - Continued.

(c) Stagnation temperature, T_o, 119.3 K

Reading	Stagnation temperature, T_o, K	Stagnation pressure, P_o, N/cm^2	Pressures at stations 1 to 15, N/cm^2															Backpressure, P_b, N/cm^2	Temperature at back condition, T_b, K	Ratio of throat pressure to stagnation pressure, P_t/P_o	Maximum mass flux, G_{max}, g/cm^2 · sec	Stagnation entropy, S_o, J/g · K	Saturation pressure at stagnation entropy, $P_{sat}(S_o)$, N/cm^2	Saturation pressure at stagnation temperature, $P_{sat}(T_o)$, N/cm^2
			P_1	P_2	P_3	P_4	P_5	P_6	P_7	P_8	P_9	P_{10}	P_{11}	P_{12}	P_{13}	P_{14}	P_{15}							
101-612	119.2	263	262	259	252	246	231	168	163	160	157	156	129	62	31	37	41	43	92.4	0.608	2990	1.387	236	242
648	*119.3*	*281*	*280*	*276*	*268*	*260*	*243*	*169*	*161*	*156*	*152*	*152*	*134*	*69*	*24*	*29*	*32*	34	89.6	.555	3270	1.381	234	243
587	119.3	289	288	285	275	268	249	167	158	152	147	148	135	73	58	67	71	71	98.9	.524	3440	1.377	232	243
669	119.1	294	293	289	279	270	250	162	152	145	139	140	132	76	26	31	34	37	90.5	.492	3570	1.368	228	240
657	119.1	313	312	307	295	285	263	164	151	141	133	135	129	80	40	47	52	54	95.3	.451	3790	1.362	225	240
656	118.8	317	316	311	299	289	265	162	147	136	124	127	123	83	28	33	37	40	91.3	.428	3900	1.351	221	237
603	118.8	322	321	316	303	293	269	163	148	136	123	126	123	83	28	34	38	40	91.5	.423	3950	1.350	220	237
606	119.2	345	344	339	325	314	288	175	156	141	122	126	123	83	62	73	77	78	100.2	.410	4110	1.351	221	241
597	119.1	361	359	354	340	329	301	183	164	147	111	118	116	85	30	36	40	42	92.0	.407	4210	1.343	217	240
572	119.8	379	378	371	357	344	315	192	172	154	125	129	125	85	55	67	72	73	99.2	.408	4340	1.355	223	249
615	119.7	407	406	399	383	369	338	205	187	169	118	121	119	85	30	37	41	44	92.8	.416	4540	1.345	218	248
617	119.0	441	440	432	413	396	359	204	188	182	126	87	90	82	35	42	47	50	93.9	.412	4970	1.316	206	239
590	119.4	474	472	464	443	425	384	209	192	190	132	92	97	86	58	73	79	80	100.5	.400	5260	1.318	207	244
649	119.9	503	501	491	468	448	403	213	194	195	138	95	99	88	68	85	91	91	102.6	.387	5480	1.323	209	251
578	119.5	525	523	512	487	466	417	210	189	192	138	94	87	81	58	73	80	81	100.9	.366	5760	1.307	202	245
619	119.5	549	547	535	508	485	433	210	187	191	139	96	76	74	35	45	52	56	95.8	.348	5980	1.301	200	245
651	119.6	578	576	563	534	509	452	210	186	191	141	97	71	72	55	71	79	81	100.8	.330	6260	1.296	198	246
594	119.8	602	600	587	556	531	470	212	186	192	144	100	70	71	54	70	79	80	100.8	.319	6430	1.296	198	249
671	119.2	624	621	607	574	546	481	206	178	185	141	99	68	54	37	48	56	61	96.8	.297	6690	1.278	190	241
592	119.2	661	658	643	607	577	507	208	177	185	142	101	70	45	48	66	75	78	100.3	.281	6970	1.272	187	242

TABLE VI. - Continued.

(d) Stagnation temperature, T_o, 124.3 K

Reading	Stagnation temperature, T_o, K	Stagnation pressure, P_o, N/cm^2	Pressures at stations 1 to 15, N/cm^2															Backpressure, P_b, N/cm^2	Temperature at back condition, T_b, K	Ratio of throat pressure to stagnation pressure, P_t/P_o	Maximum mass flux, G_{max}, $g/cm^2 \cdot sec$	Stagnation entropy, S_o, $J/g \cdot K$	Saturation pressure at stagnation entropy, $P_{sat}(S_o)$, N/cm^2	Saturation pressure at stagnation temperature, $P_{sat}(T_o)$, N/cm^2
			P_1	P_2	P_3	P_4	P_5	P_6	P_7	P_8	P_9	P_{10}	P_{11}	P_{12}	P_{13}	P_{14}	P_{15}							
101-690	124.1	339	339	336	330	325	313	264	258	258	222	142	94	47	17	23	27	29	87.7	0.762	2530	1.526	292	308
692	124.1	358	358	355	347	340	324	257	249	248	237	169	113	57	20	26	30	33	89.2	.692	2980	1.508	285	↓
627	124.1	375	375	371	361	353	334	252	241	239	232	186	125	65	22	29	34	37	90.4	.637	3310	1.492	280	↓
694	124.1	392	392	387	376	366	343	248	236	232	225	195	133	70	23	30	35	38	90.9	.592	3590	1.483	276	↓
696	124.3	409	408	402	390	379	354	248	233	228	221	199	138	74	25	33	38	41	91.7	.557	3820	1.478	274	310
702	124.4	423	421	415	402	390	363	247	231	224	217	201	142	77	53	67	73	73	99.4	.531	4000	1.472	272	312
628	124.4	429	428	422	408	396	368	248	232	224	216	201	144	78	35	46	53	55	95.6	.521	4080	1.469	270	312
705	124.1	437	436	429	414	401	371	242	225	215	206	197	146	80	27	35	41	44	92.7	.491	4250	1.455	265	307
708	124.5	450	449	442	427	413	382	249	231	221	212	201	147	82	47	62	69	70	98.8	.491	4320	1.463	268	314
712	124.2	451	450	443	427	413	381	244	226	215	205	197	148	83	50	64	70	71	99.1	.476	4400	1.452	263	309
673	124.0	456	455	447	431	416	383	242	223	210	197	192	148	84	28	35	41	45	93.0	.460	4460	1.445	261	306
714	124.3	457	456	449	432	417	385	245	227	214	203	196	149	83	39	51	58	61	96.9	.469	4430	1.453	264	310
719	124.3	473	472	464	447	431	396	247	228	214	198	193	150	86	45	60	68	69	98.7	.452	4610	1.446	261	311
722	124.1	483	482	474	455	439	402	246	227	212	190	188	152	87	29	38	45	48	93.8	.440	4730	1.436	257	307
631	124.4	492	491	483	464	447	410	250	231	217	193	190	152	88	29	38	45	49	93.9	.440	4780	1.441	259	312
726	124.5	511	510	501	481	463	423	252	234	222	190	189	154	89	30	39	46	50	94.3	.435	4950	1.437	258	314
677	124.3	530	528	519	497	478	435	250	231	223	179	180	157	91	30	39	47	50	94.6	.421	5170	1.425	252	311
633	124.7	562	560	549	525	504	457	254	233	230	178	181	160	93	31	42	50	54	95.4	.410	5430	1.425	252	317
733	124.5	584	582	571	545	522	471	251	229	229	167	170	159	95	51	68	77	79	100.5	.392	5680	1.410	246	313
678	124.5	598	596	584	557	533	480	249	226	228	165	167	158	95	55	73	83	84	101.3	.382	5810	1.406	244	313
636	124.8	632	630	617	588	562	505	254	228	231	168	167	158	98	56	76	86	88	102.1	.366	6070	1.405	244	319
680	124.9	666	664	650	618	590	527	253	225	229	167	158	154	99	55	75	85	86	102.0	.344	6320	1.397	240	319

TABLE VI. - Concluded.

(e) Stagnation temperature, T_o, 130.0 K

Reading	Stagnation temperature, T_o, K	Stagnation pressure, P_o, N/cm^2	Pressures at stations 1 to 15, N/cm^2															Back-pressure, P_b, N/cm^2	Temperature at back condition, T_b, K	Ratio of throat pressure to stagnation pressure, P_t/P_o	Maximum mass flux, G_{max}, g/cm^2 · sec	Stagnation entropy, S_o, J/g · K	Saturation pressure at stagnation entropy, $P_{sat}(S_o)$, N/cm^2	Saturation pressure at stagnation temperature, $P_{sat}(T_o)$, N/cm^2
			P_1	P_2	P_3	P_4	P_5	P_6	P_7	P_8	P_9	P_{10}	P_{11}	P_{12}	P_{13}	P_{14}	P_{15}							
101-762	129.9	377	376	374	368	363	350	262	244	231	170	111	72	34	7	16	21	23	85.5	0.613	1740	2.008	322	(a)
766	129.9	393	393	390	384	379	367	279	260	246	181	117	75	36	9	19	24	26	86.3	.626	1950	1.891	339	
768	130.0	411	411	408	402	396	383	294	269	256	196	133	87	42	11	21	26	28	87.5	.622	2250	1.795	341	
746	130.3	418	418	415	408	402	389	302	274	261	201	137	89	44	42	56	59	59	96.3	.624	2300	1.791	341	
773	130.0	425	424	421	414	407	393	315	286	276	215	147	96	47	39	53	57	58	96.2	.651	2480	1.737	338	
781	130.0	427	427	424	417	410	395	324	289	279	217	148	98	48	13	24	30	32	88.4	.653	2520	1.733	338	
778	130.0	431	431	427	420	413	398	330	304	282	220	151	100	49	35	49	54	54	95.4	.654	2590	1.721	337	
805	129.9	434	434	431	423	416	400	332	325	317	222	154	102	51	21	35	41	43	92.2	.729	2650	1.704	335	
806	129.9	↓	434	430	423	↓	↓	332	325	308	221	154	101	50	13	23	30	32	88.7	.709	2630	1.708	336	
789	129.9	↓	434	431	423	↓	↓	331	324	319	223	155	102	51	49	64	67	67	98.2	.734	2660	1.702	335	
790	129.9	↓	433	430	422	↓	↓	332	325	310	221	154	101	50	13	24	30	32	88.8	.715	2640	1.708	336	
791	130.1	↓	433	430	422	↓	↓	332	324	289	220	153	101	50	25	39	44	45	93.0	.668	2600	1.719	337	
787	130.0	438	438	434	426	419	404	333	326	323	226	157	104	51	72	85	86	87	101.8	.737	2670	1.703	335	
796	129.9	440	440	437	428	421	405	332	324	325	233	161	107	53	13	24	31	33	89.1	.737	2750	1.691	334	
793	130.0	445	445	442	433	425	408	331	323	324	243	166	110	55	60	75	78	78	100.2	.727	2850	1.684	333	
799	130.1	451	451	447	437	430	411	332	323	324	250	169	113	56	66	81	83	83	101.5	.719	2880	1.682	332	
802	129.9	458	458	454	443	435	414	326	317	317	271	180	121	61	15	26	33	36	90.2	.692	3100	1.658	328	
845	129.9	465	464	459	449	439	418	324	313	314	278	185	127	63	30	45	51	53	94.9	.676	3230	1.647	326	
834	130.0	472	471	465	455	445	423	324	314	314	281	189	128	64	17	29	36	39	91.1	.667	3310	1.645	326	
813	130.1	481	481	475	464	453	429	324	312	313	284	194	133	67	17	30	37	40	91.4	.650	3440	1.639	325	
814	130.1	498	498	491	478	466	439	320	307	307	285	203	141	72	42	60	66	67	98.2	.616	3720	1.621	321	
819	130.2	517	517	509	495	481	450	317	302	302	283	211	148	77	20	33	42	44	92.6	.584	3940	1.607	317	
755	130.0	531	530	522	506	491	458	312	296	295	278	217	153	81	21	34	43	46	93.0	.557	4190	1.590	313	
821	130.0	547	547	538	521	504	468	309	291	290	273	222	157	85	22	35	44	48	93.6	.531	4390	1.578	309	
848	129.7	562	560	551	532	515	476	304	285	283	266	226	161	88	24	37	46	50	94.1	.504	4630	1.558	303	
826	130.3	586	585	575	555	536	494	308	288	287	268	230	165	91	66	89	94	95	103.0	.490	4810	1.563	304	
851	129.9	597	595	585	563	544	500	302	281	279	259	230	166	93	51	73	81	83	101.0	.468	4980	1.545	298	
835	130.3	637	635	623	598	577	527	305	280	280	255	232	170	97	64	88	96	97	103.4	.439	5320	1.537	296	
751	130.0	658	656	644	617	594	540	300	274	275	246	230	170	99	27	43	54	58	96.0	.418	5570	1.521	290	
852	130.1	681	679	666	637	613	556	302	273	275	243	229	171	101	51	76	86	87	102.0	.404	5750	1.514	288	
717	273.0	356	356	353	345	339	323	218	198	186	129	77	45	21	96	97	98	98	266.9	.522	843	3.239	(a)	
718	271.2	356	356	353	346	339	323	218	199	186	129	77	45	21	7	12	16	18	263.4	.522	850	3.232	(a)	↓

[a]Not applicable.

TABLE VII. - DATA FOR NITROGEN - 3.5° CONICAL NOZZLE

(a) Stagnation temperature, T_o, 110.1 K

Reading	Stagnation temperature, T_o, K	Stagnation pressure, P_o, N/cm^2	Pressures at stations 1 to 15, N/cm^2															Back-pressure, P_b, N/cm^2	Temperature at back condition, T_b, K	Ratio of throat pressure to stagnation pressure, P_t/P_o	Maximum mass flux, G_{max}, g/cm^2·sec	Stagnation entropy, S_o, J/g·K	Saturation pressure at stagnation entropy, $P_{sat}(S_o)$, N/cm^2	Saturation pressure at stagnation temperature, $P_{sat}(T_o)$, N/cm^2
			P_1	P_2	P_3	P_4	P_5	P_6	P_7	P_8	P_9	P_{10}	P_{11}	P_{12}	P_{13}	P_{14}	P_{15}							
101-1425	109.8	150	150	150	150	144	134	123	107	91	86	75	28	24	20	17	24	26	86.1	0.503	2370	1.165	145	145
1465	110.0	175	175	176	176	166	153	137	116	98	94	82	31	25	21	24	26	28	87.6	.470	2830	1.164	145	146
1461	110.2	184	184	185	185	175	161	144	123	106	101	89	77	78	80	82	85	88	102.0	.483	2890	1.166	146	148
1457	110.1	185	185	186	186	176	162	145	124	107	101	89	32	27	25	31	33	35	88.7	.479	2890	1.164	145	147
1420	110.0	199	199	199	199	188	172	153	131	112	105	91	31	25	21	28	30	32	88.6	.459	3090	1.160	143	147
1476	110.0	207	207	207	207	196	179	158	135	116	108	94	32	25	20	27	29	30	88.8	.453	3170	1.158	142	147
1473	110.4	214	213	214	214	202	185	163	139	119	111	96	32	26	20	27	29	31	88.5	.449	3250	1.165	145	150
1409	109.8	223	223	223	223	211	192	169	143	124	116	100	33	26	22	30	32	33	89.4	.447	3390	1.150	139	145
1481	110.0	234	233	233	234	221	201	175	147	127	119	104	34	27	21	29	31	33	89.4	.445	3500	1.152	140	147
1402	110.1	244	244	244	244	230	208	182	151	131	124	109	36	28	22	31	32	35	89.7	.446	3640	1.148	139	146
1432	109.8	269	269	269	269	252	225	194	157	134	126	116	39	30	24	33	35	38	90.6	.433	4000	1.140	136	145
1398	110.2	283	282	282	282	264	235	202	162	138	129	121	41	35	45	52	57	60	96.4	.428	4180	1.147	138	148
1375	110.1	333	332	333	332	308	271	225	173	140	130	125	44	34	27	40	43	46	92.6	.376	4760	1.137	135	148
1376	110.1	380	380	380	379	349	303	247	182	141	128	125	46	36	33	52	57	59	96.6	.329	5320	1.128	131	147
1387	110.2	442	442	442	441	403	346	277	196	145	128	126	83	87	87	88	90	95	103.0	.285	5950	1.120	129	148
1379	110.1	507	508	507	505	460	391	307	210	148	126	124	50	39	40	62	71	78	100.1	.244	6580	1.108	125	148
1391	110.1	518	519	518	517	470	399	313	212	148	126	123	50	40	31	46	52	---	95.5	.238	6670	1.106	124	147
1393	110.0	579	580	579	577	524	440	341	224	151	125	123	51	40	32	47	54	---	96.4	.212	7190	1.097	121	147
1451	110.2	598	599	598	596	541	454	351	229	153	126	124	51	41	32	46	53	58	96.1	.207	7330	1.097	121	148
1447	109.7	654	655	654	651	590	491	377	240	155	124	122	51	41	32	54	62	67	98.0	.186	7820	1.080	115	144
1452	110.4	666	668	667	664	601	501	386	247	160	129	126	52	42	35	65	76	82	100.8	.189	7850	1.091	119	150

TABLE VII. - Concluded.

(b) Stagnation temperature, T_o, 119.3 K

Reading	Stagnation temperature, T_o, K	Stagnation pressure, P_o, N/cm^2	Pressures at stations 1 to 15, N/cm^2															Backpressure, P_b, N/cm^2	Temperature at back condition, T_b, K	Ratio of throat pressure to stagnation pressure, P_t/P_o	Maximum mass flux, G_{max}, g/cm^2 · sec	Stagnation entropy, S_o, J/g · K	Saturation pressure at stagnation entropy, $P_{sat}(S_o)$, N/cm^2	Saturation pressure at stagnation temperature, $P_{sat}(T_o)$, N/cm^2
			P_1	P_2	P_3	P_4	P_5	P_6	P_7	P_8	P_9	P_{10}	P_{11}	P_{12}	P_{13}	P_{14}	P_{15}							
101-1484	119.1	246	246	246	246	238	225	208	187	171	167	163	114	75	52	29	41	46	93.1	0.661	2600	1.393	239	241
1552	119.3	254	253	254	254	244	232	211	187	168	164	159	120	81	56	25	29	41	89.5	.628	2730	1.394	239	242
1546	119.2	284	283	283	284	270	252	225	193	167	160	149	123	102	68	31	30	35	89.7	.524	3270	1.377	232	242
1491	119.2	298	297	297	297	283	260	233	200	173	164	150	164	167	170	177	188	193	115.1	.504	3420	1.370	229	241
1506	119.2	298	298	298	298	283	262	233	199	171	162	146	120	105	73	33	47	54	95.1	.491	3440	1.370	229	241
1564	119.3	317	317	317	317	300	278	245	206	177	166	147	116	107	78	38	58	68	98.2	.464	3650	1.366	227	243
1493	119.4	327	326	326	326	309	282	250	212	181	169	149	114	107	80	64	76	86	101.6	.455	3740	1.365	227	244
1576	119.2	344	343	343	343	324	301	263	223	191	178	156	104	101	84	67	80	90	102.4	.454	3740	1.353	222	242
1534	119.3	347	346	346	346	327	298	262	220	188	175	152	105	102	85	39	32	39	91.2	.438	3920	1.353	222	242
1496	119.3	350	349	349	348	329	299	264	221	190	177	153	106	103	85	44	68	77	100.0	.437	3960	1.353	222	243
1555	119.4	350	350	350	350	330	303	265	222	190	177	154	107	104	85	39	37	44	92.9	.439	3960	1.356	223	244
1531	119.3	366	365	365	365	345	313	274	229	196	183	159	101	100	87	40	33	40	91.7	.435	4110	1.348	219	243
1512	119.3	370	370	370	369	348	317	277	231	198	185	161	100	99	87	41	34	41	91.8	.435	4160	1.347	219	243
1557	119.2	395	395	395	394	370	336	290	239	205	193	171	90	92	85	44	41	49	93.8	.434	4430	1.335	214	241
1540	119.3	403	403	402	402	378	339	295	240	206	195	174	89	91	85	45	38	47	93.7	.432	4490	1.336	214	243
1566	119.3	433	433	433	432	404	364	310	246	209	196	182	78	84	81	49	43	53	94.6	.419	4850	1.326	210	243
1578	119.1	433	433	432	432	403	365	310	247	208	194	185	73	80	77	51	69	80	100.7	.427	4710	1.321	208	240
1503	119.5	447	447	446	446	417	373	317	253	212	199	186	80	86	82	50	38	47	93.3	.416	4950	1.327	211	245
1587	119.1	509	510	509	508	471	416	346	263	210	193	187	57	65	65	55	72	86	101.5	.367	5650	1.300	199	240
1589	119.3	553	553	553	551	510	444	367	274	213	194	189	123	137	146	163	191	206	116.3	.342	6040	1.296	198	243
1584	119.2	564	564	563	562	517	453	371	271	213	193	192	59	53	56	51	70	86	101.3	.341	5910	1.292	196	242
1591	119.1	580	580	580	578	534	462	379	278	212	191	187	84	88	90	94	96	105	104.5	.322	6280	1.285	193	240
1593	119.2	631	632	632	629	579	497	404	290	215	191	187	121	126	126	127	130	140	109.4	.296	6720	1.277	190	242
1383	277.6	350	350	350	350	339	321	296	257	217	206	188	42	31	42	52	63	73	272.5	.537	817	3.263	(a)	(a)
1384	275.4	351	350	350	350	339	321	296	257	217	206	188	42	31	20	8	13	18	261.8	.537	820	3.254	(a)	(a)

[a]Not applicable.

TABLE VIII. - DATA FOR NITROGEN - TWO-DIMENSIONAL NOZZLE

(a) Stagnation temperature, T_o, 95.3 K

Reading	Stagnation temperature, T_o, K	Stagnation pressure, P_o, N/cm^2	Pressures at stations 1 to 15, N/cm^2															Back-pressure, P_b, N/cm^2	Temperature at back condition, T_b, K	Ratio of throat pressure to stagnation pressure, P_t/P_o	Maximum mass flux, G_{max}, $g/cm^2 \cdot sec$	Stagnation entropy, S_o, $J/g \cdot K$	Saturation pressure at stagnation entropy, $P_{sat}(S_o)$, N/cm^2	Saturation pressure at stagnation temperature, $P_{sat}(T_o)$, N/cm^2
			P_1	P_2	P_3	P_4	P_5	P_6	P_7	P_8	P_9	P_{10}	P_{11}	P_{12}	P_{13}	P_{14}	P_{15}							
1-386	94.8	71	71	72	71	71	68	62	52	45	38	39	40	41	61	45	38	42	91.8	0.626	1730	0.833	53	53
299	95.2	108	108	109	108	106	99	86	60	51	46	51	56	63	85	51	45	71	95.4	.468	2710	.839	54	55
114	95.4	150	149	150	149	146	133	111	69	55	43	41	51	54	112	55	44	67	96.0	.366	3530	.838	54	56
115	95.3	185	184	185	183	179	162	133	77	57	44	41	42	49	134	57	44	58	95.7	.309	4100	.832	53	55
117	95.6	217	216	216	215	210	189	153	84	60	44	42	41	50	154	60	45	61	96.1	.276	4530	.835	53	57
291	95.6	248	247	247	245	239	215	172	90	62	44	44	65	66	174	62	45	102	96.1	.251	4920	.833	53	57
119	95.1	287	286	286	284	276	246	196	97	65	41	42	43	58	197	64	43	90	95.7	.225	5430	.818	50	55
111	95.3	341	340	340	338	329	293	230	112	70	43	45	45	61	233	71	44	89	97.4	.205	6010	.815	50	55
290	95.2	373	372	372	369	359	319	249	117	73	41	42	36	56	252	72	42	86	95.9	.196	6340	.812	49	55
121	95.8	417	415	415	412	400	355	276	126	78	42	43	35	54	280	77	43	82	96.6	.188	6730	.819	50	57
[a]136	95.5	462	461	460	457	444	393	304	135	80	41	41	41	69	309	80	42	130	96.5	.174	7150	.809	48	56
[a]137	95.1	524	522	521	518	502	443	342	147	85	39	39	36	63	347	83	39	127	96.1	.161	7690	.794	46	54
[a]141	95.4	526	524	522	519	503	445	343	147	84	40	40	35	58	348	84	40	121	96.4	.161	7700	.800	47	56
125	95.6	555	553	551	548	533	480	[b]208	162	90	45	42	37	39	[b]189	92	47	90	96.7	.161	7570	.803	47	57
[a]144	95.4	590	588	587	583	565	499	383	162	92	40	38	33	52	389	90	39	109	96.5	.156	8200	.796	46	56
288	95.4	611	609	607	603	585	517	397	167	95	40	38	33	55	402	92	39	105	96.6	.155	8350	.793	46	56
375	95.1	627	625	623	619	600	530	408	172	96	40	38	44	97	413	95	39	203	96.2	.153	8510	.787	45	55
127	95.1	656	654	652	648	631	568	[b]245	[b]81	[b]53	42	40	34	31	[b]266	[b]54	38	94	96.5	.080	8080	.783	44	54
372	95.4	674	671	669	665	644	569	436	182	100	41	38	33	51	442	99	39	108	96.7	.149	8810	.788	45	56

(b) Stagnation temperature, T_o, 109.9 K

Reading	T_o, K	P_o, N/cm^2	P_1	P_2	P_3	P_4	P_5	P_6	P_7	P_8	P_9	P_{10}	P_{11}	P_{12}	P_{13}	P_{14}	P_{15}	P_b	T_b	P_t/P_o	G_{max}	S_o	$P_{sat}(S_o)$	$P_{sat}(T_o)$
1-280	109.1	155	154	155	154	153	146	135	109	88	67	60	51	50	135	89	67	57	95.9	0.568	2320	1.148	139	140
278	109.2	169	168	168	168	166	158	145	116	93	67	59	50	48	145	94	68	55	96.9	.551	2520	1.147	139	140
[c]52	110.3	173	172	173	172	170	163	149	119	96	71	63	52	43	149	97	71	49	93.2	.557	2490	1.172	148	149
[d]42	109.8	188	187	188	187	190	176	160	127	100	70	60	50	44	160	103	70	46	93.5	.533	2490	1.157	142	145
[c]51	109.2	203	202	203	202	199	189	170	134	106	71	65	70	75	170	107	71	83	101.1	.521	3020	1.140	136	140
276	108.9	254	253	253	252	248	231	202	145	119	82	66	55	63	203	120	82	75	98.1	.467	3790	1.122	129	137
[c]48	109.9	267	266	266	265	260	244	213	154	126	84	68	53	60	214	128	85	72	99.6	.474	3720	1.145	137	146
[d]40	110.4	273	271	272	271	275	249	217	156	128	86	69	52	50	219	132	86	64	98.6	.471	3550	1.153	141	150
274	109.1	313	312	312	310	304	280	239	157	126	90	73	60	72	241	127	90	86	101.7	.402	4550	1.118	128	139
[d]38	109.9	345	343	343	342	345	308	260	167	133	94	76	56	55	262	135	94	80	100.6	.385	4720	1.130	132	146
[d]36	110.1	407	406	406	404	407	361	300	181	137	98	80	58	58	302	139	98	87	102.3	.337	5310	1.123	130	147
272	109.8	447	446	445	443	432	393	323	188	137	97	82	62	81	327	139	98	109	104.9	.306	5900	1.112	126	145
[d]34	109.8	517	516	515	513	516	452	366	201	141	96	84	60	70	372	143	96	104	104.2	.273	6330	1.100	122	145
269	110.0	567	565	563	561	546	493	398	214	144	96	87	89	127	405	147	98	206	109.9	.254	6920	1.097	121	147
267	110.0	619	617	615	612	695	535	429	230	148	93	87	75	114	437	150	96	190	109.8	.240	7410	1.089	118	146
[d]44	110.9	663	661	660	657	660	575	460	241	159	96	90	63	63	468	159	99	114	105.5	.239	7160	1.103	123	155
[c]54	111.3	665	663	662	658	640	576	462	243	161	98	90	63	67	469	159	100	119	106.6	.243	7320	1.111	126	158

[a]Gas checks outside of tolerance.
[b]Readings appear to be in error but data record offers no reason as to why they should be.
[c]Flow rates based on downstream flowmeters.
[d]Transducers not zero adjusted and flow rates based on downstream flowmeters.

TABLE VIII. - Continued.

(c) Stagnation temperature, T_o, 118.9 K

Reading	Stagnation temperature, T_o, K	Stagnation pressure, P_o, N/cm^2	Pressures at stations 1 to 15, N/cm^2 P_1	P_2	P_3	P_4	P_5	P_6	P_7	P_8	P_9	P_{10}	P_{11}	P_{12}	P_{13}	P_{14}	P_{15}	Backpressure, P_b, N/cm^2	Temperature at back condition, T_b, K	Ratio of throat pressure to stagnation pressure, P_t/P_o	Maximum mass flux, G_{max}, $g/cm^2 \cdot sec$	Stagnation entropy, S_o, $J/g \cdot K$	Saturation pressure at stagnation entropy, $P_{sat}(S_o)$, N/cm^2	Saturation pressure at stagnation temperature, $P_{sat}(T_o)$, N/cm^2
1-368	118.8	245	244	244	244	242	233	217	182	162	157	116	53	48	218	164	158	62	96.1	0.661	2770	1.381	234	236
249	118.2	246	245	246	245	242	232	214	173	145	139	127	59	40	214	146	139	59	96.6	.591	2710	1.363	226	229
360	119.6	247	247	247	247	245	239	228	203	185	127	81	55	71	228	187	128	78	100.1	.379	2060	1.408	245	246
354	119.2	247	247	247	247	245	236	222	189	171	163	105	97	102	223	174	164	108	105.2	.444	2420	1.394	239	241
154	118.9	270	270	270	269	266	254	234	189	160	152	132	63	77	235	160	152	93	102.9	.591	2920	1.375	231	238
245	118.5	314	314	313	312	307	291	263	204	156	123	121	78	50	264	159	124	75	99.9	.499	3560	1.344	218	233
156	119.2	356	355	355	354	348	328	293	224	175	127	124	82	55	295	178	128	92	102.6	.491	3900	1.347	219	241
219	119.0	390	389	389	388	381	357	315	234	188	114	111	87	60	318	191	115	94	103.3	.482	4290	1.332	213	239
217	119.0	423	422	422	420	413	384	336	241	195	120	103	90	65	339	197	120	110	105.6	.462	4660	1.321	208	239
252	118.9	441	440	439	437	428	399	345	243	195	121	93	88	67	349	196	122	95	102.7	.443	4900	1.314	205	237
254	118.4	460	459	458	456	446	414	356	243	194	123	95	76	69	360	195	124	95	102.9	.422	5160	1.297	198	231
159	118.6	461	460	459	457	448	415	357	245	196	123	95	82	69	361	197	124	102	104.0	.424	5120	1.303	200	234
258	118.4	482	481	480	478	467	433	371	249	197	129	100	72	68	375	198	130	95	103.3	.409	5310	1.291	196	231
215	119.0	517	516	515	513	502	462	393	259	201	131	101	77	85	397	202	132	124	107.5	.390	5560	1.297	198	238
162	118.9	568	567	565	563	550	505	423	265	202	134	103	73	100	429	202	134	145	110.0	.355	6100	1.283	192	237
164	119.2	614	612	610	607	594	543	453	278	206	137	106	76	108	459	207	137	158	111.5	.335	6450	1.281	191	241
212	118.8	678	676	674	671	655	596	492	289	205	134	107	74	80	497	205	135	125	107.5	.302	7030	1.260	183	237

(d) Stagnation temperature, T_o, 124.3 K

Reading	Stagnation temperature, T_o, K	Stagnation pressure, P_o, N/cm^2	P_1	P_2	P_3	P_4	P_5	P_6	P_7	P_8	P_9	P_{10}	P_{11}	P_{12}	P_{13}	P_{14}	P_{15}	Backpressure, P_b, N/cm^2	Temperature at back condition, T_b, K	P_t/P_o	G_{max}, $g/cm^2 \cdot sec$	S_o, $J/g \cdot K$	$P_{sat}(S_o)$, N/cm^2	$P_{sat}(T_o)$, N/cm^2
1-231	123.7	327	327	327	327	324	315	300	269	256	140	94	47	40	301	256	140	57	95.6	0.784	2390	1.519	289	302
353	124.0	329	328	328	328	326	317	303	274	261	132	89	45	41	304	264	133	55	95.2	.794	2300	1.528	292	305
288	124.8	330	330	330	329	327	319	306	253	209	125	85	42	38	307	209	126	53	94.6	.633	2151	1.576	308	317
82	123.7	346	346	345	345	342	330	310	270	250	165	112	57	43	311	251	165	64	97.2	.724	2770	1.498	282	301
232	124.7	358	358	358	357	354	342	323	383	266	160	109	55	42	324	266	161	63	96.7	.744	2710	1.533	294	317
210	123.6	377	376	376	375	371	354	325	267	234	200	136	69	46	327	235	201	72	99.0	.621	3380	1.474	272	301
93	124.5	393	393	393	392	386	371	341	283	254	195	135	69	47	343	254	195	73	99.5	.644	3340	1.495	281	314
236	124.7	410	410	409	409	403	383	349	280	242	207	145	75	50	351	243	208	79	100.4	.590	3650	1.489	278	316
207	124.2	426	425	425	424	418	396	357	278	234	212	152	82	100	358	236	213	131	108.1	.550	3970	1.464	268	309
96	123.6	456	455	454	453	446	419	372	280	227	196	157	89	68	375	230	196	123	107.3	.499	4380	1.432	255	300
200	123.7	486	484	483	482	474	443	390	285	231	189	160	92	63	393	234	190	92	103.1	.476	4730	1.424	252	302
84	124.3	528	527	526	525	515	480	420	298	242	193	165	97	68	423	244	193	107	104.5	.458	5070	1.425	252	311
100	124.3	563	562	562	558	548	509	440	301	243	182	165	100	70	444	244	183	123	107.3	.431	5380	1.412	247	310
197	124.0	602	600	598	597	585	540	461	303	240	165	160	104	76	465	241	166	146	109.9	.399	5840	1.392	238	305
87	125.3	636	634	633	630	618	571	490	322	254	184	170	105	75	494	254	185	118	106.3	.399	5880	1.415	248	325
105	125.3	636	635	633	630	618	571	490	323	255	187	171	105	74	495	256	188	114	106.0	.401	5850	1.417	249	326
103	124.5	640	638	636	633	621	572	488	316	245	163	159	105	75	492	246	163	118	106.4	.383	6040	1.394	239	313
101	124.6	670	669	667	663	650	599	509	323	250	164	162	107	76	513	250	164	121	106.9	.373	6230	1.390	237	315

TABLE VIII. - Concluded.

(e) Stagnation temperature, T_o, 129.5 K

Reading	Stagnation temperature, T_o, K	Stagnation pressure, P_c, N/cm^2	Pressures at stations 1 to 15, N/cm^2															Backpressure, P_b, N/cm^2	Temperature at back condition, T_b, K	Ratio of throat pressure to stagnation pressure, P_t/P_o	Maximum mass flux, G_{max}, g/cm^2·sec	Stagnation entropy, S_o, J/g·K	Saturation pressure at stagnation entropy, $P_{sat}(S_o)$, N/cm^2	Saturation pressure at stagnation temperature, $P_{sat}(T_o)$, N/cm^2
			P_1	P_2	P_3	P_4	P_5	P_6	P_7	P_8	P_9	P_{10}	P_{11}	P_{12}	P_{13}	P_{14}	P_{15}							
1-191	126.4	339	339	339	338	337	327	310	256	204	112	73	73	95	311	204	113	105	104.8	0.600	1590	[e]1.967	330	(f)
186	128.5	361	361	360	360	358	348	330	272	227	115	77	37	24	331	227	116	42	91.8	.628	1690	[e]1.992	324	
351	128.8	374	374	373	373	371	361	344	283	236	121	80	39	25	345	239	123	46	92.9	.631	1800	[e]1.922	336	
188	129.4	379	379	379	378	376	365	348	288	241	123	81	39	25	349	241	124	47	92.9	.635	1820	[e]1.955	333	
172	129.6	402	402	401	401	398	387	369	312	254	141	95	48	32	370	254	142	55	94.9	.633	2190	1.798	344	
347	129.3	406	405	405	405	402	390	371	317	261	148	99	50	37	372	264	149	59	95.4	.644	2310	1.745	339	
174	129.8	423	422	422	422	418	406	385	340	280	157	106	53	35	386	281	159	60	96.1	.664	2480	1.731	338	
329	129.3	433	433	432	432	427	414	390	341	324	169	115	58	38	392	328	171	61	96.7	.748	2760	1.668	330	
331	129.4	444	444	444	443	438	423	397	342	322	180	123	62	41	398	326	181	64	97.2	.725	2950	1.654	328	
183	130.1	462	461	461	460	455	439	410	350	326	188	128	66	81	412	327	189	106	104.7	.707	3050	1.661	329	
344	129.0	475	474	473	473	467	446	411	338	307	206	144	75	113	413	311	208	137	108.9	.646	3530	1.598	315	
176	129.8	512	511	510	509	502	476	435	346	310	223	157	82	55	437	311	223	86	101.4	.606	3900	1.597	315	
343	129.5	545	545	543	542	534	505	453	346	300	234	167	91	60	456	305	235	88	102.0	.550	4380	1.562	304	
97	130.1	564	563	561	560	552	520	466	351	304	239	171	93	62	468	305	239	95	103.0	.539	4490	1.568	306	
340	129.6	597	596	594	592	583	547	485	355	298	246	178	137	209	488	303	246	238	119.2	.500	4910	1.537	296	
332	129.9	638	638	636	633	621	582	511	362	298	246	183	184	232	515	303	247	275	122.0	.467	5250	1.526	292	
314	129.5	663	662	660	657	646	601	523	360	292	242	182	106	74	527	296	244	117	105.1	.440	5580	1.506	285	
178	129.9	680	679	677	675	662	616	536	368	296	244	184	108	74	540	296	245	113	105.5	.435	5650	1.510	286	
336	284.7	343	343	343	342	339	327	305	240	194	86	52	76	85	306	196	82	107	280.4	.566	870	3.298	(f)	
337	283.5	343	343	342	342	339	327	305	239	194	86	52	24	15	306	196	82	25	274.3	.565	874	3.293	(f)	

[e] $S_o > S_c = 1.813$.

[f] Not applicable.

TABLE IX. - DATA FOR NITROGEN - ELLIPTICAL NOZZLE

Reading	Stagnation temperature, T_o, K	Stagnation pressure, P_o, N/cm^2	Pressures at stations 1 to 9, N/cm^2									Back-pressure, P_b, N/cm^2	Temperature at back condition, T_b, K	Ratio of throat pressure at stagnation pressure, P_t/P_o	Maximum mass flux, G_{max}, $g/cm^2 \cdot sec$	Stagnation entropy, S_o, $J/g \cdot K$	Saturation pressure at stagnation entropy, $P_{sat}(S_o)$, N/cm^2	Saturation pressure at stagnation temperature, $P_{sat}(T_o)$, N/cm^2
			P_1	P_2	P_3	P_4	P_5	P_6	P_7	P_8	P_9							
(a) Stagnation temperature, T_o, 89 K																		
117-457	87.5	562	559	534	173	57	25	21	34	191	198	199	88.4	0.045	8 470	0.629	24	29
464	87.6	717	714	682	218	67	26	↓	59	288	296	295	88.7	.036	9 630	.619	23	↓
907	87.7	773	769	734	233	71	27	↓	44	275	285	285	89.1	.034	10 060	.617	23	↓
449	87.4	857	852	814	256	76	26	↓	94	364	374	372	88.9	.030	10 570	.605	22	↓
459	90.3	353	353	337	122	50	31	24	32	104	113	115	90.7	.088	6 490	.707	33	37
466	90.6	475	474	453	155	58	32	26	44	184	188	189	91.1	.067	7 610	.703	33	38
452	90.5	632	630	602	199	67	32	25	41	216	224	224	91.4	.050	8 890	.689	31	38
(b) Stagnation temperature, T_o, 97 K																		
117-485	94.3	444	443	424	156	67	42	33	68	197	201	202	94.6	0.096	7 160	0.785	44	51
462	96.8	156	157	152	83	61	53	49	61	94	93	96	96.6	.337	3 540	.868	60	62
841	96.5	183	185	178	91	61	52	45	53	92	93	96	96.3	.283	4 050	.858	58	61
876	96.3	289	289	277	120	66	49	34	37	51	73	78	96.2	.171	5 500	.843	55	60
735	96.4	433	432	414	157	74	48	37	82	205	209	211	96.6	.112	6 950	.831	52	60
490	96.4	509	506	485	180	78	49	38	125	256	261	261	96.8	.097	7 620	.823	51	60
741	96.5	681	678	649	225	87	48	37	118	317	324	323	97.0	.070	8 940	.810	49	61
842	98.3	148	150	145	87	66	58	55	63	91	91	95	97.9	.392	3 280	.902	67	69
877	98.6	216	217	209	106	73	60	39	48	64	77	81	98.4	.277	4 400	.901	67	71
847	98.5	218	219	211	107	71	60	37	44	55	68	73	98.2	.274	4 410	.898	66	70
488	99.2	223	224	216	111	74	63	49	64	112	113	116	99.1	.281	4 420	.913	69	74
736	98.6	255	255	246	117	73	59	44	64	122	124	127	98.5	.230	4 900	.896	66	71
742	98.1	492	490	470	178	81	54	40	91	231	236	237	98.3	.110	7 370	.861	58	69
783	99.8	778	773	738	262	101	57	41	79	303	310	308	100.5	.073	9 430	.868	60	77
(c) Stagnation temperature, T_o, 104 K																		
117-786	103.2	361	359	344	147	95	75	45	69	137	142	144	103.1	0.209	5 750	0.982	86	97
797	103.2	375	373	357	161	97	75	45	72	150	153	154	103.1	.200	5 910	.980	86	97
790	103.2	613	609	582	226	105	70	47	90	260	265	264	103.3	.115	8 020	.953	79	97
801	103.2	621	616	589	228	106	71	47	87	254	260	258	103.3	.114	8 070	.952	79	97
802	103.2	784	778	744	275	114	69	47	94	318	326	322	103.5	.088	9 250	.935	75	97
500	106.5	357	357	345	173	114	96	63	103	181	184	186	106.1	.270	5 480	1.053	107	119
502	106.4	492	491	472	208	117	91	63	139	258	262	263	106.1	.185	6 810	1.033	101	118
699	106.6	837	831	798	306	138	90	58	101	316	327	325	107.0	.108	9 330	.997	90	120

TABLE IX. - Continued.

(d) Stagnation temperature, T_o, 111 K

Reading	Stagnation temperature, T_o, K	Stagnation pressure, P_o, N/cm^2	Pressures at stations 1 to 9, N/cm^2 P_1	P_2	P_3	P_4	P_5	P_6	P_7	P_8	P_9	Back-pressure, P_b, N/cm^2	Temperature at back condition, T_b, K	Ratio of throat pressure at stagnation pressure, P_t/P_o	Maximum mass flux, G_{max}, g/cm^2 · sec	Stagnation entropy, S_o, J/g · K	Saturation pressure at stagnation entropy, $P_{sat}(S_o)$, N/cm^2	Saturation pressure at stagnation temperature, $P_{sat}(T_o)$, N/cm^2
117-637	111.9	422	421	407	216	151	129	57	85	128	149	151	109.7	0.306	5590	1.160	143	164
710	111.8	427	426	413	217	151	129	59	91	141	160	163	111.0	.303	5660	1.157	142	163
711	111.8	492	491	474	235	154	128	61	83	135	163	166	111.0	.260	6290	1.146	138	163
512	110.7	560	559	539	249	149	119	63	114	236	244	244	110.3	.213	6980	1.113	126	153
712	111.9	570	567	548	256	156	125	63	76	129	166	169	111.0	.219	6950	1.136	134	164
638	111.0	608	604	582	261	151	117	62	65	111	153	158	110.2	.193	7320	1.112	126	155
639	110.6	827	822	790	318	155	109	63	57	100	151	164	110.0	.131	8950	1.076	114	152

(e) Stagnation temperature, T_o, 117 K

Reading	T_o	P_o	P_1	P_2	P_3	P_4	P_5	P_6	P_7	P_8	P_9	P_b	T_b	P_t/P_o	G_{max}	S_o	$P_{sat}(S_o)$	$P_{sat}(T_o)$
117-827	116.3	215	218	213	148	117	109	105	75	111	115	119	105.1	0.507	3040	1.318	207	208
642	116.6	348	348	338	196	125	110	110	146	200	204	206	115.6	.315	4610	1.284	192	211
643	116.7	496	494	479	262	182	157	74	123	199	211	213	115.3	.316	5820	1.251	178	212
644	116.7	641	638	616	298	187	154	70	113	217	238	239	115.2	.240	7080	1.223	167	212
645	116.9	777	774	747	335	190	147	74	118	259	281	280	115.4	.189	8080	1.205	160	215

(f) Stagnation temperature, T_o, 120 K

Reading	T_o	P_o	P_1	P_2	P_3	P_4	P_5	P_6	P_7	P_8	P_9	P_b	T_b	P_t/P_o	G_{max}	S_o	$P_{sat}(S_o)$	$P_{sat}(T_o)$
117-526	119.9	277	278	273	205	183	177	159	153	181	183	185	113.3	0.641	3020	1.402	243	250
854	119.8	296	296	290	206	174	166	156	110	156	159	162	111.2	.560	3420	1.389	238	249
853	119.7	350	349	340	212	154	142	136	125	183	187	190	114.2	.407	4290	1.364	226	248
527	119.3	418	418	406	241	164	139	108	154	218	224	226	117.6	.332	4950	1.331	212	243
852	119.9	447	446	433	258	177	149	113	117	200	207	209	116.1	.333	5120	1.337	215	250
851	119.6	546	542	526	290	203	173	81	108	200	214	216	116.7	.318	6010	1.304	201	246
528	119.5	571	568	551	295	205	176	72	125	210	229	230	117.3	.309	6240	1.296	197	245
647	119.3	604	601	582	302	204	174	71	134	226	244	244	117.2	.287	6480	1.285	192	243
529	119.7	708	706	682	333	209	173	77	113	210	244	244	117.3	.244	7340	1.273	187	248
530	120.6	818	814	786	369	216	172	85	197	388	397	395	119.1	.211	8040	1.271	187	259

(g) Stagnation temperature, T_o, 122 K

Reading	T_o	P_o	P_1	P_2	P_3	P_4	P_5	P_6	P_7	P_8	P_9	P_b	T_b	P_t/P_o	G_{max}	S_o	$P_{sat}(S_o)$	$P_{sat}(T_o)$
117-863	121.4	302	302	297	236	212	205	148	56	108	116	119	105.5	0.677	2910	1.441	259	270
538	121.8	346	346	339	245	206	196	169	211	243	246	247	118.9	.568	3590	1.429	254	275
862	121.3	387	386	376	243	183	166	155	79	151	162	164	111.3	.429	4360	1.394	240	268
534	121.2	489	488	475	280	198	168	127	217	290	294	295	119.6	.344	5320	1.357	223	267
540	122.3	501	500	486	289	205	176	143	198	275	281	281	120.2	.352	5320	1.381	234	282
442	122.3	708	703	680	347	226	189	112	290	411	417	413	120.8	.267	7020	1.328	211	282

TABLE IX. - Continued.

(h) Stagnation temperature, T_o, 124 K

Reading	Stagnation temperature, T_o, K	Stagnation pressure, P_o, N/cm^2	Pressures at stations 1 to 9, N/cm^2									Backpressure, P_b, N/cm^2	Temperature at back condition, T_b, K	Ratio of throat pressure at stagnation pressure, P_t/P_o	Maximum mass flux, G_{max}, g/cm^2·sec	Stagnation entropy, S_o, J/g·K	Saturation pressure at stagnation entropy, $P_{sat}(S_o)$, N/cm^2	Saturation pressure at stagnation temperature, $P_{sat}(T_o)$, N/cm^2
			P_1	P_2	P_3	P_4	P_5	P_6	P_7	P_8	P_9							
117-550	124.3	359	359	354	284	259	251	140	96	124	136	139	108.2	0.699	2980	1.514	288	311
548	124.4	506	504	491	306	226	200	174	161	245	252	254	120.1	.394	5060	1.435	257	312
547	124.4	558	556	541	321	232	201	165	152	248	258	259	120.5	.361	5530	1.417	249	312
546	124.5	630	627	609	341	241	209	153	181	285	295	295	121.4	.332	6170	1.398	241	314
545	124.4	701	698	677	361	242	207	198	415	485	492	490	123.1	.296	6760	1.377	232	312
544	124.5	809	805	779	389	243	201	181	435	528	536	534	123.2	.249	7580	1.355	223	314

(i) Stagnation temperature, T_o, 125 K

Reading	T_o	P_o	P_1	P_2	P_3	P_4	P_5	P_6	P_7	P_8	P_9	P_b	T_b	P_t/P_o	G_{max}	S_o	$P_{sat}(S_o)$	$P_{sat}(T_o)$
117-569	125.1	356	356	352	298	279	273	119	137	179	182	185	113.8	0.765	2560	1.556	302	323
568	124.9	429	428	419	296	247	233	175	235	284	286	289	122.6	.542	4000	1.487	278	320
553	125.0	434	434	424	298	246	232	178	187	249	253	253	120.0	.535	4080	1.487	278	321
567	125.1	496	495	482	309	236	212	181	250	317	320	322	122.8	.428	4830	1.460	267	323
566	125.3	634	632	614	348	247	212	165	269	375	379	380	123.1	.335	6100	1.417	249	326
565	125.3	771	768	743	383	249	208	141	280	427	433	433	123.1	.270	7160	1.381	234	326
564	125.1	890	887	856	413	248	197	120	364	510	518	517	123.3	.221	8060	1.352	221	323

(j) Stagnation temperature, T_o, 126 K

Reading	T_o	P_o	P_1	P_2	P_3	P_4	P_5	P_6	P_7	P_8	P_9	P_b	T_b	P_t/P_o	G_{max}	S_o	$P_{sat}(S_o)$	$P_{sat}(T_o)$
117-600	126.1	387	388	382	312	287	279	135	55	117	129	132	107.1	0.721	2910	1.567	306	338
582	125.8	428	428	419	308	264	251	169	122	178	187	190	114.1	.587	3770	1.519	290	334
599	125.8	432	432	423	309	264	251	170	117	146	161	165	111.4	.581	3810	1.517	289	334
581	126.0	500	499	487	320	251	230	187	260	325	327	329	123.6	.459	4690	1.484	277	337
598	126.0	565	564	549	335	249	217	184	90	191	213	214	116.5	.385	5370	1.457	266	337
437	126.1	572	569	553	334	248	217	362	451	488	493	490	125.4	.379	5450	1.456	266	338
605	125.8	573	572	556	332	247	214	181	243	333	337	339	123.1	.374	5490	1.449	263	334
436	125.9	632	629	611	350	250	216	364	477	523	528	252	125.2	.342	6010	1.432	256	335
597	126.2	699	697	676	370	256	219	167	98	212	245	245	119.3	.313	5610	1.419	250	340
604	126.0	700	699	677	368	255	217	164	236	358	365	365	123.0	.311	6540	1.414	248	337
603	125.8	864	861	832	409	253	205	134	227	395	405	404	122.8	.237	7810	1.372	230	337
577	126.2	873	870	840	417	256	207	178	467	566	574	572	124.6	.237	7840	1.378	233	340

TABLE IX. - Continued.

(k) Stagnation temperature, T_o, 127 K

Reading	Stagnation temperature, T_o, K	Stagnation pressure, P_o, N/cm^2	Pressures at stations 1 to 9, N/cm^2									Back-pressure, P_b, N/cm^2	Temperature at back condition, T_b, K	Ratio of throat pressure at stagnation pressure, P_t/P_o	Maximum mass flux, G_{max}, $g/cm^2 \cdot sec$	Stagnation entropy, S_o, $J/g \cdot K$	Saturation pressure at stagnation entropy, $P_{sat}(S_o)$, N/cm^2	Saturation pressure at stagnation temperature, $P_{sat}(T_o)$, N/cm^2
			P_1	P_2	P_3	P_4	P_5	P_6	P_7	P_8	P_9							
117-575	126.9	392	391	386	324	303	295	124	87	111	123	127	106.5	0.753	2680	1.602	316	(a)
612	127.4	395	395	390	331	312	300	119	81	106	118	122	105.7	.760	2570	1.626	322	
611	127.2	426	426	418	327	294	283	153	103	131	145	149	109.4	.665	3310	1.574	308	
574	126.9	503	502	490	329	265	245	186	142	182	200	203	115.4	.487	4540	1.509	286	
610	127.1	562	562	547	343	262	233	192	148	188	211	214	116.6	.415	5170	1.486	278	
573	127.0	639	637	619	361	262	227	186	163	217	244	246	119.5	.355	5900	1.455	265	
609	127.4	699	698	677	377	266	228	182	164	252	277	278	122.0	.326	6370	1.445	261	
572	127.0	773	770	746	394	262	220	166	105	250	281	281	122.1	.285	6980	1.417	249	
608	127.4	845	841	814	415	265	218	160	140	295	322	321	122.7	.258	7490	1.408	246	
571	126.8	897	892	862	426	260	209	143	106	247	293	292	121.8	.233	7910	1.385	236	

(l) Stagnation temperature, T_o, 130 K

Reading	T_o, K	P_o	P_1	P_2	P_3	P_4	P_5	P_6	P_7	P_8	P_9	P_b	T_b	P_t/P_o	G_{max}	S_o	$P_{sat}(S_o)$	$P_{sat}(T_o)$
117-894	130.5	418	419	414	354	281	253	111	48	104	117	120	105.5	0.604	2320	1.809	341	(a)
899	130.7	428	427	422	359	293	263	117	48	107	120	123	105.8	.613	2420	1.784	341	
624	130.1	444	444	437	361	334	322	135	90	119	135	138	108.0	.725	2800	1.695	334	
687	130.7	444	444	439	366	338	307	129	53	118	132	135	107.6	.692	2690	1.733	338	
757	130.3	453	453	446	364	333	321	141	132	198	203	206	115.8	.710	3000	1.689	333	
680	130.1	463	463	457	363	328	316	151	102	134	151	155	110.1	.681	3200	1.661	329	
679	130.6	520	502	493	370	324	308	171	118	154	173	177	112.7	.613	3730	1.635	323	
770	130.3	527	526	516	369	312	294	181	76	170	187	189	114.0	.558	4210	1.601	315	
884	130.3	561	560	548	375	306	284	191	206	293	298	300	123.6	.507	4590	1.577	309	
622	130.4	568	566	554	375	306	283	192	141	182	204	207	115.9	.499	4630	1.576	308	

(m) Stagnation temperature, T_o, 131 K

Reading	T_o, K	P_o	P_1	P_2	P_3	P_4	P_5	P_6	P_7	P_8	P_9	P_b	T_b	P_t/P_o	G_{max}	S_o	$P_{sat}(S_o)$	$P_{sat}(T_o)$
117-945	130.9	385	384	380	318	256	230	94	107	158	161	164	110.0	0.598	1730	[b]2.026	317	(a)
932	130.9	439	438	433	364	305	280	123	83	146	155	157	110.5	.637	2560	1.762	340	
811	130.8	449	447	440	366	338	313	128	78	143	152	153	110.3	.699	2660	1.727	338	
760	131.3	462	462	456	372	340	327	140	208	259	261	264	120.9	.709	2930	1.728	338	
883	131.2	700	698	679	411	303	267	211	238	354	361	362	126.0	.381	5850	1.533	295	
621	130.9	708	706	687	407	298	261	210	98	223	252	253	120.0	.368	5960	1.523	291	
620	131.1	863	861	834	448	295	246	201	106	246	289	289	122.8	.285	7180	1.478	275	

[a]Not applicable.

[b]$S_o > S_c = 1.813$.

TABLE IX. - Continued.

(n) Stagnation temperature, T_o, 132 K

Reading	Stagnation temperature, T_o, K	Stagnation pressure, P_o, N/cm^2	Pressures at stations 1 to 9, N/cm^2 P_1	P_2	P_3	P_4	P_5	P_6	P_7	P_8	P_9	Back-pressure, P_b, N/cm^2	Temperature at back condition, T_b, K	Ratio of throat pressure at stagnation pressure, P_t/P_o	Maximum mass flux, G_{max}, g/cm^2 · max	Stagnation entropy, S_o, J/g · K	Saturation pressure at stagnation entropy, $P_{sat}(S_o)$, N/cm^2	Saturation pressure at stagnation temperature, $P_{sat}(T_o)$, N/cm^2
117-900	132.2	468	466	460	378	344	329	136	52	123	139	140	108.3	0.704	2800	1.767	340	(a)
928	131.8	481	482	474	378	340	327	151	135	208	214	216	116.7	.678	3110	1.718	337	↓
929	132.2	500	499	491	383	340	325	161	143	219	225	227	117.8	.650	3340	1.706	335	↓
809	132.1	559	556	544	389	326	306	184	122	211	222	222	117.5	.547	4150	1.636	324	↓
684	131.9	570	569	558	391	325	303	190	80	180	200	201	115.3	.531	4380	1.621	320	↓
882	132.0	901	897	870	469	304	251	206	236	395	407	406	126.6	.278	7350	1.487	278	↓
768	132.1	918	914	887	473	303	250	205	108	255	301	301	123.7	.272	7560	1.484	277	↓

(o) Stagnation temperature, T_o, 133 K

Reading	T_o	P_o	P_1	P_2	P_3	P_4	P_5	P_6	P_7	P_8	P_9	P_b	T_b	P_t/P_o	G_{max}	S_o	$P_{sat}(S_o)$	$P_{sat}(T_o)$
117-893	132.4	476	476	470	381	345	331	143	92	127	145	148	109.3	0.695	2920	1.760	340	(a)
915	132.9	476	476	469	382	346	331	139	94	166	176	178	112.9	.694	2910	1.789	341	↓
688	132.8	565	563	553	398	335	314	187	76	174	194	195	114.6	.555	4150	1.655	328	↓
685	133.0	669	665	650	419	324	293	209	92	209	235	235	118.5	.439	5250	1.591	313	↓
808	133.1	682	678	660	421	321	289	209	138	259	273	272	121.7	.423	5330	1.588	312	↓

(p) Stagnation temperature, T_o, 134 K

Reading	T_o	P_o	P_1	P_2	P_3	P_4	P_5	P_6	P_7	P_8	P_9	P_b	T_b	P_t/P_o	G_{max}	S_o	$P_{sat}(S_o)$	$P_{sat}(T_o)$
117-662	133.7	483	482	476	387	348	332	139	53	129	144	147	109.2	0.687	2750	[b]1.816	341	(a)
661	133.8	486	486	479	388	349	332	140	65	142	155	158	110.6	.684	2780	[b]1.814	341	↓
663	134.1	490	489	483	390	348	333	141	53	132	148	150	109.6	.679	2790	[b]1.821	341	↓
892	134.2	559	558	549	407	347	326	181	121	163	185	188	113.9	.583	3810	1.711	336	↓
759	133.9	667	666	651	426	332	302	208	307	403	407	409	128.6	.452	5180	1.616	319	↓
754	133.8	845	840	417	468	320	273	221	238	383	393	394	127.3	.324	6780	1.540	297	↓
807	133.7	846	838	314	467	318	271	219	136	295	320	317	125.0	.321	6650	1.537	296	↓

(q) Stagnation temperature, T_o, 135 K

Reading	T_o	P_o	P_1	P_2	P_3	P_4	P_5	P_6	P_7	P_8	P_9	P_b	T_b	P_t/P_o	G_{max}	S_o	$P_{sat}(S_o)$	$P_{sat}(T_o)$
117-946	135.9	429	429	423	339	290	275	110	125	186	189	192	114.4	0.644	1960	[b]2.088	298	(a)
817	134.9	431	429	422	343	302	279	108	93	154	159	161	111.2	.647	1910	[b]2.043	312	↓
942	135.2	460	460	454	370	330	309	123	106	170	177	180	113.1	.672	2250	[b]1.964	330	↓
664	135.1	521	519	512	401	351	332	157	58	144	162	164	111.3	.638	3090	1.805	341	↓
902	135.2	577	574	564	417	350	328	184	72	169	190	190	114.2	.568	3880	1.727	338	↓
922	136.1	577	574	564	420	353	330	180	119	216	228	228	117.9	.572	3710	1.760	340	↓
758	134.9	848	842	420	477	329	283	226	310	459	466	466	129.5	.334	6640	1.562	304	↓
689	136.0	860	855	833	490	330	292	230	105	250	288	287	122.7	.340	6470	1.581	310	↓

[a]Not applicable.

[b]$S_o > S_c = 1.813$.

TABLE IX. - Concluded.

(r) Stagnation temperature, T_o, 138 K

Reading	Stagnation temperature, T_o, K	Stagnation pressure, P_o, N/cm^2	Pressures at stations 1 to 9, N/cm^2									Back-pressure, P_b, N/cm^2	Temperature at back condition, T_b, K	Ratio of throat pressure at stagnation pressure, P_t/P_o	Maximum mass flux, G_{max}, g/cm$^2\cdot$sec	Stagnation entropy, S_o, J/g·K	Saturation pressure at stagnation entropy, $P_{sat}(S_o)$, N/cm^2	Saturation pressure at stagnation temperature, $P_{sat}(T_o)$, N/cm^2
			P_1	P_2	P_3	P_4	P_5	P_6	P_7	P_8	P_9							
117-940	138.0	559	557	549	420	355	331	172	210	287	291	293	123.1	0.592	3180	[b]1.858	341	(a)
658	138.2	692	690	677	463	363	327	207	269	373	378	379	128.5	.473	4630	1.718	337	↓
912	138.2	765	763	745	482	361	319	223	162	297	313	314	124.6	.416	5370	1.672	331	↓
890	138.2	928	925	900	528	358	301	237	179	258	303	304	123.9	.325	6700	1.604	316	↓

(s) Stagnation temperature, T_o, 140 K

Reading	T_o	P_o	P_1	P_2	P_3	P_4	P_5	P_6	P_7	P_8	P_9	P_b	T_b	P_t/P_o	G_{max}	S_o	$P_{sat}(S_o)$	$P_{sat}(T_o)$
117-669	139.8	536	535	528	408	339	317	154	55	138	159	161	111.0	0.591	2670	[b]1.968	330	(a)
668	139.3	596	595	586	439	361	332	182	67	167	189	190	114.2	.558	3400	[b]1.849	341	↓
657	139.1	766	763	747	490	368	324	223	283	406	411	412	130.0	.423	5200	1.694	334	↓
923	139.9	779	774	757	499	372	326	223	153	292	311	309	124.3	.419	5240	1.706	335	↓
656	139.8	857	853	833	520	373	319	237	298	441	448	449	131.1	.373	5870	1.665	329	↓
938	139.3	865	862	841	520	369	315	237	293	441	448	448	131.0	.364	6040	1.650	327	↓
911	139.5	920	915	891	535	368	310	240	179	342	365	365	127.6	.337	6460	1.633	323	↓
904	140.3	937	931	908	548	376	314	242	107	261	304	301	123.8	.336	6470	1.643	325	↓

(t) Stagnation temperature, T_o, 156 K

Reading	T_o	P_o	P_1	P_2	P_3	P_4	P_5	P_6	P_7	P_8	P_9	P_b	T_b	P_t/P_o	G_{max}	S_o	$P_{sat}(S_o)$	$P_{sat}(T_o)$
117-729	158.4	666	665	656	497	374	319	138	139	227	240	240	130.1	0.479	2660	[b]2.211	244	(a)
671	156.3	693	691	682	512	385	329	150	61	158	187	188	119.3	.474	2860	[b]2.149	274	↓
751	155.1	705	703	693	518	389	331	155	63	163	192	194	118.0	.470	3090	[b]2.116	289	↓
948	153.8	756	753	742	546	406	345	173	211	324	333	332	129.8	.456	3500	[b]2.046	313	↓
670	154.4	870	865	851	610	445	373	204	87	221	257	257	120.4	.429	4100	[b]1.964	330	↓
947	157.8	950	946	929	661	479	398	211	252	400	412	410	134.9	.419	4480	[b]1.975	328	↓

(u) Stagnation temperature, T_o, 177 K

Reading	T_o	P_o	P_1	P_2	P_3	P_4	P_5	P_6	P_7	P_8	P_9	P_b	T_b	P_t/P_o	G_{max}	S_o	$P_{sat}(S_o)$	$P_{sat}(T_o)$
117-506	179.3	473	471	464	360	274	236	78	47	109	125	127	281.8	0.500	1450	[b]2.623	58	(a)
697	175.0	590	587	579	447	338	290	97	59	140	161	162	269.4	.492	1950	[b]2.483	106	↓
691	176.8	696	694	685	523	396	339	113	119	202	221	221	268.8	.487	2330	[b]2.416	36	↓
672	175.5	880	877	865	650	486	413	149	65	201	234	234	142.3	.469	3140	[b]2.275	210	↓
690	178.2	912	906	894	672	502	426	148	156	262	289	288	263.8	.467	3200	[b]2.290	207	↓

(v) Stagnation temperature, T_o, 234 K

Reading	T_o	P_o	P_1	P_2	P_3	P_4	P_5	P_6	P_7	P_8	P_9	P_b	T_b	P_t/P_o	G_{max}	S_o	$P_{sat}(S_o)$	$P_{sat}(T_o)$
117-726	234.7	85	87	85	68	53	45	15	18	31	30	34	232.3	0.527	200	[b]3.526	(c)	(a)
725	234.8	149	151	148	117	90	77	26	32	53	54	58	231.5	.515	340	[b]3.353	(c)	(a)
747	233.1	313	311	308	241	182	155	97	159	187	188	191	227.5	.495	820	[b]3.105	(c)	(a)

[a]Not applicable.

[b]$S_o > S_c = 1.813$.

[c]$P_{sat}(S_o) < 10$ N/cm^2.

TABLE X. - DATA FOR METHANE - ELLIPTICAL NOZZLE

Reading	Stagnation temperature, T_o, K	Stagnation pressure, P_o, N/cm^2	Pressures at stations 1 to 9, N/cm^2									Back-pressure, P_b, N/cm^2	Temperature at back condition, T_b, K	Ratio of throat pressure at stagnation pressure, P_t/P_o	Maximum mass flux, G_{max}, g/cm^2 · sec	Stagnation entropy, S_o, J/g · K	Saturation pressure at stagnation entropy, $P_{sat}(S_o)$, N/cm^2	Saturation pressure at stagnation temperature, $P_{sat}(T_o)$, N/cm^2
			P_1	P_2	P_3	P_4	P_5	P_6	P_7	P_8	P_9							
(a) Stagnation temperature, T_o, 123 K																		
117-1098	123.4	149	152	146	58	31	23	22	20	22	30	38	124.1	0.154	3030	5.268	24	24
1093	123.0	182	185	177	65	32	23	21	23	61	64	69	124.0	.125	3420	5.254	23	↓
969	123.0	292	295	281	100	43	28	26	---	51	84	82	125.2	.094	4370	5.244	22	↓
965	123.1	324	326	311	106	41	23	21	---	38	72	79	124.4	.073	4690	5.244	22	↓
966	121.8	425	426	406	133	47	22	20	---	42	87	93	123.4	.052	5430	5.197	20	22
1036	123.9	478	478	455	153	51	24	21	50	200	205	208	125.0	.050	5710	5.253	23	25
967	121.1	510	510	487	155	51	21	19	---	45	101	106	122.9	.042	5980	5.169	19	21
1035	122.6	613	613	583	187	59	26	21	77	271	278	279	124.3	.042	6540	5.204	20	23
968	121.5	717	715	682	209	65	26	20	---	90	158	161	124.0	.036	7100	5.164	19	21
(b) Stagnation temperature, T_o, 126 K																		
117-1096	127.7	65	69	67	40	32	28	28	26	28	30	36	127.8	0.425	1680	5.400	32	32
1095	125.6	89	92	89	44	30	25	26	25	38	38	44	125.8	.284	2170	5.338	28	28
1097	124.8	112	115	111	49	31	25	24	22	23	29	36	125.3	.221	2520	5.313	26	27
1094	124.2	116	118	114	50	30	23	24	23	43	45	50	124.6	.203	2590	5.295	25	26
1038	127.6	278	280	267	99	44	29	27	42	123	125	130	128.2	.105	4200	5.377	30	32
1037	125.8	358	360	342	121	46	26	24	44	154	157	161	126.6	.074	4870	5.318	26	28
1010	127.8	618	619	590	192	63	31	26	90	280	285	288	129.3	.050	6430	5.351	28	32
1009	126.3	737	737	701	222	71	33	24	36	233	244	246	128.6	.045	7100	5.299	25	29
(c) Stagnation temperature, T_o, 133 K																		
117-1040	132.8	160	162	155	74	47	39	34	34	39	48	56	133.0	0.242	2910	5.533	42	43
1013	136.1	216	217	209	93	57	45	42	49	101	101	107	136.3	.207	3410	5.616	50	52
1039	129.6	220	222	212	85	44	32	29	34	35	87	92	130.1	.147	3640	5.438	35	36
1012	133.3	284	285	272	108	54	39	35	50	130	131	136	133.8	.136	4100	5.533	42	45
1011	131.2	391	392	374	136	56	35	30	58	176	179	183	132.1	.991	4970	5.465	37	40

TABLE X. - Concluded.

(d) Stagnation temperature, T_o, 154 K

Reading	Stagnation temperature, K_o, K	Stagnation pressure, P_o, N/cm^2	Pressures at stations 1 to 9, N/cm^2									Back-pressure, P_b, N/cm^2	Temperature at back condition, T_b, K	Ratio of throat pressure to stagnation pressure, P_t/P_o	Maximum mass flux, G_{max}, g/cm^2 · sec	Stagnation entropy, S_o, J/g · K	Saturation pressure at stagnation entropy, $P_{sat}(S_o)$, N/cm^2	Saturation pressure at stagnation temperature, $P_{sat}(T_o)$, N/cm^2
			P_1	P_2	P_3	P_4	P_5	P_6	P_7	P_8	P_9							
117- 988	156.6	226	230	225	150	115	101	98	100	132	135	143	156.1	0.448	2650	6.164	135	139
989	156.4	283	288	280	171	130	112	90	95	133	142	148	156.2	.397	3200	6.148	132	138
987	155.1	293	296	288	169	127	110	87	97	145	149	156	155.1	.375	3360	6.111	125	131
986	154.0	352	354	343	181	127	107	80	105	181	184	190	154.0	.304	3930	6.072	117	125
990	155.1	425	428	413	203	135	111	68	87	151	168	174	155.3	.262	4420	6.090	120	131
985	152.8	427	428	413	196	125	100	74	118	222	226	232	153.0	.235	4550	6.029	109	118
991	154.4	559	561	540	237	136	104	69	97	222	231	235	154.7	.185	5330	6.051	113	127
984	151.5	573	574	553	232	126	91	68	145	293	299	303	151.9	.159	5560	5.975	99	112
992	153.9	693	694	666	272	140	100	69	103	276	286	289	154.4	.144	6080	6.020	107	124
993	154.3	747	747	718	288	144	100	70	105	297	308	310	154.8	.134	6330	6.023	108	126
983	150.1	772	773	741	284	130	86	66	190	389	398	401	150.9	.112	6680	5.914	89	105
(e) Stagnation temperature, T_o, 167 K																		
117-1044	167.3	424	424	412	248	175	149	126	156	218	226	230	166.6	0.351	3740	6.413	195	211
1043	166.9	492	492	477	272	200	172	101	148	216	229	233	166.1	.349	4190	6.387	189	208
1042	166.6	599	599	578	301	208	176	87	143	236	252	256	165.7	.295	4900	6.357	181	206
(f) Stagnation temperature, T_o, 184 K																		
117-1017	182.1	501	500	489	327	258	238	221	177	226	241	245	169.3	0.475	3420	6.786	315	351
1023	184.1	555	555	542	359	281	257	232	117	240	254	255	170.6	.464	3620	6.818	326	374
1025	185.5	576	575	562	377	300	275	241	190	243	262	265	171.9	.477	3620	6.849	337	391
1016	182.3	628	627	611	369	263	225	194	198	301	310	314	177.3	.358	4230	6.737	298	353
1024	185.6	737	735	714	423	305	261	216	131	285	307	308	176.7	.355	4620	6.781	313	393
1015	182.3	746	746	723	411	293	252	168	166	304	320	324	178.3	.337	4860	6.697	284	353
(g) Stagnation temperature, T_o, 195 K																		
117- 996	194.4	625	627	618	476	425	406	223	199	293	303	307	176.5	0.649	2910	7.158	429	---
995	195.6	724	725	711	498	417	388	259	242	356	366	369	182.7	.536	3630	7.108	417	---
994	194.7	747	748	733	498	405	373	268	258	374	384	388	184.3	.499	3900	7.060	405	---
(h) Stagnation temperature, T_o, 200 K																		
117-1101	198.2	690	690	680	519	454	436	236	161	211	238	242	169.0	0.632	2980	7.247	444	---
1100	200.0	802	800	785	551	452	424	268	194	255	288	292	174.8	.529	3690	7.199	436	---
1099	201.2	925	920	901	585	449	410	294	219	295	335	338	179.7	.443	4390	7.150	427	---

TABLE XI. - DATA FOR HYDROGEN - ELLIPTICAL NOZZLE

(a) Stagnation temperature, T_o, 28 K

Reading	Stagnation temperature, T_o, K	Stagnation pressure, P_o, N/cm^2	Pressures at stations 1 to 9, N/cm^2 P_1	P_2	P_3	P_4	P_5	P_6	P_7	P_8	P_9	Back-pressure, P_b, N/cm^2	Temperature at back condition, T_b, K	Ratio of throat pressure to stagnation pressure, P_t/P_o	Maximum mass flux, G_{max}, g/cm^2·sec	Stagnation entropy, S_o, J/g·K	Saturation pressure at stagnation entropy, $P_{sat}(S_o)$, N/cm^2	Saturation pressure at stagnation temperature, $P_{sat}(T_o)$, N/cm^2
117-1199	27.8	293	295	284	118	58	42	18	26	65	82	87	28.4	0.143	1700	10.80	39	57
1200	27.2	340	231	327	127	57	38	17	24	59	85	90	28.2	.113	1870	10.39	33	51
1212	28.7	431	430	413	161	68	45	20	37	127	136	138	29.6	.104	2090	10.80	39	66
1210	28.7	471	470	452	172	69	46	20	33	103	128	129	29.7	.098	2210	10.70	38	66
1222	28.1	582	579	557	206	72	43	20	55	209	216	217	29.9	.074	2500	10.19	31	60
1216	28.6	589	587	564	210	76	44	20	36	133	160	161	30.2	.075	2510	10.38	33	65

(b) Stagnation temperature, T_o, 30 K

Reading	T_o, K	P_o, N/cm^2	P_1	P_2	P_3	P_4	P_5	P_6	P_7	P_8	P_9	P_b, N/cm^2	T_b, K	P_t/P_o	G_{max}, g/cm^2·sec	S_o, J/g·K	$P_{sat}(S_o)$, N/cm^2	$P_{sat}(T_o)$, N/cm^2
117-1197	30.7	129	133	128	75	51	47	43	41	62	64	69	28.7	0.364	890	13.27	83	92
1198	29.0	219	222	213	101	62	51	18	34	70	76	82	29.0	.232	1370	11.66	53	70
1207	30.3	288	288	277	126	72	63	24	64	133	135	137	30.4	.220	1570	12.02	59	86
1213	29.5	356	356	342	142	69	49	21	41	118	124	126	29.8	.139	1840	11.38	48	76
1206	29.5	360	360	346	145	69	67	22	49	137	141	143	30.0	.185	1850	11.37	48	76
1219	30.6	370	370	356	152	77	57	22	37	98	113	115	30.5	.154	1830	11.84	56	90
1211	29.1	422	421	405	160	69	46	20	34	100	120	122	29.8	.110	2050	11.00	43	71
1217	30.3	421	420	405	166	77	54	22	43	126	137	138	30.6	.128	1990	11.53	51	86
1223	29.8	425	425	409	165	74	51	22	56	163	169	170	30.3	.119	2020	11.30	47	80

(c) Stagnation temperature, T_o, 32 K

Reading	T_o, K	P_o, N/cm^2	P_1	P_2	P_3	P_4	P_5	P_6	P_7	P_8	P_9	P_b, N/cm^2	T_b, K	P_t/P_o	G_{max}, g/cm^2·sec	S_o, J/g·K	$P_{sat}(S_o)$, N/cm^2	$P_{sat}(T_o)$, N/cm^2
117-1215	32.3	167	168	164	106	83	75	59	69	95	95	98	31.1	0.448	900	14.10	97	117
1214	31.0	223	224	217	112	74	62	35	67	111	113	115	30.7	.276	1270	12.72	72	96
1221	32.2	221	222	215	119	80	66	50	48	87	91	93	30.7	.298	1190	13.47	86	115
1224	31.3	281	285	272	131	79	65	32	75	138	141	143	31.0	.231	1500	12.56	69	101
1218	32.3	285	284	275	140	89	74	39	73	127	130	132	31.6	.260	1430	13.09	79	117
1220	31.3	290	291	281	132	80	65	22	45	98	105	107	30.7	.225	1520	12.52	69	101
1201	32.2	294	295	286	152	96	74	33	36	76	90	95	30.1	.252	1420	12.98	77	115

TABLE XII. - DATA FOR NITROGEN WITH SPECIAL EMPHASIS ON THERMODYNAMIC

CRITICAL REGION - ELLIPTICAL NOZZLE

Reading	Stagnation temperature, T_o, K	Pressures at stations 1 to 9, N/cm^2									Ratio of throat pressure to stagnation pressure, P_t/P_o	Maximum mass flux, G_{max}, g/cm^2 · sec	Stagnation entropy, S_o, J/g · K	Saturation pressure at stagnation entropy, $P_{sat}(S_o)$, N/cm^2	Saturation pressure at stagnation temperature, $P_{sat}(T_o)$, N/cm^2
		P_1	P_2	P_3	P_4	P_5	P_6	P_7	P_8	P_9					
416- 79	118.3	389	381	220	143	121	98	87	100	117	0.311	4850	1.314	205	231
80	118.6	391	382	221	144	123	103	88	148	158	.315	4890	1.321	208	234
81	119.4	421	412	242	162	136	112	89	101	119	.323	5030	1.332	213	244
82	119.7	421	412	243	163	138	120	89	146	160	.328	5000	1.340	216	248
102	120.0	290	288	210	183	175	161	62	72	83	.603	3190	1.399	242	251
103	120.1	291	289	212	184	177	162	63	117	125	.608	3160	1.402	243	253
108	121.5	389	382	249	191	174	163	79	84	107	.447	4350	1.399	242	271
109	121.8	391	384	252	196	178	166	79	156	167	.455	4290	1.407	245	275
84	125.3	326	325	275	216	193	89	34	51	61	.592	1980	1.644	325	326
85	125.3	327	327	276	216	194	91	61	101	109	.593	2030	1.638	324	326
48	125.5	340	339	284	221	199	96	36	54	66	.585	2180	1.612	318	328
49	125.4	340	339	286	221	200	96	64	105	111	.588	2210	1.603	316	327
87	126.2	358	357	309	235	212	102	38	55	67	.592	2260	1.623	321	340
88	126.2	358	358	309	236	213	102	72	108	116	.595	2260	1.623	321	↓
32	126.2	342	339	286	221	199	89	33	50	63	.582	2050	1.702	335	↓
33	126.2	344	341	287	222	200	89	52	60	103	.581	2040	1.682	332	↓
93	126.2	342	342	287	225	202	92	34	52	63	.591	2010	1.702	335	↓
94	126.2	343	344	288	↓	202	91	69	115	121	.589	2000	1.691	333	↓
95	126.3	344	344	289	↓	203	91	112	157	159	.590	2000	1.706	335	342
96	126.3	345	345	289	↓	203	94	151	192	192	.588	1990	1.694	334	342
97	126.4	345	345	290	226	203	149	202	227	227	.588	1980	1.725	337	(a)
98	126.4	346	345	291	225	203	210	250	271	270	.587	1970	1.709	336	↓
26	126.7	367	363	313	240	217	103	38	57	71	.591	2280	1.640	325	↓
27	126.7	370	367	317	242	218	104	76	105	115	.589	2330	1.632	323	↓
91	127.9	422	420	340	314	302	138	54	71	88	.716	3000	1.611	318	↓
92	128.0	424	421	341	314	303	138	55	121	134	.715	2980	1.613	318	↓
54	128.0	396	394	336	264	240	113	42	60	76	.606	2440	1.666	330	↓
55	128.0	393	391	334	260	236	111	45	97	109	.601	2390	1.674	331	↓
42	130.3	421	418	355	282	251	114	42	---	77	.596	2300	1.778	341	↓
43	130.5	423	420	356	285	253	114	60	120	131	.598	2320	1.787	341	↓

[a]Not applicable.

TABLE XIII. - DATA FOR NITROGEN FROM INITIAL FLOW RATE STUDIES -

ELLIPTICAL NOZZLE

Reading	Stagnation temperature, T_o, K	Pressures at stations 1, 5, and 9, N/cm^2			Ratio of throat pressure to stagnation pressure, P_t/P_o	Maximum mass flux, G_{max}, g/cm^2 · sec	Stagnation entropy, S_o, J/g · K	Saturation pressure at stagnation entropy, $P_{sat}(S_o)$, N/cm^2	Saturation pressure at stagnation temperature, $P_{sat}(T_o)$, N/cm^2
		P_1	P_5	P_9					
616-352	89.9	113	30	38	0.265	3340	0.719	35	36
338	89.9	152	30	43	.197	4050	.716	34	↓
356	89.9	202	28	54	.139	4890	.711	34	↓
367	90.0	253	29	66	.115	5520	.709	33	↓
298	90.1	294	29	43	.009	5890	.708	33	↓
375	90.0	323	29	72	.090	6280	.703	33	↓
409	90.0	344	28	80	.081	6530	.701	32	↓
312	90.4	384	30	42	.078	6850	.707	33	37
393	90.0	425	28	88	.066	7330	.694	32	36
340	99.9	154	58	56	.377	3340	.936	75	77
358	99.8	202	63	67	.312	4140	.928	73	77
370	99.9	253	62	76	.245	4880	.924	72	77
299	100.1	295	62	100	.210	5290	.924	72	78
377	100.1	319	61	95	.191	5660	.921	71	↓
403	100.1	344	61	104	.177	5920	.918	71	↓
314	100.1	384	60	79	.156	6320	.914	70	↓
396	100.1	426	59	78	.138	6770	.909	68	↓
342	109.1	153	66	62	.431	2810	1.167	145	146
372	110.0	253	81	88	.320	4200	1.148	139	147
302	110.0	297	102	93	.343	4550	1.140	136	147
380	110.1	324	107	99	.330	4840	1.138	135	148
406	110.0	346	110	100	.318	5110	1.132	133	147
316	110.0	386	113	105	.293	5480	1.125	130	147
398	110.0	426	111	109	.261	5970	1.118	128	147
374	120.1	255	189	70	.741	2470	1.423	252	253
303	120.0	295	170	135	.576	3340	1.396	241	251
381	120.0	326	152	145	.466	4010	1.382	234	251
407	120.0	346	146	153	.422	4260	1.374	231	251
317	120.0	385	138	152	.358	4640	1.359	224	251
387	120.0	425	138	166	.325	5040	1.346	219	251
413	125.0	345	249	112	.722	2370	1.565	305	321
319	125.0	387	255	117	.659	3250	1.519	290	321
399	125.1	427	234	166	.548	4040	1.495	281	323

TABLE XIV. - CHOKED AND UNCHOKED PRESSURE DISTRIBUTION IN 3.5° CONICAL NOZZLE

Reading	Stagnation temperature, T_o, K	Stagnation pressure, P_o, N/cm²	Pressures at stations 1 to 15, N/cm²															Backpressure, P_b, N/cm²	Temperature at back condition, T_b, K	Ratio of throat pressure to stagnation pressure, P_t/P_o	Mass flux, G, g/cm² · sec	Stagnation entropy, S_o, J/g · K	Saturation pressure at stagnation entropy, $P_{sat}(S_o)$, N/cm²	Saturation pressure at stagnation temperature, $P_{sat}(T_o)$, N/cm²
			P_1	P_2	P_3	P_4	P_5	P_6	P_7	P_8	P_9	P_{10}	P_{11}	P_{12}	P_{13}	P_{14}	P_{15}							
101-1331	109.1	471	472	471	471	451	421	385	342	318	309	308	370	379	385	398	409	412	109.3	0.654	4370	1.092	119	139
1332	109.4	465	466	466	465	431	379	317	244	199	184	182	288	304	315	336	357	360	109.5	.391	5650	1.099	122	142
1333	109.9	463	463	463	461	422	360	286	200	145	127	126	99	109	117	132	163	177	109.6	.269	6160	1.111	125	146
1334	111.0	463	463	462	461	422	362	289	204	150	133	130	50	39	31	45	51	54	95.0	.281	6050	1.133	133	155
1350	109.7	227	227	227	227	218	204	188	168	156	152	152	181	185	188	194	199	200	109.7	.669	2920	1.147	138	144
1351	109.9	226	225	226	226	214	195	173	147	130	124	116	130	134	139	150	161	162	109.7	.511	3340	1.152	140	146
1352	110.2	226	225	226	225	213	195	173	146	128	121	109	112	114	117	122	131	136	109.0	.483	3340	1.160	143	149
1353	110.5	225	225	226	225	213	195	172	146	127	119	106	102	104	106	110	116	122	106.8	.469	3330	1.166	145	151
1354	110.9	225	225	225	225	213	194	172	145	125	117	100	55	58	60	65	69	72	98.8	.446	3350	1.176	149	155
1344	283.1	353	353	354	353	342	324	299	259	218	208	190	42	31	20	8	13	18	269.9	.537	879	3.282	---	---
1345	277.9	354	353	353	353	342	324	299	259	219	207	190	42	31	27	45	56	66	272.5	.537	824	3.262	---	---

TABLE XV. - CORRESPONDING-STATES NORMALIZING PARAMETERS

Fluid	Critical pressure, P_c, N/cm²	Critical temperature, T_c, K	Critical density, ρ_c, g/cm³	Critical entropy, S_c, J/g · K	Compressibility factor, Z_c	Mass flux G*, g/cm² · sec
Nitrogen	341.7	126.3	0.3105	1.813	0.2937	6010.4
Methane	462.7	190.8	.162	4.214	.2889	5093.7
Hydrogen	129.3	32.98	.03143	17.773	.3023	1158

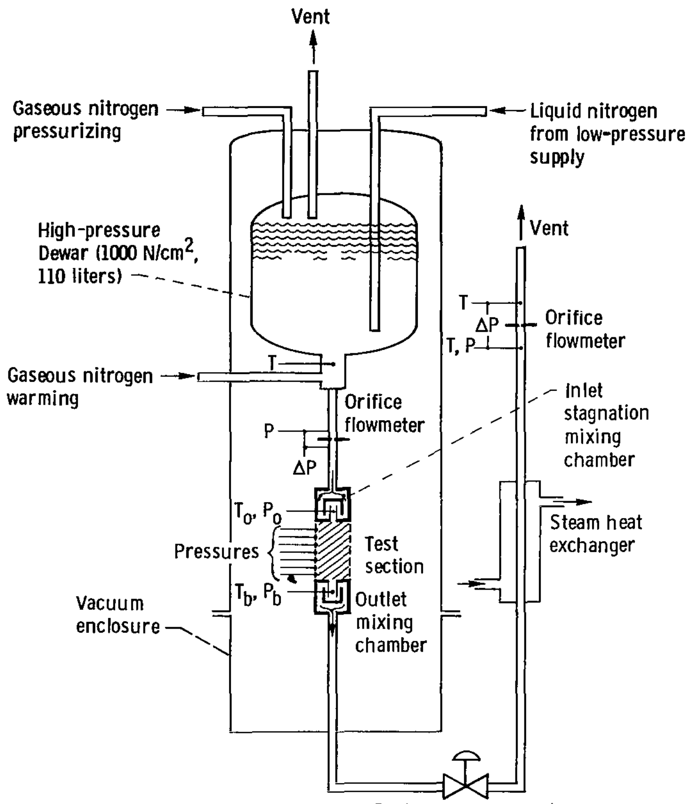

Figure 1. - Flow system schematic for nitrogen two-phase-choked-flow rig (110-liter capacity).

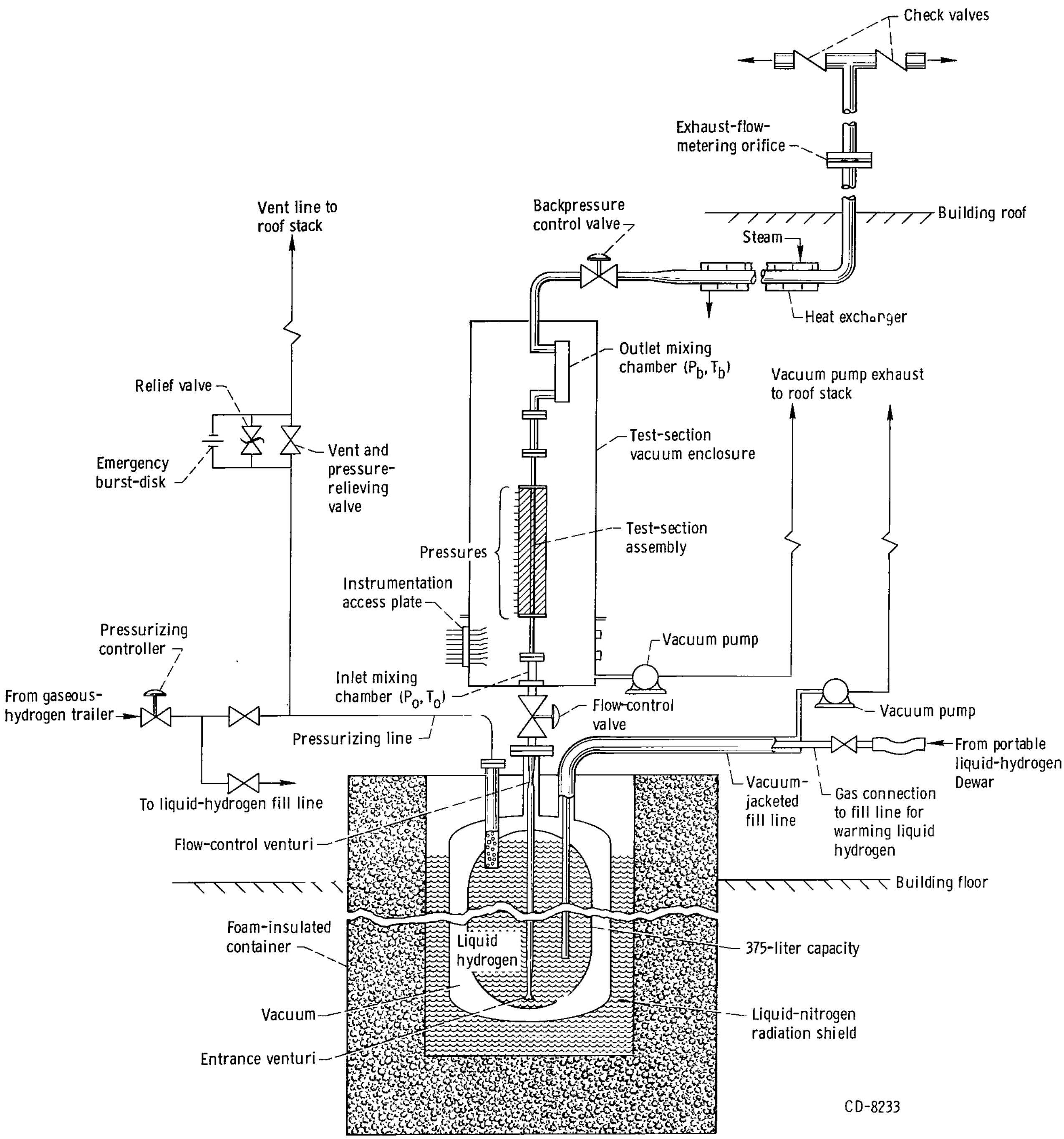

Figure 2. - Flow system schematic for liquid-hydrogen and -methane choked-flow rig (375-liter capacity).

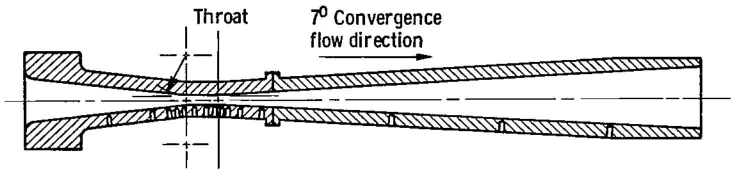

Figure 3. - Axisymmetric converging-diverging nozzle with conical convergence and divergence. Throat area, A_t, 0.0993 cm^2.

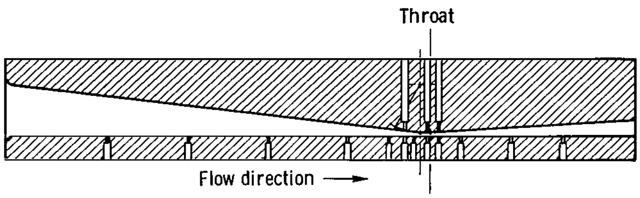

Figure 4. - Two-dimensional converging-diverging nozzle. Convergence at 7° and divergence at 3.5°; throat area, A_t, 0.1104 cm^2.

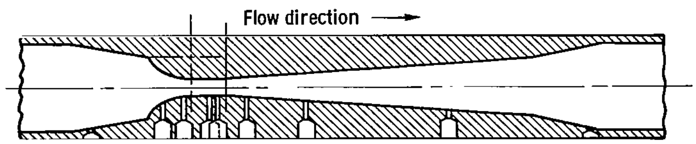

Figure 5. - Axisymmetric converging-diverging nozzle with 2:1 elliptical convergence. Throat area, A_t, 0.0676 cm^2.

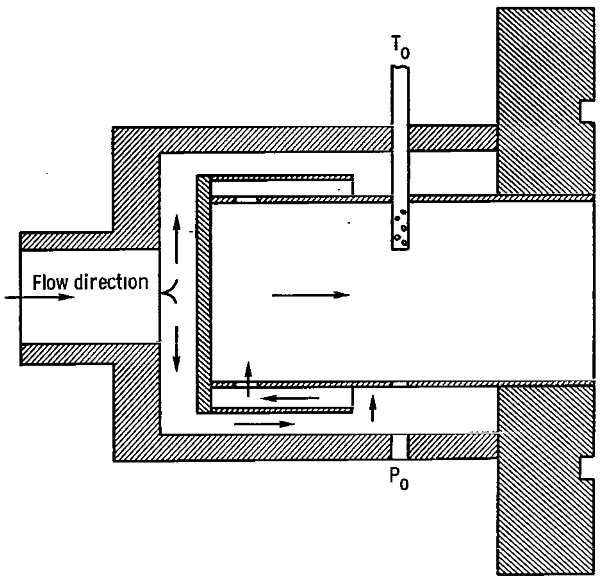

Figure 6. - Inlet and outlet mixing chambers for conical and two-dimensional nozzles.

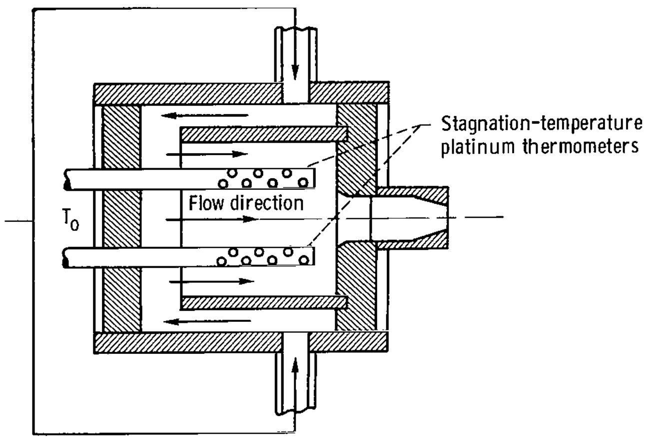

Figure 7. - Inlet mixing (stagnation) chamber for elliptical nozzle.

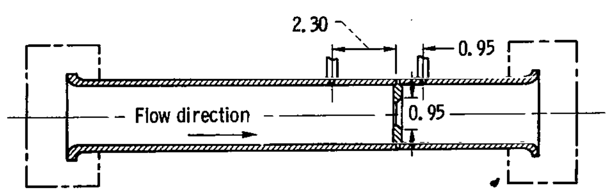

Figure 8. - Flowmeter used in two-phase-critical-flow rig. (All dimensions are in cm.)

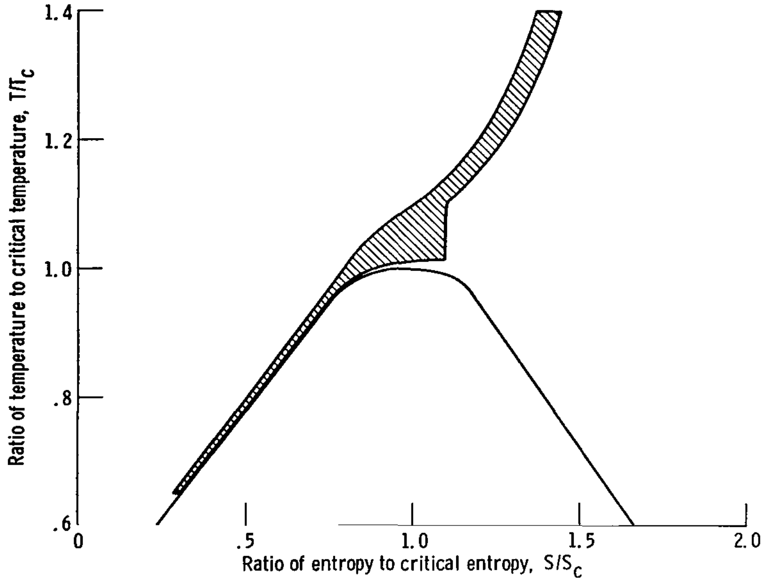

Figure 9. - Range of stagnation conditions of experiments.

Nozzle	Stagnation temperature, T_0, K	Stagnation pressure, P_0, N/cm^2	Ratio of throat to stagnation pressure: Measured	Ratio of throat to stagnation pressure: Calculated	Mass flux (maximum), $g/cm^2 \cdot sec$: Measured, G_{meas}	Mass flux (maximum), $g/cm^2 \cdot sec$: Calculated, G_{calc}	Mass flux ratio, G_{meas}/G_{calc}
○ 7^0 conical	272	356	0.522	0.524	846	872	0.970
△ 3.5^0 conical	276.5	351	.537	↓	820	852	.962
□ Two dimensional	284	343	.565	↓	790	820	.963
D Elliptical	233	313	.495	↓	820	835	.982

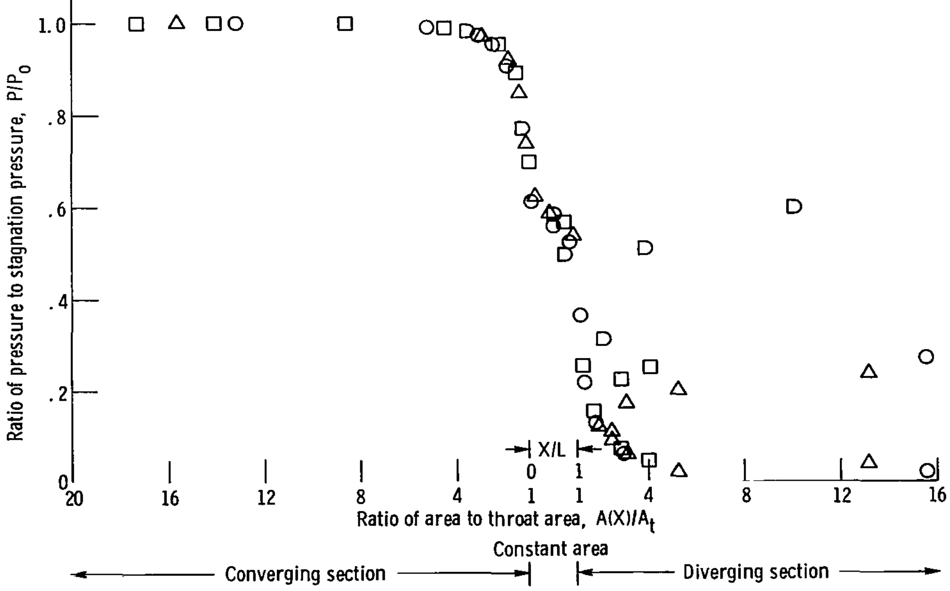

Figure 10. - Gas profiles in the four nozzles of this experiment.

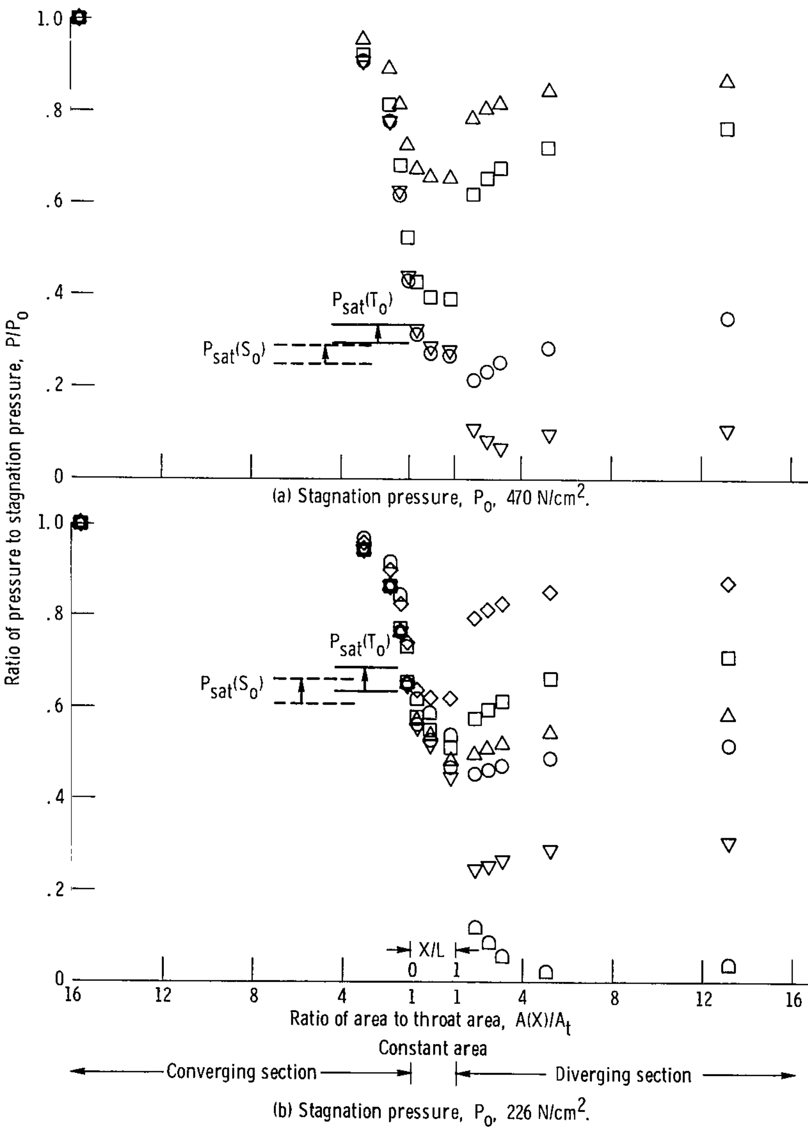

Symbol	Reading	Stagnation temperature, T_0, K	Stagnation pressure, P_0, N/cm^2	Mass flux, G, $g/cm^2 \cdot sec$	Temperature at back conditions, T_b, K	Pressure at back conditions, P_b, N/cm^2
△	1331	109.1	472	4372	109.3	412
□	1332	109.4	465	5652	109.5	360
○	1333	109.9	463	6157	109.6	177
▽	1334	111.0	463	6052	95.0	54
◇	1350	109.7	227	2922	109.7	200
□	1351	109.9	226	3337	109.7	162
△	1352	110.2	226	3342	109.0	136
○	1353	110.5	225	3333	106.8	122
▽	1354	110.9	225	3348	98.8	72
⌂	1344	283.1	354	819	269.9	18

Figure 11. - Choked and unchoked nitrogen axial pressure profiles in 3.5° conical nozzle. Stagnation temperature, T_0, 110 K.

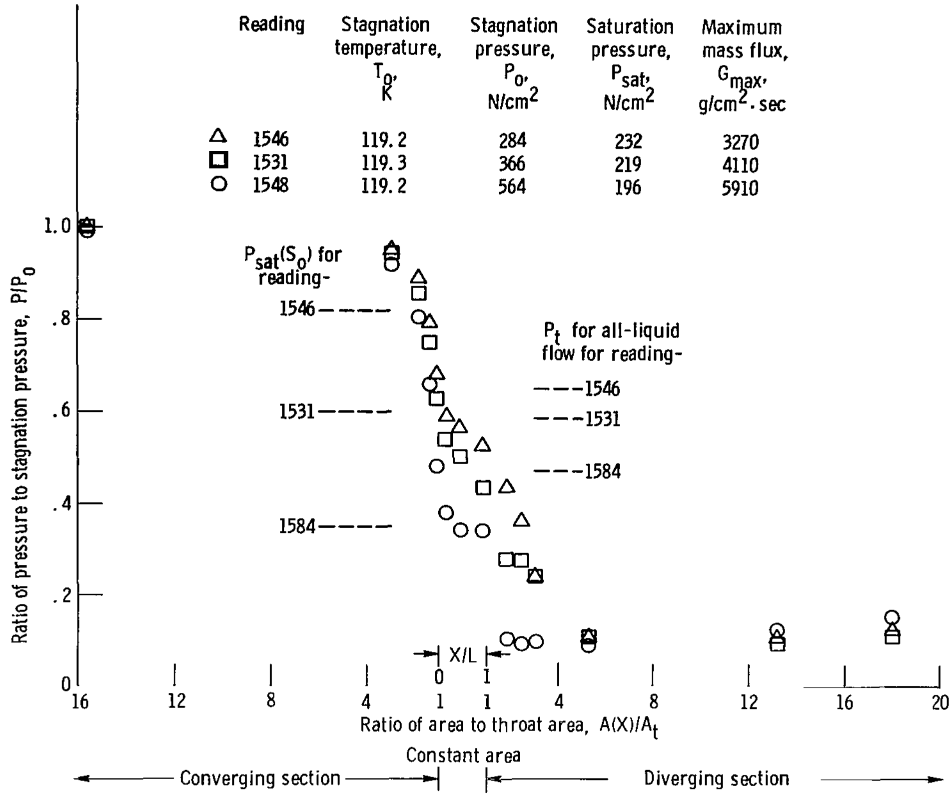

Figure 12. - Nitrogen axial pressure profiles at various stagnation pressures in 3.5° conical nozzle.

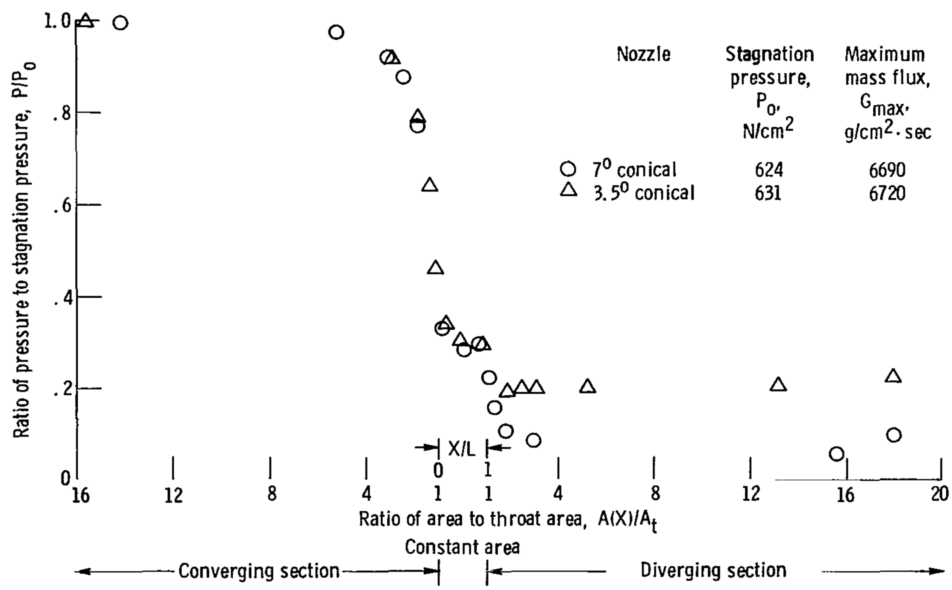

Figure 13. - Nitrogen pressure profiles in two conical nozzles at high stagnation pressure. Stagnation temperature, T_0, 119.2 K; saturation pressure at stagnation entropy, $P_{sat}(S_0)$, 190 N/cm^2.

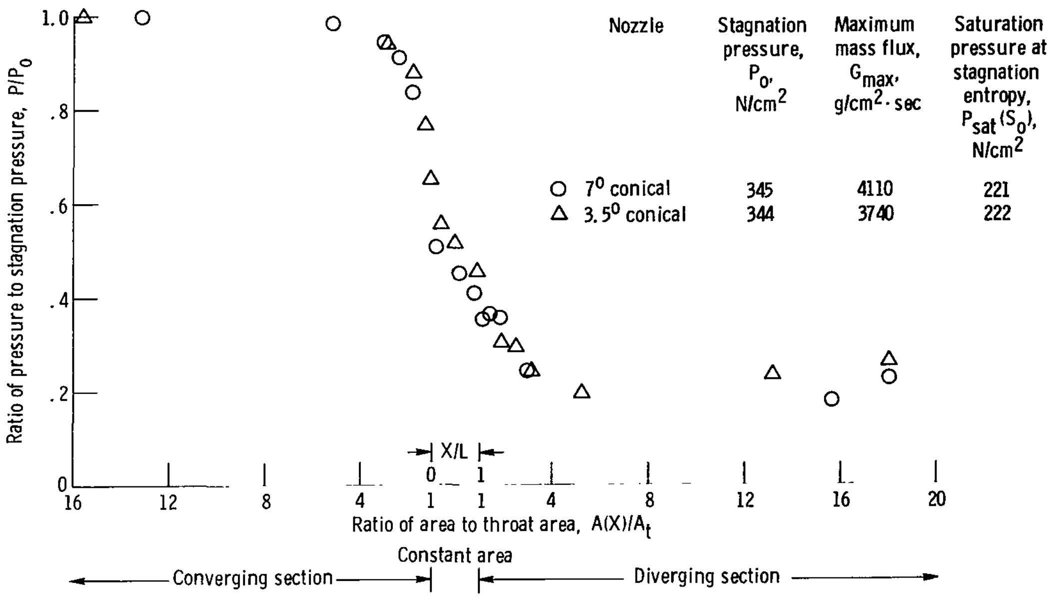

Figure 14. - Nitrogen axial pressure profiles in two conical nozzles at low stagnation pressure. Stagnation temperature, T_0, 119.2 K.

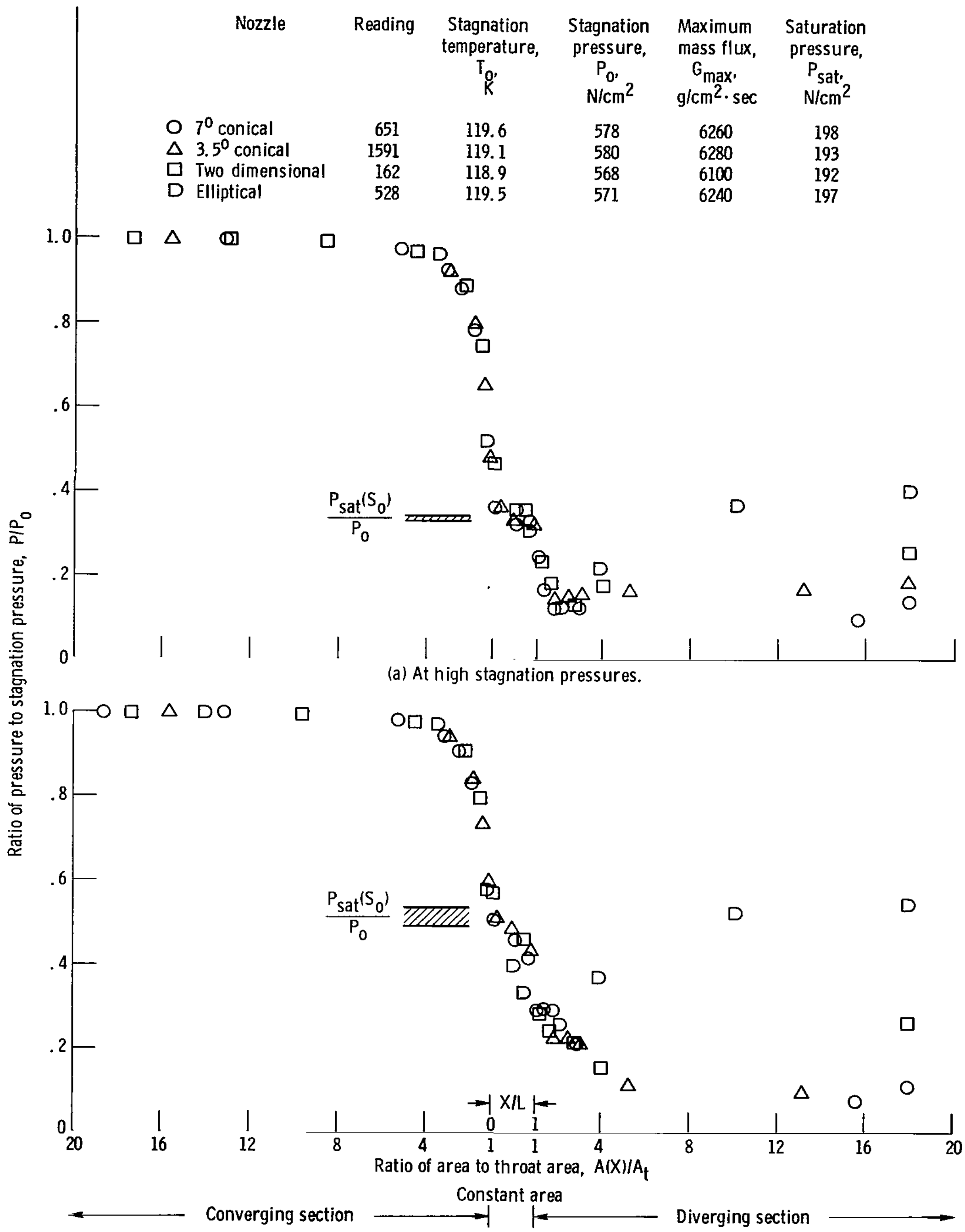

(b) At low stagnation pressures.

Figure 15. - Comparison of axial pressure profiles in all four nozzles with nitrogen profile.

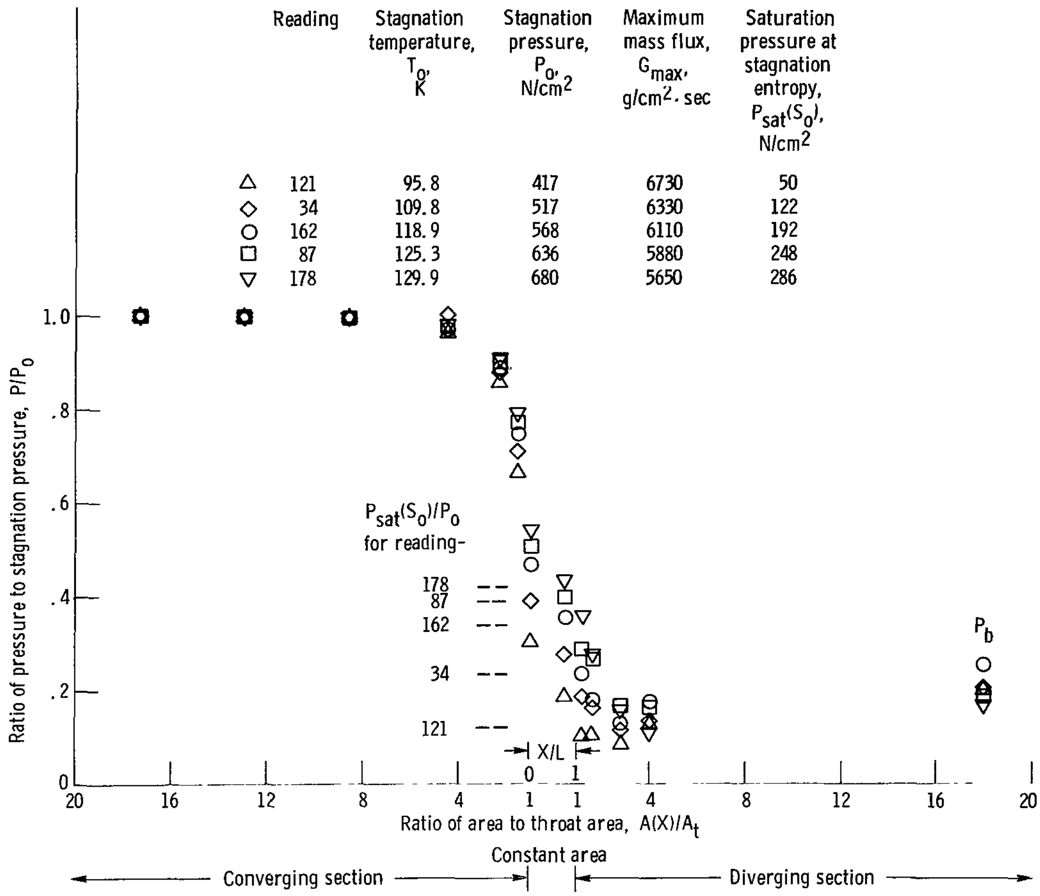

Figure 16. - Nitrogen axial pressure profiles at various stagnation temperatures in 7^0 conical nozzle.

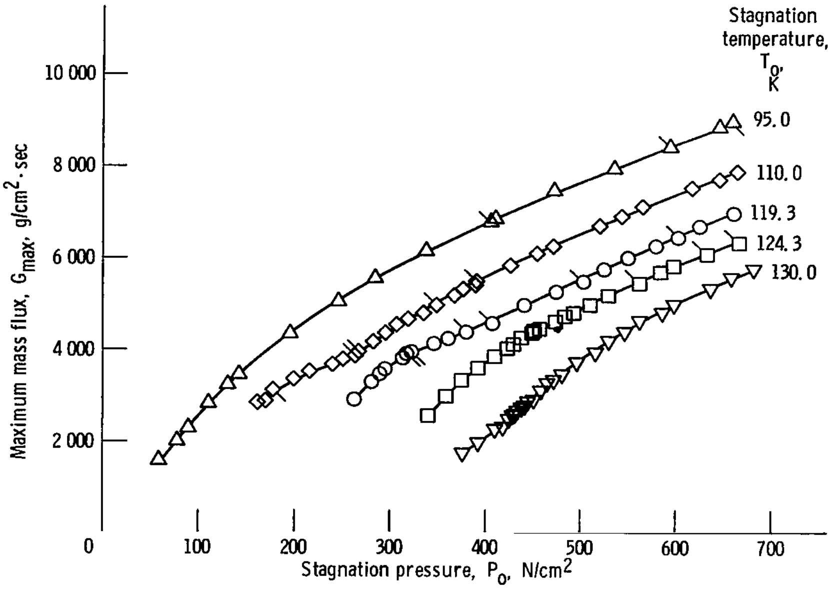

Figure 17. - Choked flow rates for subcooled nitrogen in 7° conical nozzle.

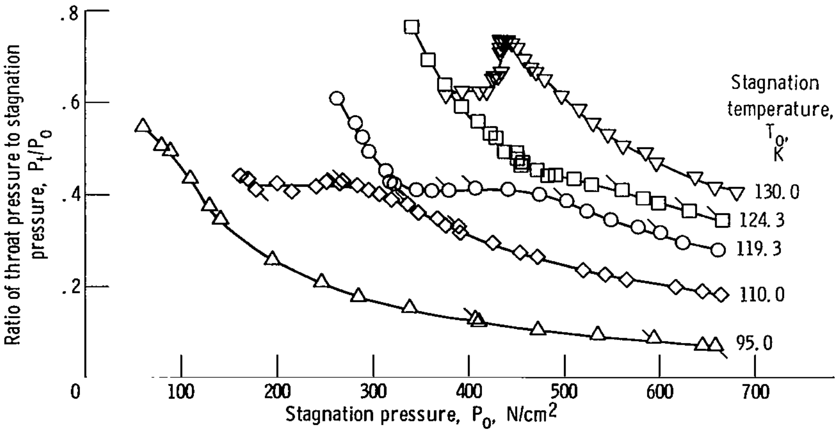

Figure 18. - Throat-stagnation pressure ratios for choked flow of subcooled nitrogen in 7° conical nozzle.

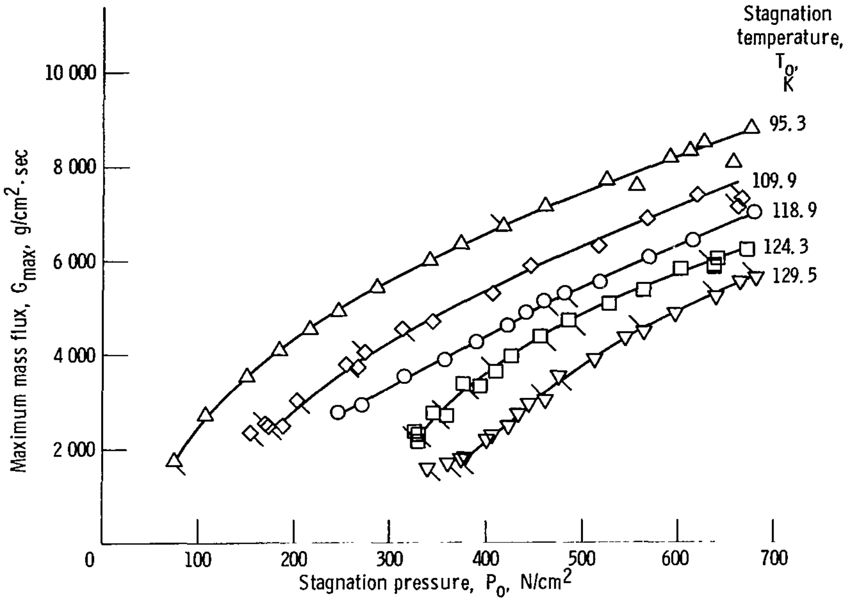

Figure 19. - Choked flow rates for subcooled nitrogen in two-dimensional nozzle.

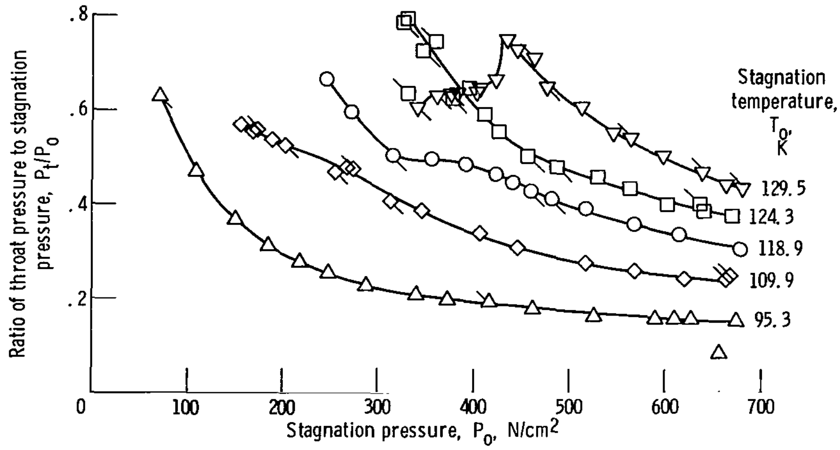

Figure 20. - Throat-stagnation pressure ratios for choked flow of subcooled nitrogen in two-dimensional nozzle.

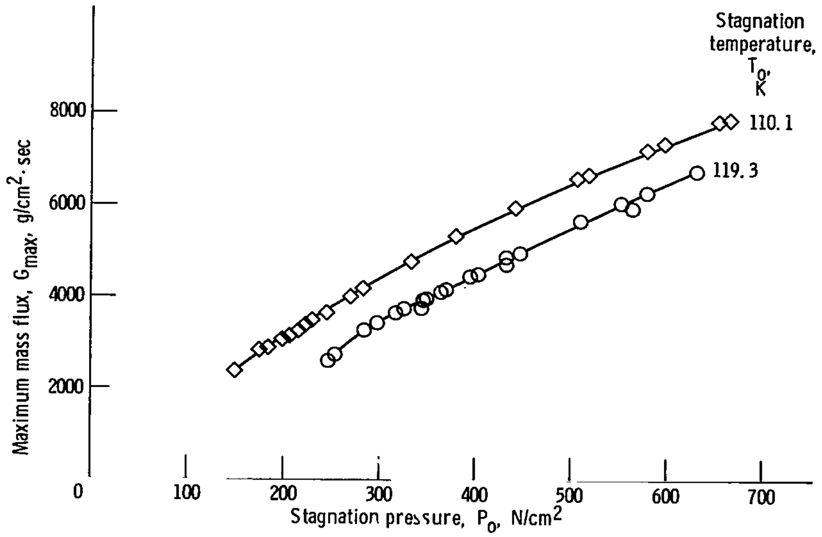

Figure 21. - Choked flow rates for subcooled nitrogen in 3.5^0 conical nozzle.

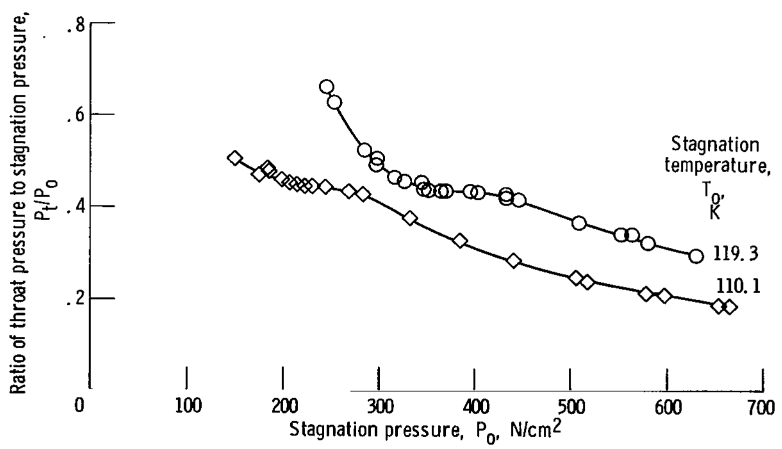

Figure 22. - Throat-stagnation pressure ratios for choked flow of subcooled nitrogen in 3.5^0 conical nozzle.

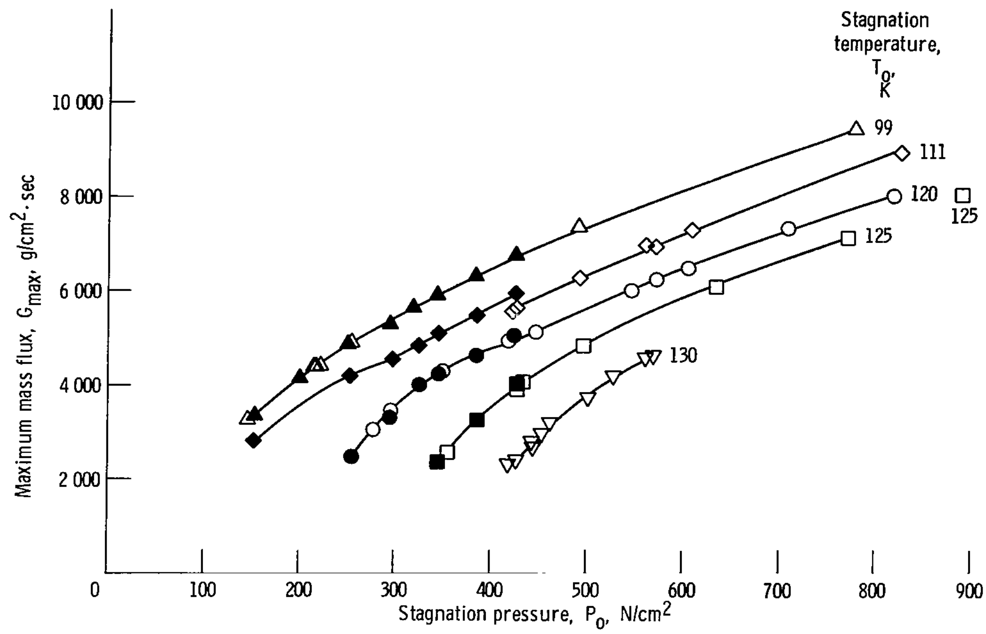

Figure 23. - Choked flow rates for subcooled nitrogen in elliptical nozzle.

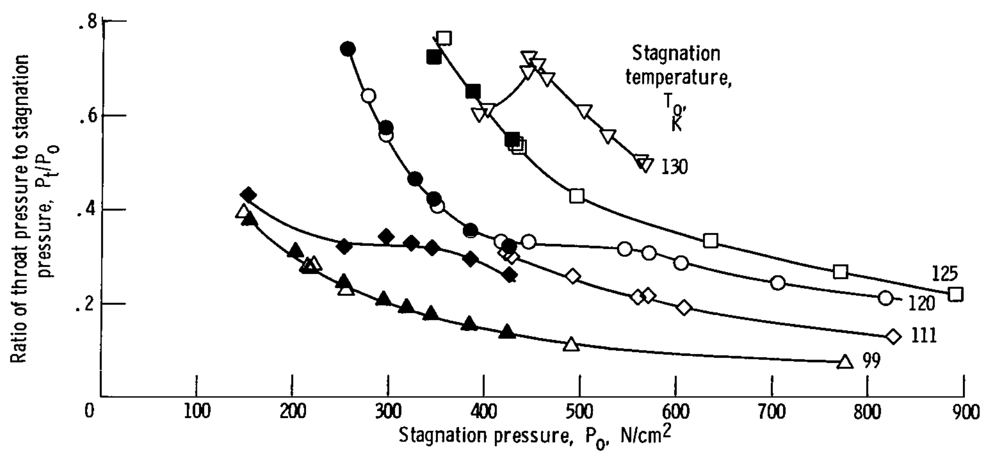

Figure 24. - Throat-stagnation pressure ratios for choked flow of subcooled nitrogen in elliptical nozzle.

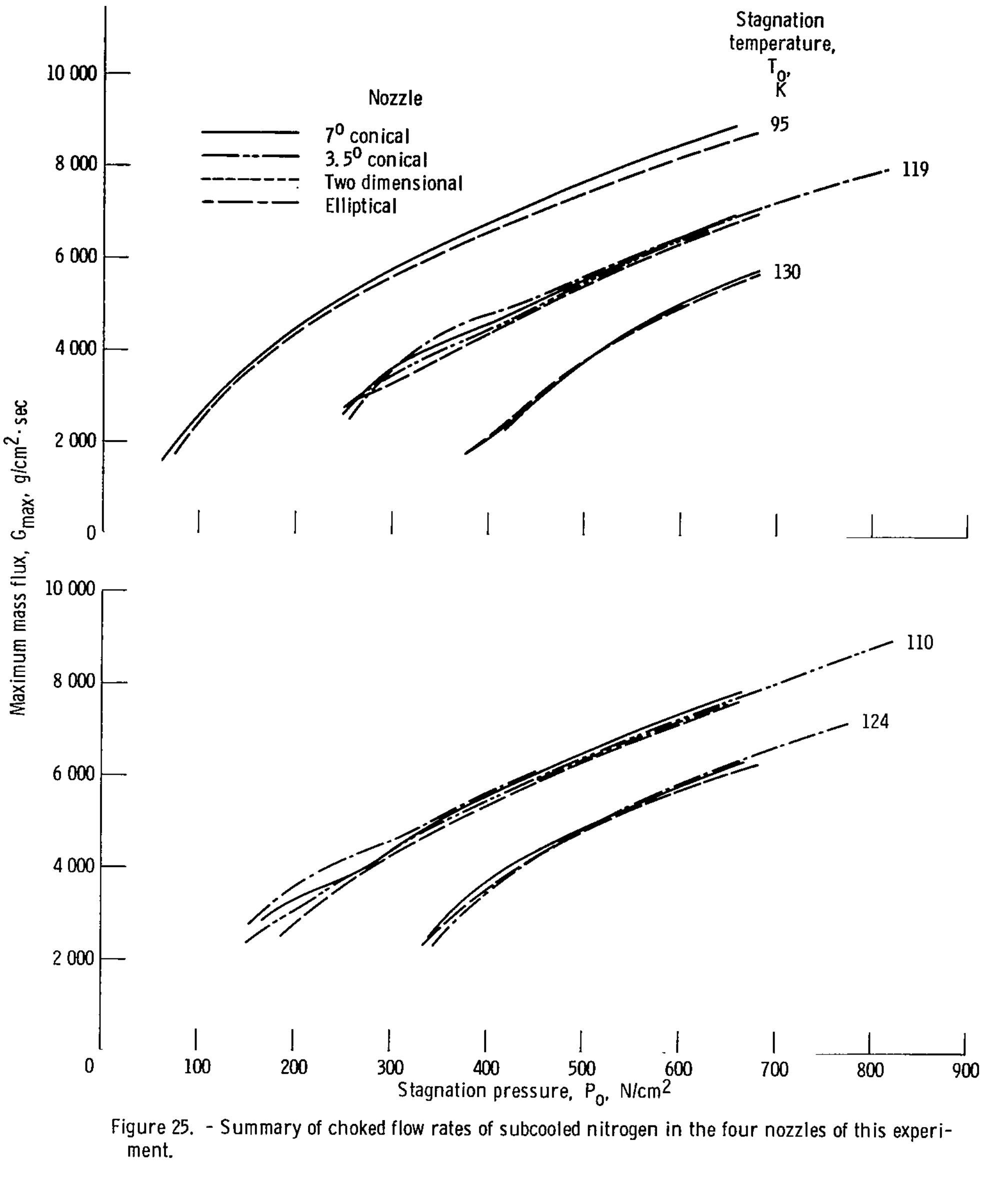

Figure 25. - Summary of choked flow rates of subcooled nitrogen in the four nozzles of this experiment.

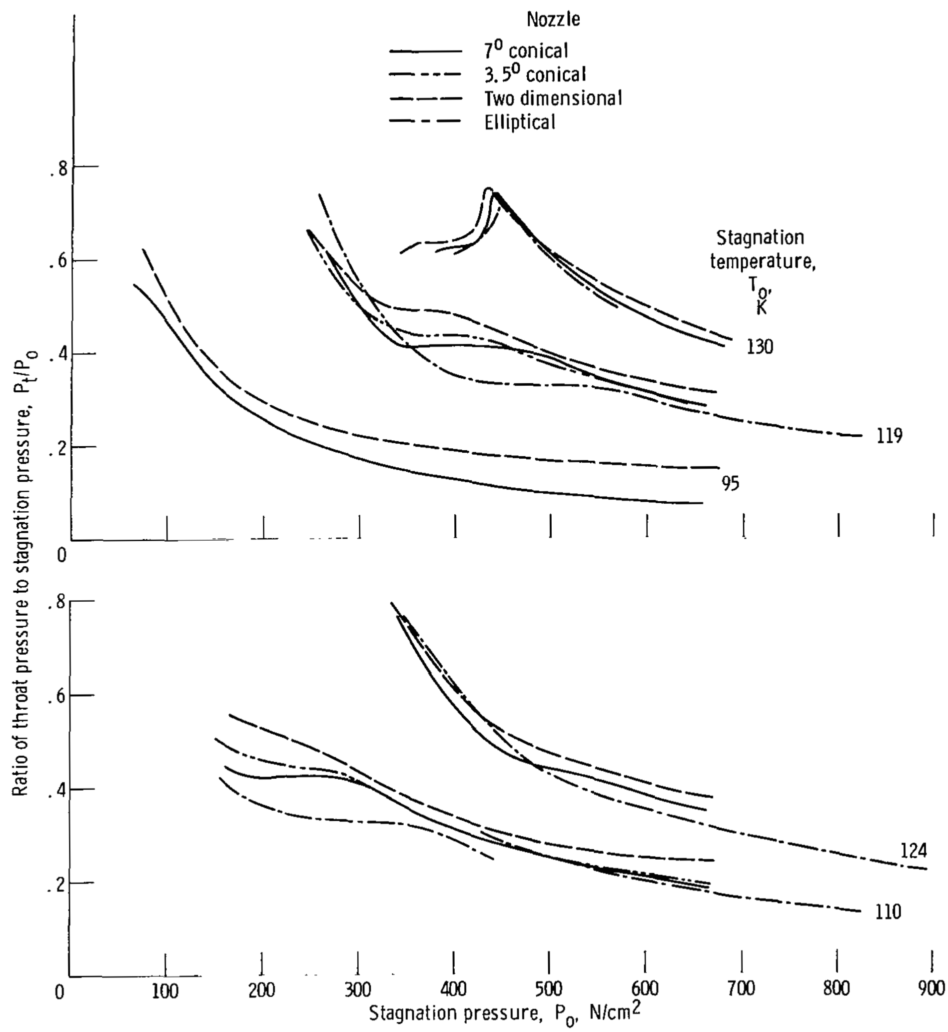

Figure 26. - Summary of throat-stagnation pressure ratios for choked flow of subcooled nitrogen in the four nozzles of this experiment.

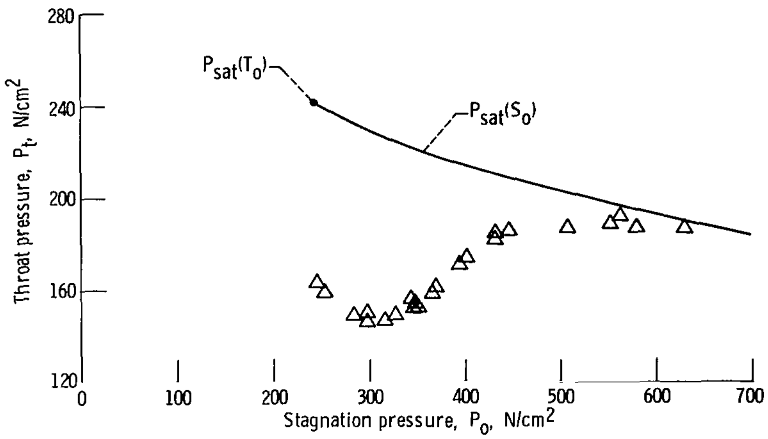

Figure 27. - Throat pressure for choked flow of subcooled nitrogen at stagnation temperature of 119.3±0.2 K - 3.5° conical nozzle.

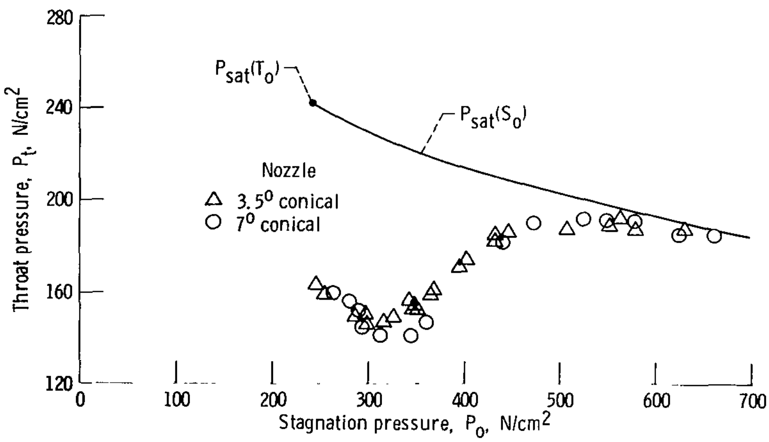

Figure 28. - Throat pressure for choked flow of subcooled nitrogen at stagnation temperature of 119.3±0.3 K - two conical nozzles.

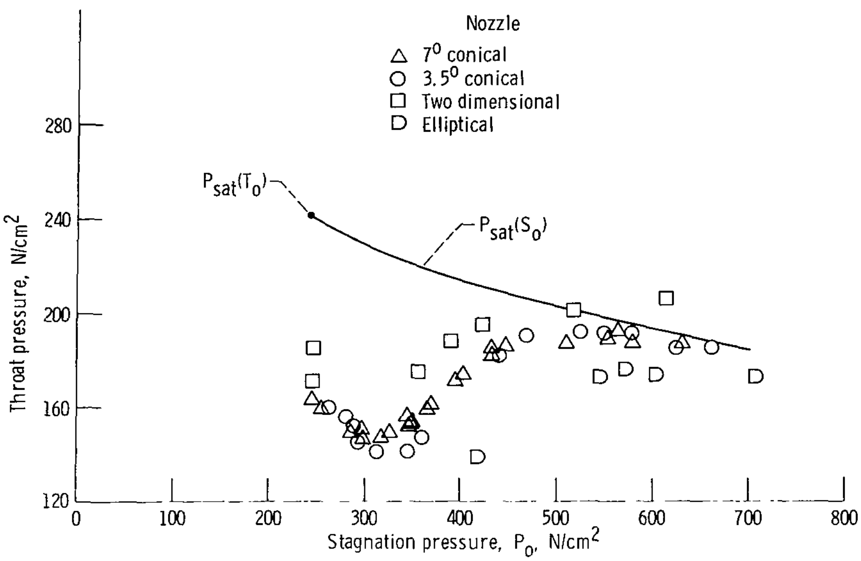

Figure 29. - Throat pressure for choked flow of subcooled nitrogen at stagnation temperature of 119.3±0.3 K - all four nozzles.

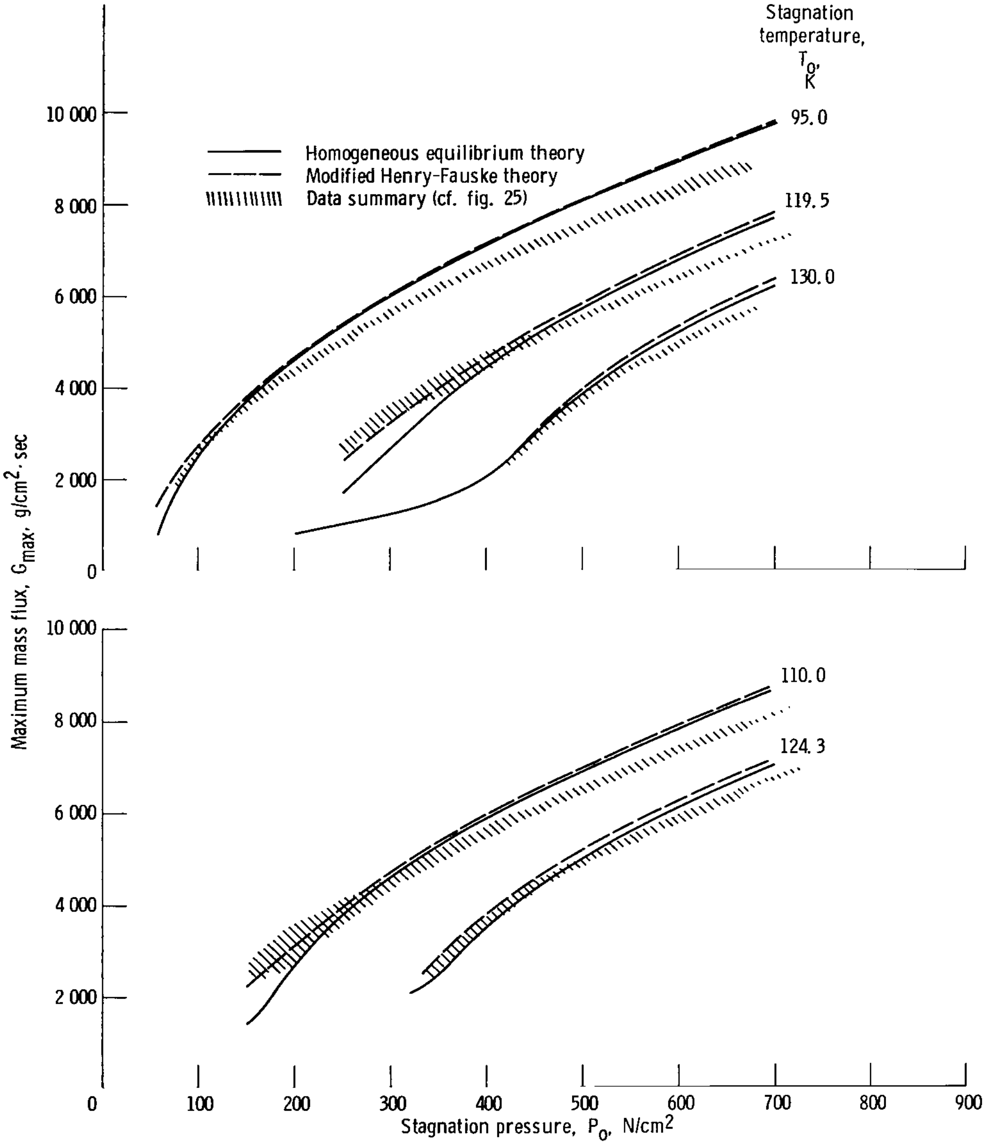

Figure 30. - Comparison of data with theory for two-phase choked flow rates.

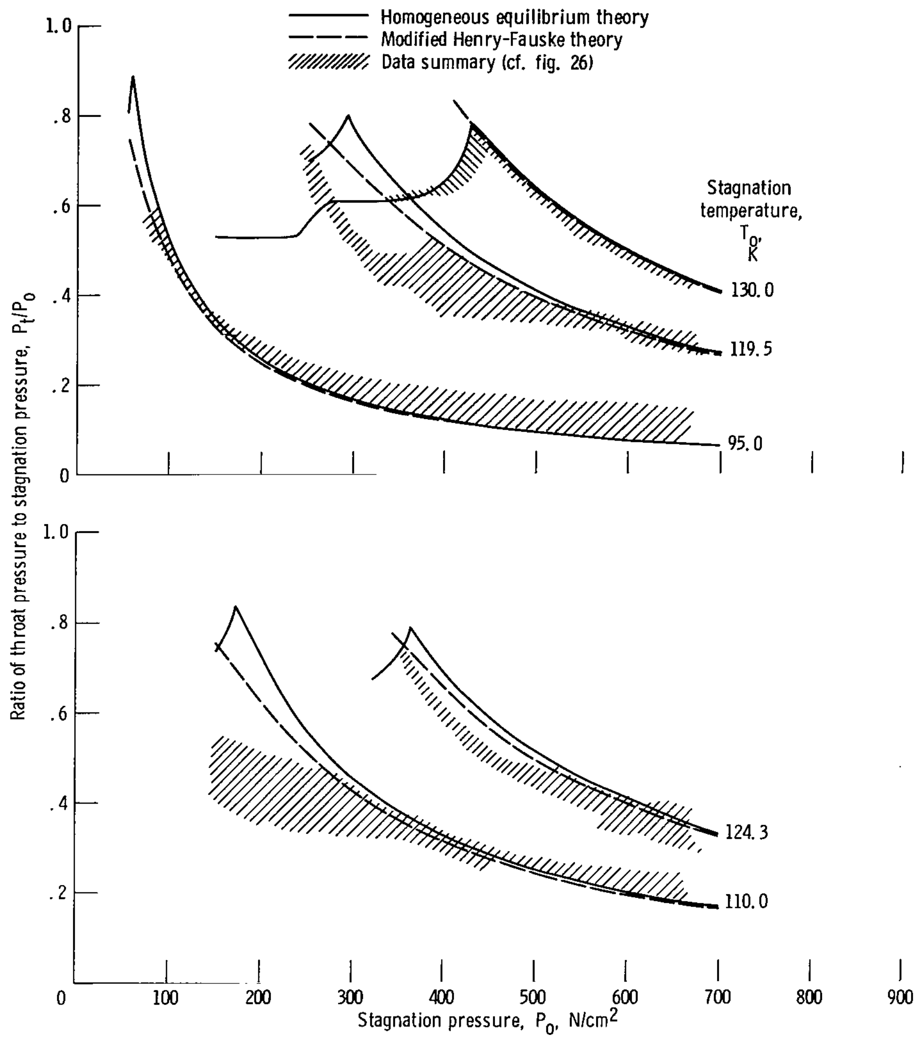

Figure 31. - Comparison of data with theory for two-phase-choked-flow throat-stagnation pressure ratios.

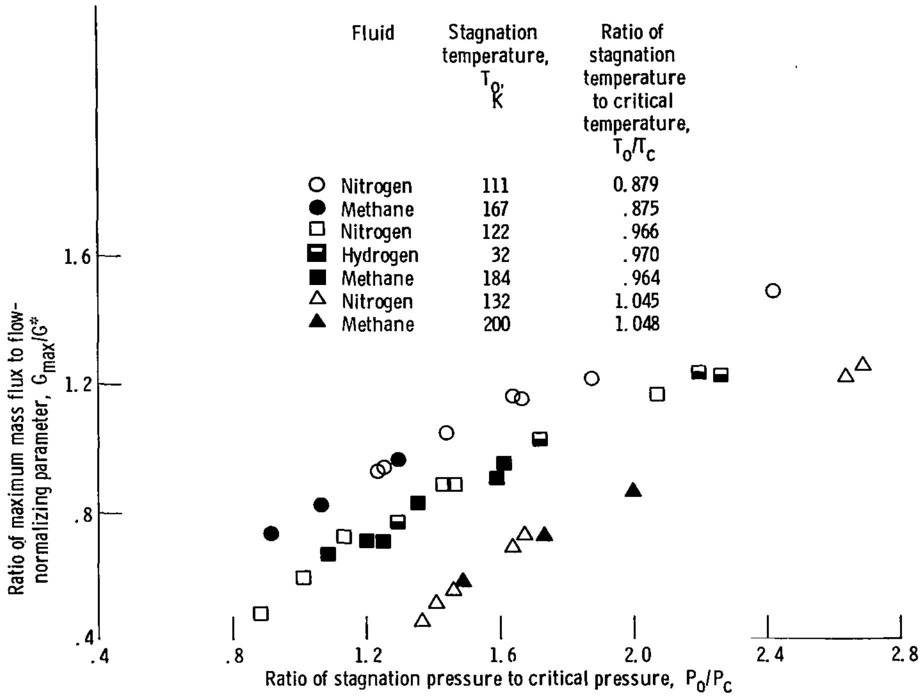

Figure 32. - Comparison of choked flow rates for nitrogen, hydrogen, and methane on a corresponding-states basis.

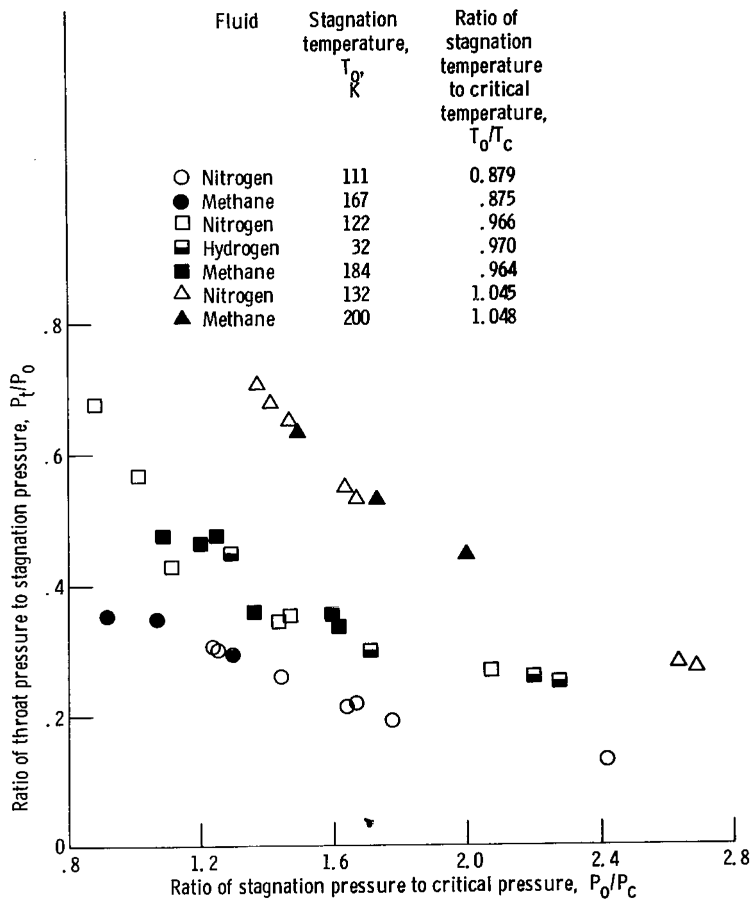

Figure 33. - Comparison of throat-stagnation pressure ratios for nitrogen, hydrogen, and methane on a corresponding-states basis.

1. Report No. TP-1484	2. Government Accession No.	3. Recipient's Catalog No.
4. Title and Subtitle TWO-PHASE CHOKED FLOW OF CRYOGENIC FLUIDS IN CONVERGING-DIVERGING NOZZLES		5. Report Date July 1979
		6. Performing Organization Code
7. Author(s) Robert J. Simoneau and Robert C. Hendricks		8. Performing Organization Report No. E-9659
		10. Work Unit No. 506-21
9. Performing Organization Name and Address National Aeronautics and Space Administration Lewis Research Center Cleveland, Ohio 44135		11. Contract or Grant No.
		13. Type of Report and Period Covered Technical Paper
12. Sponsoring Agency Name and Address National Aeronautics and Space Administration Washington, D.C. 20546		14. Sponsoring Agency Code
15. Supplementary Notes		

16. Abstract

Data are presented for the two-phase choked flow of three cryogenic fluids - nitrogen, methane, and hydrogen - in four converging-diverging nozzles. Oxygen data were reported earlier. The data cover a range of inlet stagnation conditions, all single phase, from well below to well above the thermodynamic critical conditions. In almost all cases the nozzle throat conditions were two phase. The results indicate that the choked flow rates were not very sensitive to nozzle geometry. However, the axial pressure profiles, especially the throat pressure and the point of vaporization, were very sensitive to both nozzle geometry and operating conditions. A modified Henry-Fauske model correlated all the choked-flow-rate data to within ±10 percent. Neither the equilibrium model nor the Henry-Fauske model predicted throat pressures well over the whole range of data. Above the thermodynamic critical temperature the homogeneous equilibrium model was preferred for both flow rate and pressure ratio. Like the oxygen data, the data of the three fluids could be normalized by the principle of corresponding states.

17. Key Words (Suggested by Author(s))	18. Distribution Statement
Two phase; Choked flow; Cryogenics; Nozzles; Nitrogen; Hydrogen; Methane	Unclassified - unlimited STAR Category 34

19. Security Classif. (of this report)	20. Security Classif. (of this page)	21. No. of Pages	22. Price*
Unclassified	Unclassified	81	A05

* For sale by the National Technical Information Service, Springfield, Virginia 22161

NASA-Langley, 1979

National Aeronautics and
Space Administration

Washington, D.C.
20546

Official Business
Penalty for Private Use, $300

THIRD-CLASS BULK RATE

Postage and Fees Paid
National Aeronautics and
Space Administration
NASA-451

U.S.MAIL

10 1 1U,D, 062979 S00903DS
DEPT OF THE AIR FORCE
AF WEAPONS LABORATORY
ATTN: TECHNICAL LIBRARY (SUL)
KIRTLAND AFB NM 87117

NASA

POSTMASTER: If Undeliverable (Section 158 Postal Manual) Do Not Return